République Algérienne Démocratique et Populaire
Ministère de l'Enseignement Supérieur et de la Recherche Scientifique
Université 20 Août 1955 - Skikda

Réf : D012118015D

Faculté de Technologie
Département de Génie Electrique
Laboratoire d'Automatique Skikda

THÈSE

En vue de l'obtention du diplôme de

Doctorat LMD

Domaine : **Science et Technologie**
Filière : **Génie Electrique**
Spécialité : **Automatique**

Présentée par

GANOUCHE Abderahmane

Thème

Modélisation et Commande d'une génératrice asynchrone à double stator (BDFM) : Application à une Eolienne.

Soutenue publiquement le : 18/06/2018
Devant le jury composé de :

Président	Dr. MEHENAOUI Lamine	MCA	Université de Skikda
Encadreur	Dr. BOUZEKRI Hacene	Professeur	Université de Skikda
Examinateurs	Dr. KIDOUCHE Madjid	Professeur	Université de Boumerdes
	Dr. GHERBI Sofiane	MCA	Université d'Annaba
	Dr. AHMIDA Zahir	MCA	Université de Skikda

Année 2018

People's Democratic Republic of Algeria
Ministry of Higher Education and Scientific Research
University 20 August 1955 – Skikda

Ref : D012118015D

Faculty of Technology
Department of Electrical Engineering
Automatic Laboratory of Skikda

Thesis

for the degree of

Doctor of Philosophy (LMD Doctorate)

Domain: Science and Technology
Section: Electrical Engineering
Specialty: Automatic

Presented by

GANOUCHE Abderahmane

Theme

Modelling and Control of Brushless Doubly Fed Machine (BDFM): Wind Power Application.

Presented publicly on**: 18/06/2018**

President	Dr. MEHENAOUI Lamine	Associate Professor	University of Skikda
Supervisor	Dr. BOUZEKRI Hacene	Full Professor	University of Skikda
Examiners	Dr. KIDOUCHE Madjid	Full Professor	University of Boumerdes
	Dr. GHERBI Sofiane	Associate Professor	University of Annaba
	Dr. AHMIDA Zahir	Associate Professor	University of Skikda

Year 2018

Acknowledgements

This work has been done at the automatic laboratory of Skikda under the supervision of, Dr. Hacene BOUZEKRI, professor at the department of electrical engineering, technology faculty, University 20 August 1955 Skikda

First of all, I thank Almighty God for having guided me during all my years of study and Who helped me to carry out this work, giving me strength, patience and intention. Then,

I want to express my honest gratitude and deep appreciation to my supervisor, Dr. Hacene BOUZEKRI, for directing, supporting and orienting me in my preparation of this work. His availability, feedback and scientific commitment have greatly helped me throughout these years.

I also want to thank Dr. Lamine MEHENAOUI, associate professor at the University 20 August 1955 of Skikda for the honour he gave me by accepting to be the head of the jury of my thesis.

I would also like to thank: Dr. Madjid KIDOUCHE, professor at Boumerdes University, Dr. Sofiane GHERBI, associate professor at Annaba University and, Dr. Zahir AHMIDA, associate professor at Skikda University for having accepted to evaluate this work. I would like to acknowledge Dr. Zahir AHMIDA, for his technical support. It has been a pleasure to work with you.

I would also like to express my gratitude to, Dr. Abdelmalek KHEZZAR, professor at Constantine 1 University, and Dr. Ahmed Lokmane NEMMOUR, associate professor at Constantine 1 University for permitting us to perform some

experiments in their laboratory.

Further, I want to thank my colleagues here at Skikda University who have always been present to discuss ideas with. Special thanks to Antar BEDDAR, Rochdi BOUCHEBBAT, Abderezzak LAOUAFI, Abdel Mouneim KHEMISSAT and Mehdi BOUKROUH whose support and help have proven to be invaluable.

Last but not least, I want to thank Dr. Sedat SÜNTER, professor at Firat University, for accepting and guiding me during my internship exchange as PhD international student at Firat University, Elazığ, Turkey.

Dr. Hüseyin ALTUN, professor at Firat University, and Mr. Cem CATALBAS, Miss Melike ESEN and Mr. Musab COSKUN research assistants at Firat University, and Mr. Abdul Mumin IDDRISU and Mr. Musah MUNAH international students preparing Master's degree at Firat university are all considerably acknowledged for their human qualities and technical support.

Lastly, I would like to thank my father for providing the early foundations and support that were necessary to get me where I am, and I would like to thank my lovely wife, who supported my work and without whom this research would be a much duller experience. To whom together with my daughter as well as the memory of my mother, I dedicate this dissertation.

Abderahmane Ganouche

Abstract

The Brushless Doubly Fed Machine (BDFM) continues to attract increasing interest for applications in wind power generation systems and variable speed motor drives where, robustness and low servicing costs are much desirable. As has been mentioned by various studies, the main disadvantage of this machine is its control which is relatively complex with respect to the Doubly Fed Induction Machine (DFIM). This difficulty is mainly due to the lack of a mathematical model connecting the inputs of the machine (control winding) to its outputs (power winding). To solve this problem, a new model that describes the input-output relationships of the machine is proposed. This dissertation adopts a transfer function approach to derive a mathematical model of the BDFM as a Multiple-Input Multiple-Output (MIMO) dynamic system. The proposed model is used to carry out a stability analysis of a benchmark machine under unbalanced grid voltage conditions and parameters variation. The stability study is done in an extremely wide speed range, and valid for both motor and generator operation modes. In addition to the stability investigation, the mathematical model is used to synthesise appropriate controllers for the BDFM as generator connected to the grid. The validity of the proposed model has been verified by experimentation, and the effectiveness of the control scheme has been validated by simulations.

Keywords

Brushless doubly fed machine; BDFM; linearisation; small signal model; mathematical model; stability analysis; PI controller; robust control.

الملخص

تستمر الآلة الحثية ثنائية التغذية القفصية (ا.ح.ث.ت.ق) في جذب اهتمام متزايد للتطبيقات في أنظمة توليد الطاقة من الرياح والمحركات ذات السرعة المتغيرة، حيث تكون القوة والتكاليف المنخفضة للصيانة مرغوبة إلى حد كبير. كما ذُكر في دراسات مختلفة ، فإن العيب الرئيسي لهذه الآلة هو آلية التحكم المعقدة نسبيًا مقارنة بالآلة الحثية ثنائية التغذية. وتعود هذه الصعوبة بشكل رئيسي إلى عدم وجود نموذج رياضي يربط مدخلات الآلة (لفّ التحكم) بمخرجاتها (لفّ الطاقة). لحل هذه المشكلة ، تم اقتراح نموذج جديد يصف علاقات مدخل-مخرج الآلة. تتبنى هذه الأطروحة أسلوب دالة تحويل لاشتقاق نموذج رياضي لِـ ا.ح.ث.ت.ق كنظام ديناميكي متعدد-المدخلات متعدد-المخرجات (م.م.م.م). تم استخدام النموذج المقترح لإجراء تحليل الاستقرار لآلة مقياس الأداء تحت ظروف جهد غير متوازن للشبكة الكهربائية وتغير المعلمات. تمت دراسة الاستقرار في نطاق سرعة واسع للغاية، وهي صالحة لكل من وسائط التشغيل محرك ومولد. بالإضافة إلى تحقيق للاستقرار، تم استخدام النموذج الرياضي لتطوير وحدة تحكم مناسبة ل ا.ح.ث.ت.ق كمولد متصل بشبكة الكهرباء. تم التحقق من صحة النموذج المقترح عن طريق التجريب، ومن فعالية مخطط التحكم بواسطة المحاكاة.

الكلمات المفتاحية

آلة حثية ثنائية التغذية قفصية ؛ ا.ح.ث.ت.ق؛ نموذج إشارة صغيرة؛ نموذج رياضي؛ تحليل الاستقرار؛ متحكم تناسبي تكاملي؛ تحكم قوي.

Résumé

La machine asynchrone à double stator (BDFM) continue d'attirer un intérêt croissant pour les applications dans les systèmes de production d'énergie éolienne et les entraînements de moteurs à vitesse variable où la robustesse et les faibles coûts d'entretien sont très souhaitables. Comme il a été mentionné par diverses études, l'inconvénient principal de cette machine est sa commande qui est relativement complexe par rapport à la machine asynchrone à double alimentation. Cette difficulté est principalement due à l'absence d'un modèle mathématique reliant les entrées de la machine (bobinage de contrôle) à ses sorties (bobinage de puissance). Pour résoudre ce problème, un nouveau modèle qui décrit les relations entrée-sortie de la machine est proposé. Cette thèse adopte une approche par fonction de transfert pour dériver un modèle mathématique de la BDFM en tant qu'un système dynamique entrées multiples, sorties multiples. Le modèle proposé est utilisé pour effectuer une analyse de la stabilité d'une machine prototype dans des conditions de tension de réseau déséquilibrées et de variation de paramètres. L'étude de la stabilité est réalisée dans une plage de vitesse extrêmement large, et valable pour les modes de fonctionnement moteur et générateur. En plus de l'étude de la stabilité, le modèle mathématique est utilisé pour synthétiser des contrôleurs appropriés pour la BDFM comme une génératrice connecté au réseau. La validité du modèle proposé a été vérifiée par expérimentation, et l'efficacité du schéma de contrôle a été validée par simulation.

Mots clés

machine asynchrone à double stator; BDFM; linéarisation; modèle petit signal; modèle mathématique; analyse de la stabilité; Contrôleur PI; contrôle robuste.

Contents

Acknowledgements **iii**

Abstract **v**

Contents **vii**

Table of Figures **x**

List of Tables **xiv**

Notation and Terminology **xv**

1 Introduction **1**

1.1 Review of the BDFM 3

1.1.1 History of the design and operation of the BDFM 3

1.1.2 BDFM's principle of operation 6

1.2 Objectives of the Thesis 8

1.3 Outline of the Thesis 9

2 Vector Model of the BDFM **11**

2.1 Coupled Circuit Model of the BDFM 11

2.1.1 Electrical equations 12
2.1.2 Mechanical and electromechanical equations 14
2.1.3 Active and reactive power equations 15
2.2 $d-q$ Model of the BDFM 15
2.2.1 Basics of $d-q$ transform and space vector 15
2.2.2 Electrical equations 21
2.2.3 Mechanical equations 23
2.2.4 Active and reactive power equations 23
2.3 Conclusion 24

3 Small-signal model of the BDFM **25**
3.1 Review of the BDFM Modelling 26
3.2 Small Signal Model of the BDFM 28
3.3 Control Model of the BDFM 38
3.4 Simulation Results 39
3.5 Experimental Results 44
3.6 Conclusion 47

4 BDFM Stability Analysis **50**
4.1 Definition and Basics of Stability 50
4.2 Review of the BDFM Stability Studies 53
4.3 BDFM Stability Analysis with Respect to the Operating Point . . . 54
4.4 BDFM Stability Analysis with Respect to Electric Parameters Change 55
4.5 Conclusion 59

5 Control of the BDFM **60**

5.1 History of the BDFM Control 60

5.2 PI Control of the BDFM 62

5.2.1 Decoupling matrix calculation 62

5.2.2 Order reduction of the set BDFM-Decoupling action 63

5.2.3 PI coefficients calculation: Naslin's method 67

5.2.4 Results and discussion 69

5.3 Robust Control of the BDFM 71

5.3.1 H_∞ control theory 71

5.3.2 Results and discussion 84

5.4 Application to Wind Turbine based on BDFM 87

5.4.1 Wind turbine model 87

5.4.2 Control without parameters uncertainty 91

5.4.3 Control in the presence of parameters uncertainty 95

5.5 Conclusions 98

6 Conclusions and Future Work **102**

6.1 Conclusions 102

6.2 Future Work 104

Appendix **106**

A Coefficients of the transfer Matrix **106**

Bibliography **111**

List of Figures

2.1 Clarke transformation. 16

2.2 Park transformation. 18

2.3 Rotor reference frames. 20

2.4 Different reference frames of the BDFM (electrical angles). 20

3.1 Conceptual diagram of a BDFM-based wind turbine. 28

3.2 Block diagram of the BDFM. 37

3.3 Block diagram of the BDFM control model. 39

3.4 Static gains of $\boldsymbol{G}_c(s)$ with respect to ω_{r0}. 40

3.5 Produced currents with respect to ω_{r0}. 41

3.6 Produced power with respect to ω_{r0}. 42

3.7 Step response of the BDFM. 43

3.8 Step response of the BDFM with shifted voltages. 45

3.9 Experimental test rig. 46

3.10 Power winding currents when ω_{r0}=500 rpm. 46

3.11 Power winding currents when ω_{r0}=750 rpm. 47

3.12 Power winding currents when ω_{r0}=1000 rpm. 47

3.13 Power winding currents in the reference $d-q$. 48

4.1 Geometric explanation of marginal and asymptotic stabilities. . . . 52

4.2 Geometric explanation of instability and global asymptotic stability. 52

4.3 Real part of the poles with respect to ω_{r0}. 55

4.4 Imaginary part of the poles with respect to ω_{r0}. 55

4.5 Real part of the poles with respect to rotor resistance variations. . . 56

4.6 Real part of the poles with respect to rotor inductance variations. . 57

4.7 Stability regions with respect to variations in the rotor self-inductance and resistance. 57

4.8 Stability regions with respect to variations in the stator power winding self-inductance and resistance. 58

4.9 Stability regions with respect to variations in the stator control winding self-inductance and resistance. 58

5.1 Step response of $sys(s)$ and its reduced-order approximant. 66

5.2 Bode diagram of $sys(s)$ and its reduced-order approximant. 66

5.3 Control diagram of the power winding currents using PI controller. 68

5.4 Step response of the closed-loop for different operating points. . . . 70

5.5 Schematic block diagram of the sensitivity. 72

5.6 Schematic block diagram of the complementary sensitivity. 72

5.7 Schematic block diagram of the control signal output. 73

5.8 Bode magnitude of a typically controlled system. 73

5.9 Acceptability of compensation of poles and/or zeros. 74

5.10 Nyquist diagram of a given open-loop with uncertainty. 75

5.11 Nyquist diagram of a system having small critical distance. 76

5.12 Singular values decomposition. 78

5.13 Singular values of the BDFM. 79

5.14 General formulation of the H_∞ control problem. 79

5.15 Mixed sensitivity structure for H_∞ controller design. 81

5.16 Bode diagram of the regulator. 83

5.17 Control diagram of the power winding currents. 84

5.18 Frequency and time responses of the mixed sensitivity structure-based BDFM. 85

5.19 Schematic representation of the BDFM PI control structure. 89

5.20 Schematic representation of the BDFM H_∞ control structure. . . . 90

5.21 Matlab/Simulink model. 90

5.22 Turbine Simulink model. 90

5.23 Dynamic response of constant wind speed. 92

5.24 Zoom of the dynamic response of constant wind speed. 93

5.25 Dynamic response of variable wind speed. 94

5.26 Zoom of the dynamic response of variable wind speed. 95

5.27 Dynamic response under constant wind speed in the presence of parameters uncertainty. 97

5.28 Zoom of the dynamic response for constant wind speed in the presence of parameters uncertainty. 98

5.29 Dynamic response under variable wind speed in the presence of parameters uncertainty. 99

5.30 Zoom of the dynamic response for variable wind speed in the presence of parameters uncertainty. 100

List of Tables

3.1 Electrical parameters of the BDFM 39

5.1 Routh table for model order reduction 64

5.2 Dynamic performances of the PI controller 71

5.3 Dynamic performances of the H_∞ controller 86

5.4 Wind turbine and BDFM mechanical parameters 88

5.5 The assumed BDFM real parameters 95

Notation and Terminology

List of Abbreviations

BDFM	brushless doubly fed machine
BDPA	brushless doubly-fed pulsed alternator
DFIM	doubly fed induction machine
DSBDFM	dual-stator brushless doubly-fed machine
LVRT	low voltage ride through
MIMO	multiple-input multiple-output
MMF	magneto motive forces
PI	proportional-integral controller
PWM	pulse width modulation
rpm	revolutions per minute
SISO	single-input single-output
TSIM	twin stator induction machine

Control Theory Nomenclature

α_i	characteristic ratios
$\|\cdot\|_\infty$	H infinity norm
ω_i	characteristic pulsatances
ϕ_m	phase margin
ξ	damping ratio
A_m	gain margin
d_{crit}	distance between the Nyquist locus and the critical point
$G(s)$	generalised plant
$L(s)$	open-loop function
$P(s)$	plant
$R(s)$	control function
s	Laplace variable
$S(s)$	sensitivity function
$T(s)$	complementary sensitivity function
x^*	reference of x, desired signal of x
dB	decibel

Mathematical Terminology

$'$	derivative

$[x]$, $\boldsymbol{x}$	indicates that x is non-scalar; lowercase letters refer to vectors such as $\boldsymbol{x}$, $[x]$ and $[\boldsymbol{x}]$, and capital letters refer to matrices such as $\boldsymbol{X}$, $[X]$ and $[\boldsymbol{X}]$
$\bar{a}_{xy}$	vector notation of $a_x + \jmath a_y$
$\mathbf{0}$	zero matrix of compatible dimension
$\boldsymbol{X}^T$	indicating transpose or complex-conjugate transpose of matrix $\boldsymbol{X}$
Δx	change in x
$\dot{x}$, px	time derivative of x, i.e. $\frac{dx}{dt}$
$\jmath$	the imaginary unit, i.e. $\sqrt{-1}$
$\|\cdot\|_\infty$	infinity norm
$\mathbb{R}$	field of real numbers
$\triangleq$	defined as
∂	partial derivative
σ, $\bar{\sigma}$	singular value, largest singular value
e	mathematical constant = 2.71828
X^{-1}	indicating inverse of matrix X
$\mathbb{R}_0^+$	the set of positive real numbers
I	the identity matrix of compatible dimension
ß	end of note

BDFM Nomenclature

ω_p, ω_c	power winding, control winding supply frequencies
ω_r	rotor's mechanical angular speed
θ_r	mechanical rotor-shaft displacement
$a-b-c$	natural reference frame
B	friction coefficient of the mechanical system
$d-q$	arbitrary reference frame in a p_p-type pole-pair distribution
$dc-qc$	control winding reference frame in a p_p-type pole-pair distribution
$dr-qr$	rotor reference frame in a p_p-type pole-pair distribution
J	moment of inertia
L_p, L_c, L_r	self inductance of the power winding, control winding, rotor
L_{lp}, L_{lc}, L_{lr}	leakage inductance of the power winding, control winding, rotor
L_{mp}, L_{mc}, L_{mr}	magnetising inductance of the power winding, control winding, rotor
M_p, M_c	power winding, control winding -rotor mutual inductances
p_p, p_c	power winding, control winding number of pole pairs
P_p, Q_p	active power, reactive power of the power winding
p_r	number of rotor nests
R_p, R_c, R_r	resistance of the power winding, control winding, rotor
T_{em}, T_m	electromagnetic torque, mechanical torque
v, i, φ	instantaneous voltage, current, flux vectors

W_c	coenergy

Subscripts

0	equilibrium/operating point (in Chapter 2, it refers to the zero sequence)
a, b, c	indicating phase a, b, c component
d, q	indicating direct, quadrature axis component
p, c, r	indicating power winding, control winding, rotor quantity
α, β	indicating α, β axis component

Wind Turbine Nomenclature

λ	tip-speed ratio
ω_t	turbine shaft speed
ρ	air density
θ	pitch angle
C_p	power coefficient
GB	gear box ratio
P_w	mechanical power on the rotor shaft of the wind turbine
R	turbine rotor-plane radius
T_t	turbine torque
V_w	wind velocity

Chapter 1

Introduction

After the global warming as well as the environmental pollution caused by the use of petroleum, coal and gas which are known as fossil fuel, the world is now moving towards the adoption of clean and renewable energy sources as an alternative [1,2].

The wind energy is one of the most important renewable energies currently known which is considered to be the most promising compared to all other renewable sources.

The wind energy is converted into electric energy by means of wind turbines. To increase the spread of wind turbines around the world, technological progress aims to reduce the costs of its construction and installation, as it also seeks to maximise the extracted electrical power.

Wind turbines can be classified into two basic types determined by which way the turbine rotates. Wind turbines that rotate around a horizontal axis are more common (such as a windmill), while wind turbines that rotate around a vertical axis are less commonly used (Savonius and Darrieus are the most famous). A wind turbine (horizontal axis wind turbine) consists of four main parts: the base; the tower; the nacelle; and the blades. The blades capture the energy of the wind and rotate a generator located inside the nacelle. The tower contains electrical conductors, supports the nacelle and gives access to the nacelle for maintenance.

The base is made of concrete and steel, and it supports the entire structure.

The generator inside the nacelle converts the rotational movement into electricity. Basically, a wind turbine can be equipped with asynchronous (induction) machines or synchronous machines. These machines are commonly called generators in wind energy conversion systems [3].

In fact, the use of an excitation with a permanent magnet in the permanent magnet synchronous machine requires the use of a full-scale power converter so as to adjust the voltage and frequency generated to those of the grid, which increases the cost of the system. Moreover, the use of the Doubly Fed Induction Machine (DFIM) requires a partial-scale power converter, approximately 30% of the total power.

Due to the fact that installation and maintenance costs of wind turbines do not depend on the machine size, the DFIM have dominated wind turbine applications, and the output power of today's wind turbines has exceeded 9 MW (Vestas V164).

Despite of the advantage of the DFIM cited above, which is mainly its ability to operate in variable-speed constant-frequency generation using partial-rated power converter, however, the use of brushes and slip rings to transfer the power to or from the rotor windings requires perpetual maintenance which increases servicing cost. Hence, many researchers start to study the Brushless Doubly Fed Machine (BDFM) which holds the same advantages those of the DFIM and overcomes its main drawback cited thereof [4–6].

From the huge and rapidly growing literature on the BDFM design, operation, modelling and so on. Therefore, many important and valuable contributions could not be mentioned.

1.1 Review of the BDFM

1.1.1 History of the design and operation of the BDFM

The history of today's BDFM started in the beginning of the 20th century where Hunt proposed a new induction machine, known later as the 'cascaded DFIM'. He incorporated in the same frame two DFIMs with an ingenious design of the stator windings and the rotor which significantly reduces the iron losses [7, 8].

In 1920, Creedy made an important improvement, he proposed a cascaded DFIM of 3 and 1 pole-pairs, and developed a logical and simple rotor design [9].

In 1970, Broadway and Burbridge achieved a considerable contribution in the BDFM rotor design. They proposed several rotor designs, in which they had proposed a special rotor and the most used ever after known as 'nested-loop rotor'. They also proposed an equivalent circuit for the BDFM and analysed some steady-state performances [10]. Later, Broadway et al. studied the brushless doubly fed reluctance machine and they discussed saturation effects [11, 12].

In 1978, Kusko and Somuah presented results of works on the BDFM with two electrical windings in the rotor and claim that the Broadway rotor would have an improvement [13]. They were the first who noted that the BDFM behave like a synchronous machine in the synchronous mode of operation.

In 1983 and 1987, Shibata published on the BDFM in cascaded operation mode with Kohrin in [14], then on the double feed synchronous operation mode with Taka in [15].

In the end of 1980s and the beginning of 1990s, an extensive study of the BDFM was made by Oregon State University. Many researchers studied intensively the BDFM, and the acronym 'BDFM' is origin of their publications. They firstly used the nested-loop rotor BDFM and developed an equivalent circuit for their prototype machine, then used this model to study BDFM performances [16, 17]. In 1990, Rochelle et al. studied the stator winding configuration between the use of spatial

separation and the use of different pole-pairs numbers [18]. They concluded that the latter can lead to circulation currents. Henceforth, most of the work in Oregon State University use spatially separated windings. In 1992 and 1993, Ramchandran et al. offered a frequency-domain method to estimate the parameters of the BDFM $d-q$ model in the rotor reference frame [19,20]. In 1993, Wallace et al. studied the BDFM and showed that the BDFM is flexible and good candidate for electricity generation [21]. Later in 1993 and 1995, Lauw and Wallace et al. examined the rotor design, presented some analyses and suggested improvements [22,23]. In 1995, Boger and Wallace went farther and investigated the performance of the BDFM as generator and presented a preferred operation region [24].

In 1996, Gorti et al. discussed the analysis of power distribution [25], but only real power was considered. In the same year, Liao studied the BDFM and compared it with the squirrel cage induction machine for variable speed applications and found that the BDFM is a good alternative [26].

A year later, Boger, Williamson and Ferreira studied the inter-bar rotor currents and showed by experiments that these currents reduce the efficiency of the BDFM [27–29]. To deal with the inter-bar rotor currents, Koch et al. have just proposed methods to achieve bar-to-stack insulation [30].

In 2002, Wang et al. compared experimentally between performances of the cage rotor and the axially laminated anisotropic reluctance rotor for the BDFM [31]. They found that the cage rotor has better starting and asynchronous performances; moreover, the axially laminated anisotropic rotor is advantageous in synchronous and double-feed adjustable speed characteristics.

In 2006, McMahon et al. gave investigations on performance of the BDFM in motor and generator modes by comparing the BDFM rating to those of the DFIM and the cascaded-DFIM [32].

In 2009, a new formulation of the operating principle of BDFM in synchronous mode was presented by Blazquez et al. [33]. This formulation was used to define conditions for operation in synchronous mode and to evaluate the magnetic flux

density distribution in the BDFM air gap.

In the early 2010s, several studies on the BDFM have been done by Gorginpour et al. In order to analyse the stator defects of the BDFM, Gorginpour et al. introduced a finite element model [34]. The simulation results of the finite element model are compared with those of the dynamic one of Gorginpour et al. [35]. Later, to investigate the operation modes of the BDFM which are the simple induction mode, the cascade induction mode and the synchronous mode, Gorginpour et al. presented a complete and comprehensive analytical study of these three operation modes of the BDFM based on simple electromagnetic relations [36]. Due to the fact that the BDFM suffers from lower efficiency in comparison to DFIM with the same dimension, Gorginpour et al. proposed two years later a novel modelling approach based on magnetic equivalent circuit aiming to optimise the BDFM design [37]. In 2014, Gorginpour et al. proposed a magnetic equivalent circuit model for the BDFM. This model is used to predict different performance aspects [38]. In the meantime, on the one hand, Gorginpour et al. developed a multi-objective optimisation using an imperialist competitive algorithm to significantly improved the power-to-weight ratio of the BDFM [39]. On the other hand, Gorginpour et al. presented analytical equations for calculating stray load loss and core loss in BDFMs [40].

In 2015, El Achkar et al. investigated the steady-state operating limits of a cascaded DFIM in terms of active and reactive power [41]. They showed that the consumed reactive power is limited by the power winding current for the entire operating speed; whereas the produced reactive power is limited by the control winding current for a limited speed range. Two years later, the same research group extended their investigation on the power capability of the cascaded DFIM, where a generic analytic method is suggested to systematically derive the active and reactive power domain [42]. The analytical approach is applicable to different types of doubly fed machines and validated experimentally for the cascaded DFIM.

In 2017, Cheng et al. proposed a new machine design similar to the BDFM and call it Brushless Doubly-fed Pulsed Alternator (BDPA) for high-energy pulsed

lasers [43]. For the BDFM, the power and control windings are both three-phase winding. Whereas for Cheng's BDPA, as long as the load is single-phase (flash lamp load), the power winding (armature winding) must be single phase as well, and the control winding (field winding) can be designed either single-phase winding or three-phase winding. In the meantime, Djadi et al. presented an offline parameters identification for the BDFM [44]. They used the recursive least squares minimisation in the identification algorithm, and the BDFM was exited using pseudorandom binary sequence combined with sinusoidal signal.

In 2018, Gholizadeh et al. introduced analytically the BDFM dynamic behaviour during various voltage dips [45]. Additionally, they carried out a comparison between different voltage dips in order to identify critical operating points for Low Voltage Ride Through (LVRT) assessment. Gholizadeh et al. proved also in [46] the importance of the control winding current amplitude, and the overvoltage across the crowbar resistor and BDFM side converter for improving LVRT capability of the BDFM during asymmetrical voltage dips.

1.1.2 BDFM's principle of operation

As mentioned earlier, the BDFM has two separate tri-phase sinusoidally distributed windings. One set of windings, the primary, is directly connected to the grid. The other set of windings, the secondary, is also connected to the grid, but, through a bidirectional converter.

When the two stator winding sets are fed from a set of tri-phase symmetric currents, two rotating Magneto Motive Forces (MMF) are produced along the air-gap of the BDFM. Since the two sets of BDFM stator windings are of different pole-pair number, p_p for power windings and p_c for control windings, and each of them is fed by a different excitation current, ω_p for power windings and ω_c for control windings, the rotating MMFs differ from each other and have no useful interaction for electromechanical energy in safety conditions, except for torque and force oscillations. However, with the magnetic modulation of the rotor, the two

MMFs do have useful interaction for electromechanical energy conversion [47, 48].

The BDFM rotor can be built in one of the two styles: the rotor with nested cages of p_r circuits or the rotor with reluctance segments of p_r pieces. The first configuration is considered in this dissertation. Equation (1.1) is to achieve magnetic separation between the two sets of BDFM stator windings, whereas Eq. (1.2) is to allow indirect-cross-coupling between them:

$$p_p \neq p_c \tag{1.1}$$

$$p_r = p_p + p_c \tag{1.2}$$

The BDFM can operate in both asynchronous and synchronous modes [5,27,49].

The asynchronous mode includes simple induction mode and cascade mode of operation where the shaft speed depends on the machine load and the supply excitation. These modes are important for understanding and analysing the BDFM as well as for parameter estimation.

The synchronous mode is preferable for the reason that the rotor speed is independent of the machine torque provided that this torque is less than the breakdown torque. In fact, the rotor angular speed is only determined by the excitation of the two stator windings.

Considering that the power winding has p_p pole-pairs and the control winding has p_c pole-pairs, the BDFM rotor speed can be expressed as follows:

$$\omega_r = \frac{\omega_p + \omega_c}{p_p + p_c} \tag{1.3}$$

In synchronous conditions, the two coils of the stator cooperate to induce the same frequency and distribution of currents in the rotor cage. The synchronous operating speed equals to:

$$\omega_{sync} = \frac{\omega_p + \omega_c}{p_p + p_c} \tag{1.4}$$

To obtain synchronous operation when the power winding is connected to the grid, the frequency of currents and voltages in the control winding must verify:

$$\omega_c = (p_p + p_c)\omega_r - \omega_p \tag{1.5}$$

1.2 Objectives of the Thesis

Over the last two decades, research concerning the BDFM focuses mostly on developing a competitive BDFM which could replace the regularly applied DFIM in commercial wind power applications. Actually, the BDFM is a special machine type which is attractive for use as generator in wind power systems, particularly in offshore. In fact, brush and slip-ring issues account for more than 50% of generator failures in DFIM-based wind power systems which make the BDFM more advantageous with higher reliability and lower maintenance cost. Even though the BDFM has similar operating characteristics to the DFIM, nevertheless, its operating principle is far more complex and its control remains difficult, thus inhibiting its commercialisation [50, 51]. Therefore, the aim of this dissertation is to propose robust control schemes for the BDFM, which can be used in practical applications. To fulfil this aim, this thesis is concerned with the derivation of new mathematical model for the BDFM which should be usable for applying conventional and advanced control theories.

The tasks requested in the PhD research will be conducted according to the following work plan:

- Development of new mathematical model for the BDFM;
- Investigation of the BDFM stability in open-loop operation;
- Determination of the optimal control structure for the BDFM.

1.3 Outline of the Thesis

The current section addresses briefly the remainder of this dissertation which is organised in six chapters and one appendix. Apart from the introduction and conclusion chapters, it remains four chapters form the body of dissertation.

The first Chapter presents the introduction, the BDFM history, the BDFM principle of operation, the objectives and aims, and the scope of the thesis.

In Chapter 2, the coupled circuit model of the BDFM has been presented. Then, this model is used to derive the $d-q$ vector model of the BDFM in a unified reference frame. The d-axis was aligned with the power winding flux. Additionally, basic notions of the transformation from the natural reference frame to the $d-q$ reference frame in which machine parameters and variables have constant values in the steady-state have been presented.

In Chapter 3, a small signal mathematical model for the BDFM in generation mode has been proposed. The linearisation has been done around an operating point and the BDFM has been considered connected to the grid. The proposed model is used to derive a control model for the BDFM which has been verified by simulations in Matlab/Simulink environment as well as by some experiments.

In Chapter 4, the developed mathematical model in Chapter 3 has been used to investigate the stability of the BDFM under unbalanced grid voltage conditions. The stability is done for a wide speed range, and under parameters variation.

In Chapter 5, the control model of the BDFM has been used to develop two control strategies for the BDFM: a PI controller and a robust controller. The coefficients of the PI controller are calculated using Naslin's method, and the robust controller is calculated by minimising the H_∞-norm of the weighted mixed sensitivity. Simulation validation on the non-linear BDFM-based wind turbine model has been conducted, and comparison between the two proposed control schemes has been given.

Finally, in Chapter 6, the main findings and conclusions together with propos-

itions for future work have been cited.

After these six Chapters, an Appendix is presented. The purpose of having an Appendix is mainly to smooth the thesis readability where bulky equations are presented in it.

In addition to these Chapters and the Appendix, a worthwhile list of references pertinent to the subjects treated in the thesis is given under the heading 'Bibliography'.

Chapter 2

Vector Model of the BDFM

In this chapter we will present the dynamic model of the BDFM. The dynamic model is often used to express and model the behaviour of a machine over time. Like all three-phase electrical machines, the induction machine can be simply modelled by two orthogonal components rather than by what is familiar, three sinusoidal components [3, 52–54]. Given that the BDFM had several independent reference frames: a reference frame linked to the first stator, a reference frame linked to the second stator and a reference frame linked to the rotor, its modelling remains difficult.

2.1 Coupled Circuit Model of the BDFM

To simplify the model of the BDFM, we call on simplifying assumptions perpetually used. They are briefly described by [55]:

- Constant air gap;
- Neglecting of: conductors heating, notches effect, ferromagnetic losses, iron losses and skin effect;
- The windings of each stator are identical, distributed sinusoidally and spa-

tially displaced by 120^o;

- Unsaturated magnetic circuit with fixed permeability.

2.1.1 Electrical equations

The equations of the voltages of the two stators and the rotor are obtained by Kirchhoff and Faraday's laws:

$$v_{abcp} = R_p i_{abcp} + p\varphi_{abcp} \tag{2.1}$$

$$v_{abcc} = R_c i_{abcc} + p\varphi_{abcc} \tag{2.2}$$

$$v_{abcr} = R_r i_{abcr} + p\varphi_{abcr} \tag{2.3}$$

where

$$\mathrm{f}_{abcp} = \begin{bmatrix} \mathrm{f}_{ap} & \mathrm{f}_{bp} & \mathrm{f}_{cp} \end{bmatrix}^T$$

$$\mathrm{f}_{abcc} = \begin{bmatrix} \mathrm{f}_{ac} & \mathrm{f}_{bc} & \mathrm{f}_{cc} \end{bmatrix}^T$$

$$\mathrm{f}_{abcr} = \begin{bmatrix} \mathrm{f}_{ar} & \mathrm{f}_{br} & \mathrm{f}_{cr} \end{bmatrix}^T$$

and p represents the derivative operation $\dfrac{d}{dt}$

The fluxes vector is related to the currents vector by the non-stationary inductance matrix as follows:

$$\begin{bmatrix} \varphi_{abcp} \\ \varphi_{abcc} \\ \varphi_{abcr} \end{bmatrix} = \begin{bmatrix} \boldsymbol{L}_p & \underset{(3\times3)}{\mathbf{0}} & \boldsymbol{L}_{pr} \\ \underset{(3\times3)}{\mathbf{0}} & \boldsymbol{L}_c & \boldsymbol{L}_{cr} \\ \boldsymbol{L}_{rp} & \boldsymbol{L}_{rc} & \boldsymbol{L}_r \end{bmatrix} \cdot \begin{bmatrix} i_{abcp} \\ i_{abcc} \\ i_{abcr} \end{bmatrix} \tag{2.4}$$

where inductances of the coils are given by:

$$\boldsymbol{L}_p = \begin{bmatrix} L_{lp} & L_{mp} & L_{mp} \\ L_{mp} & L_{lp} & L_{mp} \\ L_{mp} & L_{mp} & L_{lp} \end{bmatrix} \tag{2.5}$$

$$\boldsymbol{L}_c = \begin{bmatrix} L_{lc} & L_{mc} & L_{mc} \\ L_{mc} & L_{lc} & L_{mc} \\ L_{mc} & L_{mc} & L_{lp} \end{bmatrix} \tag{2.6}$$

$$\boldsymbol{L}_r = \begin{bmatrix} L_{lr} & L_{mr} & L_{mr} \\ L_{mr} & L_{lr} & L_{mr} \\ L_{mr} & L_{mr} & L_{lr} \end{bmatrix} \tag{2.7}$$

$$\boldsymbol{L}_{pr} = [\boldsymbol{L}_{rp}]^T = L_{pr} \begin{bmatrix} \cos\theta_{rp} & \cos\left(\theta_{rp} + \frac{2\pi}{3}\right) & \cos\left(\theta_{rp} - \frac{2\pi}{3}\right) \\ \cos\left(\theta_{rp} - \frac{2\pi}{3}\right) & \cos\theta_{rp} & \cos\left(\theta_{rp} + \frac{2\pi}{3}\right) \\ \cos\left(\theta_{rp} + \frac{2\pi}{3}\right) & \cos\left(\theta_{rp} - \frac{2\pi}{3}\right) & \cos\theta_{rp} \end{bmatrix} \tag{2.8}$$

$$\boldsymbol{L}_{cr} = [\boldsymbol{L}_{rc}]^T = L_{cr} \begin{bmatrix} \cos\theta_{rc} & \cos\left(\theta_{rc} + \frac{2\pi}{3}\right) & \cos\left(\theta_{rc} - \frac{2\pi}{3}\right) \\ \cos\left(\theta_{rc} - \frac{2\pi}{3}\right) & \cos\theta_{rc} & \cos\left(\theta_{rc} + \frac{2\pi}{3}\right) \\ \cos\left(\theta_{rc} + \frac{2\pi}{3}\right) & \cos\left(\theta_{rc} - \frac{2\pi}{3}\right) & \cos\theta_{rc} \end{bmatrix} \tag{2.9}$$

In the above inductances equations, L_{lp}, L_{lc} and L_{lr} are leakage inductances and L_{mp}, L_{mc} and L_{mr} are magnetising inductances of power winding, control winding, and rotor, respectively. θ_{rp} and θ_{rp} are the angular position (electric angle) related to p_p and p_c pole-pair, respectively.

2.1.2 Mechanical and electromechanical equations

In order to complete the model of the BDFM, a mechanical dynamic model is given below.

The coenergy is given by:

$$W_c = \frac{1}{2}\begin{bmatrix} i_{abcp}^T & i_{abcc}^T & i_{abcr}^T \end{bmatrix} \cdot \begin{bmatrix} \varphi_{abcp} \\ \varphi_{abcc} \\ \varphi_{abcr} \end{bmatrix} \tag{2.10}$$

The partial derivative of the coenergy with respect to the mechanical angle gives the electromagnetic torque:

$$T_{em} = \frac{\partial W_c}{\partial \theta_r} \tag{2.11}$$

$$= \frac{1}{2}\begin{bmatrix} i_{abcp}^T & i_{abcc}^T & i_{abcr}^T \end{bmatrix} \cdot \frac{d}{d\theta_r}\left(\begin{bmatrix} \boldsymbol{L}_p & \mathbf{0} & \boldsymbol{L}_{pr} \\ \mathbf{0} & \boldsymbol{L}_c & \boldsymbol{L}_{cr} \\ \boldsymbol{L}_{rp} & \boldsymbol{L}_{rc} & \boldsymbol{L}_r \end{bmatrix}\right) \cdot \begin{bmatrix} i_{abcp} \\ i_{abcc} \\ i_{abcr} \end{bmatrix} \tag{2.12}$$

As long as $\boldsymbol{L}_{pr} = [\boldsymbol{L}_{rp}]^T$ and $\boldsymbol{L}_{cr} = [\boldsymbol{L}_{rc}]^T$, and $\boldsymbol{L}_p$, $\boldsymbol{L}_c$ and $\boldsymbol{L}_r$ are constants, the electromagnetic torque can be described as:

$$T_{em} = \underbrace{i_{abcp}^T \frac{\partial \boldsymbol{L}_{pr}}{\partial \theta_r} i_{abcr}}_{T_{em_p}} + \underbrace{i_{abcc}^T \frac{\partial \boldsymbol{L}_{cr}}{\partial \theta_r} i_{abcr}}_{T_{em_c}} \tag{2.13}$$

The rotor angular velocity of the generator is related to the electromagnetic torque by the fundamental equation of the dynamics (Newton differential equation of motion) [56]:

$$J\frac{d\omega_r}{dt} = T_m + T_{em} - B \cdot \omega_r \tag{2.14}$$

where J is the total inertia of the rotor and in some cases the connected load, T_m is the mechanical torque, ω_r is the angular speed of the rotor.

2.1.3 Active and reactive power equations

The instantaneous active and reactive power of the power winding and control winding of the BDFM are given by the following relationships:

$$P_p = v_{ap} i_{ap} + v_{bp} i_{bp} + v_{cp} i_{cp} \tag{2.15}$$

$$Q_p = \frac{1}{\sqrt{3}} \left(v_{cb_p} i_{ap} + v_{ac_p} i_{bp} + v_{ba_p} i_{cp} \right) \tag{2.16}$$

where v_{xy_z} is the voltage phase to phase which is described as:

$$v_{xy_z} = v_{yz} - v_{xz}. \tag{2.17}$$

2.2 $d-q$ Model of the BDFM

The model of the BDFM given in the previous section contains sinusoidal quantities. The manipulation of these quantities is very difficult, especially in the case where we are designing a corrector. In order to circumvent this obstacle, a three-phase to two-phase transformation has been used, that of Park.

2.2.1 Basics of $d-q$ transform and space vector

The idea of a reference change is to transform a sinusoidal quantity in a reference frame into a constant quantity in another reference frame. This transformation is the superposition of two consecutive transformations.

The first is to transform the three-phase sinusoidal (electric) variables from the fixed natural reference frame $a-b-c$ to a two-phase sinusoidal quantities in a fixed reference frame also and orthogonal called $\alpha-\beta$ as illustrated in Fig. 2.1.

This transformation is known as 'Clarke transformation', or more commonly '$\alpha - \beta$ transformation'. The space vector (also known as space phasor) of the three-phase power winding voltage is described as:

$$\bar{v}_{\alpha\beta p} = \frac{2}{3}\left(v_{ap} + v_{bp} \cdot a + v_{bp} \cdot a^2\right) \tag{2.18}$$

where $a = e^{\jmath\frac{2}{3}\pi}$, and the space vector can be represented by the following complex form:

$$\bar{v}_{\alpha\beta p} = v_{\alpha p} + \jmath v_{\beta p} \tag{2.19}$$

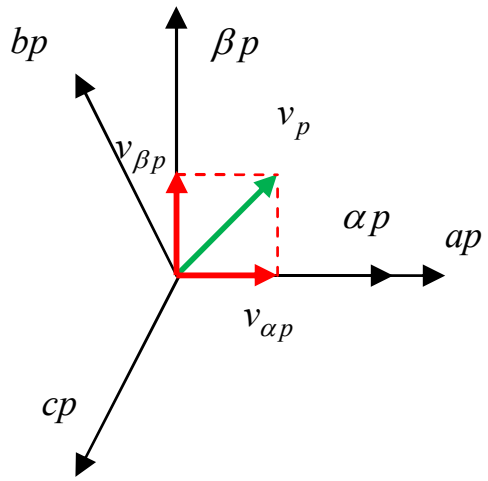

Fig. 2.1: Clarke transformation.

Note The power winding voltage is used as an example to explain how does it work. In fact, the $\alpha - \beta$ transform (also Park transformation which we will show after) is applicable to all electric variables including voltages, currents and fluxes of the power winding, the control winding and the rotor. ß

Matrix form of the $\alpha - \beta$ transformation can be written as:

$$\begin{bmatrix} v_{\alpha p} \\ v_{\beta p} \\ v_{0p} \end{bmatrix} = \frac{2}{3} \begin{bmatrix} 1 & -\frac{1}{2} & \frac{1}{2} \\ 0 & \frac{\sqrt{3}}{2} & -\frac{\sqrt{3}}{2} \\ \frac{1}{2} & \frac{1}{2} & \frac{1}{2} \end{bmatrix} \cdot \begin{bmatrix} v_{ap} \\ v_{bp} \\ v_{cp} \end{bmatrix} \tag{2.20}$$

where v_{0p} is the zero sequence or the homopolar component.

Note If we assume that the three-phase system is symmetric, so the zero sequence is always null:

$$v_{0p} = \frac{1}{3} \underbrace{(v_{ap} + v_{bp} + v_{cp})}_{\| \; 0}$$

The present dissertation concentrates only on symmetrical systems. For the sake of simplicity, the rest mathematical developments of this dissertation will omit the zero sequence. ß

Clarke and reverse Clarke transformations can be described as:

$$\begin{bmatrix} v_{\alpha p} \\ v_{\beta p} \end{bmatrix} = \frac{2}{3} \begin{bmatrix} 1 & -\frac{1}{2} & \frac{1}{2} \\ 0 & \frac{\sqrt{3}}{2} & -\frac{\sqrt{3}}{2} \end{bmatrix} \cdot \begin{bmatrix} v_{ap} \\ v_{bp} \\ v_{cp} \end{bmatrix} \tag{2.21}$$

$$\begin{bmatrix} v_{ap} \\ v_{bp} \\ v_{cp} \end{bmatrix} = \begin{bmatrix} 1 & 0 \\ -\frac{1}{2} & \frac{\sqrt{3}}{2} \\ -\frac{1}{2} & -\frac{\sqrt{3}}{2} \end{bmatrix} \cdot \begin{bmatrix} v_{\alpha p} \\ v_{\beta p} \end{bmatrix} \tag{2.22}$$

The second is to convert electrical variables from the fixed orthogonal axis system $\alpha - \beta$ to an arbitrary rotating orthogonal axis system $d - q$ as shown in

Fig. 2.2. This transformation is known as 'Park transformation' and the angle θ between the α axis and the d axis is known as Park's angle. The coordinate transformation from $\alpha - \beta$ to $d - q$ is given by:

$$\bar{v}_{dqp} = \bar{v}_{\alpha\beta p} e^{-\jmath\theta} \tag{2.23}$$

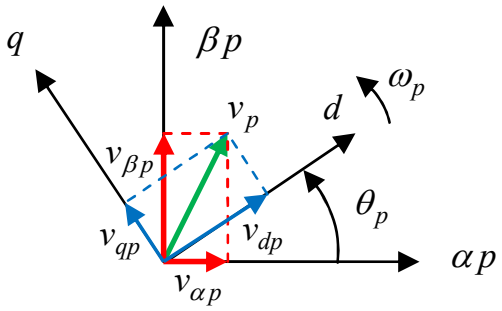

Fig. 2.2: Park transformation.

Similarly, space vector can be represented by the following complex form:

$$\bar{v}_{dqp} = v_{dp} + \jmath v_{qp} \tag{2.24}$$

where d refers to the direct component and q refers to the quadrature component.

Park and reverse park transformations can be written in matrix form as follows:

$$\begin{bmatrix} v_{dp} \\ v_{qp} \end{bmatrix} = \begin{bmatrix} \cos(\theta) & \sin(\theta) \\ -\sin(\theta) & \cos(\theta) \end{bmatrix} \cdot \begin{bmatrix} v_{\alpha p} \\ v_{\beta p} \end{bmatrix} \tag{2.25}$$

$$\begin{bmatrix} v_{\alpha p} \\ v_{\beta p} \end{bmatrix} = \begin{bmatrix} \cos(\theta) & -\sin(\theta) \\ \sin(\theta) & \cos(\theta) \end{bmatrix} \cdot \begin{bmatrix} v_{dp} \\ v_{qp} \end{bmatrix} \tag{2.26}$$

The combination of Clarke and Park transformations in one transformation leads to the well known '$d - q$ transformation' which is used to transform three-

phase sinusoidal variables into two-phase constant variables in steady-state as long as the rotating speed of the $d-q$ reference frame equals to the power winding frequency (in this case the, $d-q$ reference is called the 'synchronous reference frame'). Combining Eqs. (2.21) and (2.25) it results into:

$$\begin{bmatrix} v_{\alpha p} \\ v_{\beta p} \end{bmatrix} = \underbrace{\frac{2}{3}\begin{bmatrix} \cos(\theta) & \cos\left(\theta-\frac{2\pi}{3}\right) & \cos\left(\theta+\frac{2\pi}{3}\right) \\ -\sin(\theta) & -\sin\left(\theta-\frac{2\pi}{3}\right) & -\sin\left(\theta+\frac{2\pi}{3}\right) \end{bmatrix}}_{\mathbf{T}(\theta)} \cdot \begin{bmatrix} v_{ap} \\ v_{bp} \\ v_{cp} \end{bmatrix} \tag{2.27}$$

The reverse $d-q$ transform can be obtained using Eqs. (2.22) and (2.26):

$$\begin{bmatrix} v_{ap} \\ v_{bp} \\ v_{cp} \end{bmatrix} = \underbrace{\begin{bmatrix} \cos(\theta) & -\sin(\theta) \\ \cos\left(\theta-\frac{2\pi}{3}\right) & -\sin\left(\theta-\frac{2\pi}{3}\right) \\ \cos\left(\theta+\frac{2\pi}{3}\right) & -\sin\left(\theta+\frac{2\pi}{3}\right) \end{bmatrix}}_{\mathbf{T}^{-1}(\theta)} \cdot \begin{bmatrix} v_{\alpha p} \\ v_{\beta p} \end{bmatrix} \tag{2.28}$$

The angular position θ in the transformation $\mathbf{T}$ and its reverse $\mathbf{T}^{-1}$ is related with the angular speed ω by the following relation:

$$\theta = \omega t + \theta_0 \tag{2.29}$$

where ω refers to the angular speed at which the corresponding reference $\alpha-\beta$ is seeing the reference $d-q$ turns in the positive direction in space.

The superiority of choosing the power winding synchronous reference frame, more precisely relating the d axis to the power winding flux, can be justified by the possibility of controlling independently the active and reactive power.

Due to the fact that the BDFM has two separate three-phase electrical windings, the rotor is having two reference frames as presented in Fig. 2.3 [6, 50].

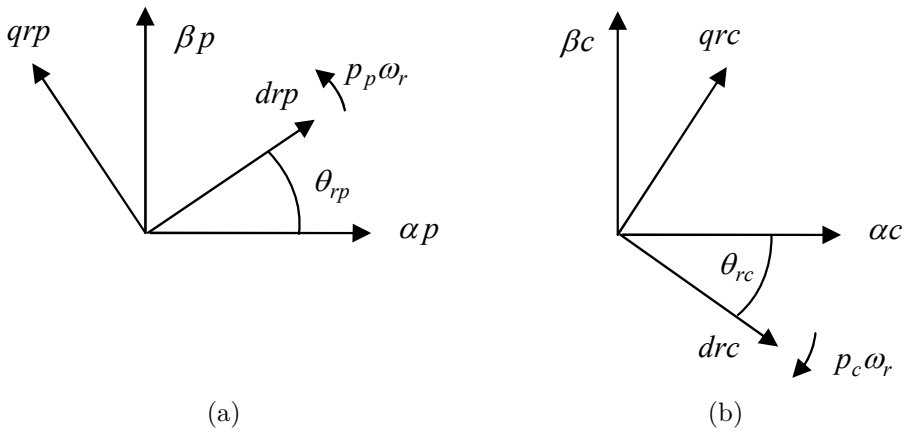

Fig. 2.3: Rotor reference frames.

Figure 2.4 presents schematically reference frames of the BDFM [57].

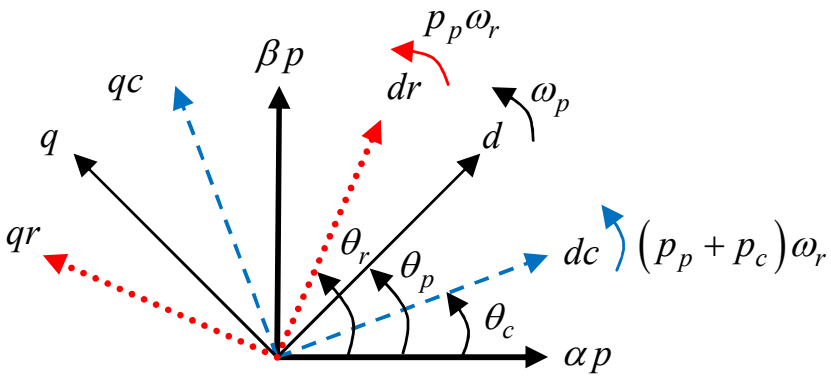

Fig. 2.4: Different reference frames of the BDFM (electrical angles).

As shown in Fig. 2.4, there are four main reference frames: (i) the stationary reference frame related to the power winding $\alpha - \beta p$, (ii) the control winding synchronous reference frame $dc - qc$ which rotates at the speed $(p_p + p_c)\omega_r$, (iii) the synchronous reference frame $d - q$ which rotates at the grid pulsatance (electrical angular speed) ω_p and (iv) the rotor synchronous reference frame $dr - qr$ which rotates at the speed $p_p\omega_r$.

2.2.2 Electrical equations

By applying the $d-q$ transform (2.27) on the power winding voltage equation (2.1) yields:

$$\begin{aligned} v_{dqp} &= \mathbf{T}(\theta_p) v_{abcp} \\ &= \mathbf{T}(\theta_p) \left(R_p i_{abcp} + p\varphi_{abcp} \right) \\ &= \mathbf{T}(\theta_p) \left(R_p \mathbf{T}^{-1}(\theta_p) i_{dqp} + \frac{d}{dt} \left(\mathbf{T}^{-1}(\theta_p) \varphi_{dqp} \right) \right) \\ &= R_p i_{dqp} + \mathbf{T}(\theta_p) \left(\mathbf{T}^{-1}(\theta_p) \frac{d}{dt} \varphi_{dqp} + \frac{d}{dt} \left(\mathbf{T}^{-1}(\theta_p) \right) \varphi_{dqp} \right) \\ &= R_p i_{dqp} + p\varphi_{dqp} + \mathbf{T}(\theta_p) \frac{d}{dt} \left(\mathbf{T}^{-1}(\theta_p) \right) \varphi_{dqp} \end{aligned} \tag{2.30}$$

Note The writing v_{dqp} is used instead of $\begin{bmatrix} v_{dp} \\ v_{qp} \end{bmatrix}$ to reduce equations' size, and will be considered later with other variables. ß

The time derivative of $\mathbf{T}^{-1}$ is calculated as follows:

$$\begin{aligned} \frac{d}{dt} \mathbf{T}^{-1}(\theta_p) &= \frac{d}{dt} \begin{bmatrix} \sin(\theta_p) & \cos(\theta_p) \\ \sin\left(\theta_p - \frac{2\pi}{3}\right) & \cos\left(\theta_p - \frac{2\pi}{3}\right) \\ \sin\left(\theta_p + \frac{2\pi}{3}\right) & \cos\left(\theta_p + \frac{2\pi}{3}\right) \end{bmatrix} \\ &= \omega_p \begin{bmatrix} \cos(\theta_p) & -\sin(\theta_p) \\ \cos\left(\theta_p - \frac{2\pi}{3}\right) & -\sin\left(\theta_p - \frac{2\pi}{3}\right) \\ \cos\left(\theta_p + \frac{2\pi}{3}\right) & -\sin\left(\theta_p + \frac{2\pi}{3}\right) \end{bmatrix} \end{aligned} \tag{2.31}$$

Since:

$$\begin{gathered}\sum_{k=0}^{2}\sin^2\left(x-(k-1)\frac{2\pi}{3}\right)=\sum_{k=0}^{2}\cos^2\left(x-(k-1)\frac{2\pi}{3}\right)=\frac{3}{2}\\ \sum_{k=0}^{2}\left(\sin\left(x-(k-1)\frac{2\pi}{3}\right)\cdot\cos\left(x-(k-1)\frac{2\pi}{3}\right)\right)=0\end{gathered}\tag{2.32}$$

the following can be written:

$$\mathbf{T}(\theta_p)\frac{d}{dt}\left(\mathbf{T}^{-1}(\theta_p)\right)=\begin{bmatrix}0 & -\omega_p\\ \omega_p & 0\end{bmatrix}\tag{2.33}$$

Thus, the power winding voltage equation can be expressed by the following complex notation:

$$\bar{v}_{dqp}=R_p\bar{i}_{dqp}+p\bar{\varphi}_{dqp}+j\omega_p\bar{\varphi}_{dqp}\tag{2.34}$$

Similarly for control winding and rotor voltage equations:

$$\bar{v}_{dqr}=R_r\bar{i}_{dqr}+p\bar{\varphi}_{dqr}+j\left(\omega_p-p_p\omega_r\right)\bar{\varphi}_{dqr}\tag{2.35}$$

$$\bar{v}_{dqc}=R_c\bar{i}_{dqc}+p\bar{\varphi}_{dqc}+j\left(\omega_p-\left(p_p+p_c\right)\omega_r\right)\bar{\varphi}_{dqc}\tag{2.36}$$

Using the $d-q$ transformation on the power winding flux equation leads to:

$$\varphi_{dqp}=\mathbf{T}\left(\theta_p\right)\left(\mathbf{L}_p\mathbf{T}^{-1}\left(\theta_p\right)i_{dqp}+\mathbf{L}_{pr}\mathbf{T}^{-1}\left(\theta_r\right)i_{dqr}\right)\tag{2.37}$$

$$\begin{bmatrix}\varphi_{dp}\\ \varphi_{qp}\end{bmatrix}=\begin{bmatrix}L_{lp}-L_{mp} & 0\\ 0 & L_{lp}-L_{mp}\end{bmatrix}\cdot\begin{bmatrix}i_{dp}\\ i_{qp}\end{bmatrix}+\begin{bmatrix}\frac{3}{2}L_{pr} & 0\\ 0 & \frac{3}{2}L_{pr}\end{bmatrix}\cdot\begin{bmatrix}i_{dr}\\ i_{qr}\end{bmatrix}\tag{2.38}$$

Therefore, fluxes equations can be expressed as:

$$\varphi_{dqp}=L_pi_{dqp}+M_pi_{dqr}\tag{2.39}$$

$$\varphi_{dqc} = L_c i_{dqc} + M_c i_{dqr} \tag{2.40}$$

$$\varphi_{dqr} = L_r i_{dqr} + M_p i_{dqp} + M_c i_{dqc} \tag{2.41}$$

where $L_x = L_{lx} - L_{mx}$ and $M_x = \frac{3}{2} L_{xr}$ and x could be p for power winding, c for control winding or r for rotor.

2.2.3 Mechanical equations

By applying the transformation (2.27) on the electromagnetic torque equation given by Eq. (2.13), this leads to:

$$\begin{aligned} T_{em_p} &= i_{abcp}^T \frac{\partial \boldsymbol{L}_{pr}}{\partial \theta_r} i_{abcr} \\ &= i_{dqp}^T \left(T^{-1}(\theta_p)\right)^T \frac{\partial \boldsymbol{L}_{pr}}{\partial \theta_r} T^{-1}(\theta_r) i_{dqr} \\ &= \frac{3}{2} p_p M_p \left(i_{qp} i_{dr} - i_{dp} i_{qr}\right) \end{aligned} \tag{2.42}$$

$$T_{em_c} = \frac{3}{2} p_c M_c \left(i_{qc} i_{dr} - i_{dc} i_{qr}\right) \tag{2.43}$$

$$T_{em} = T_{em_p} + T_{em_c} \tag{2.44}$$

2.2.4 Active and reactive power equations

The active and reactive powers of the BDFM are expressed in the reference $d-q$ by:

$$\begin{aligned} P_p &= v_{ap} i_{ap} + v_{bp} i_{bp} + v_{cp} i_{cp} \\ &= v_{abcp}^T i_{abcp} \\ &= v_{dqp}^T \left(T^{-1}(\theta_p)\right)^T T^{-1}(\theta_p) i_{dqp} \\ &= \frac{3}{2} \left(v_{dp} i_{dp} + v_{qp} i_{qp}\right) \end{aligned} \tag{2.45}$$

$$
\begin{aligned}
Q_p &= \frac{1}{\sqrt{3}}\left(v_{cb_p} i_{ap} + v_{ac_p} i_{bp} + v_{ba_p} i_{cp}\right) \\
&= \frac{1}{\sqrt{3}} v_{abcp}^T \begin{bmatrix} 0 & -1 & 1 \\ 1 & 0 & -1 \\ -1 & 1 & 0 \end{bmatrix} i_{abcp} \\
&= \frac{1}{\sqrt{3}} v_{dqp}^T \left(T^{-1}(\theta_p)\right)^T \begin{bmatrix} 0 & -1 & 1 \\ 1 & 0 & -1 \\ -1 & 1 & 0 \end{bmatrix} T^{-1}(\theta_p) i_{dqp} \\
&= \frac{3}{2}\left(v_{qp} i_{dp} - v_{dp} i_{qp}\right)
\end{aligned}
\tag{2.46}
$$

2.3 Conclusions

This chapter describes the three-phase model of the BDFM, the voltages equations, the fluxes equations, the powers equations, the electromagnetic torque equation as well as the shaft equation. This $a-b-c$ model or coupled circuit model is used to extract a two-phase model, called the $d-q$ model. The transformation from the natural reference to the Park reference is briefly described.

Chapter 3

Small-Signal Model of the BDFM

The BDFM $d-q$ model given in the previous chapter as well as in all previously published works have affine non-linearities, and do not reflect a direct relationship between the input which is the control winding and the output which is the power winding. Therefore, this model is not serviceable for control purposes. In order to overcome these disadvantages, we propose in this chapter a small signal mathematical model giving a direct relation between the input and the output of the BDFM when it works in generation mode connected to the grid. The input is the voltage vector of the control winding, and the output is the current vector produced by the BDFM and transmitted to the grid. Thanks to this developed model, we can (i) study the stability of the BDFM, (ii) reduce the model of the BDFM by the existing aggregation methods, (iii) synthesise controllers which allow the regulation of the power produced by the BDFM and (iv) implement optimal and robust control laws. As we will show, and has been stated in several studies such as [58], the obtained model for this type of machines is high order of multivariable structure and strong coupling effect [59].

3.1 Review of the BDFM Modelling

In the mid of 1960s, Smith developed for the first time a steady-state model and an equivalent circuit for the Twin Stator Induction Machine (TSIM). The TSIM is similar to the cascaded DFIM but the stators have equivalent number of pole-pairs, i.e. the magnetic separation is spatial instead of using different number of pole-pairs [60, 61]. In 1991, Li et al. proposed for the first time a dynamic model for their BDFM prototype and showed performance results by simulation [62–64]. The stator of their BDFM was composed of 3 pole-pairs for the power winding and 1 pole-pair for the control winding. Since the appearance of the initial dynamic model of the BDFM, a lot of interest was brought on this subject.

In 1994, Li et al. used the two axes BDFM model to derive an equivalent circuit for the machine, and also to consider the steady-state performances in synchronous mode [65]. In the same year, Zhou and Spée developed a synchronous reference frame model for the BDFM and used it to develop a decoupled torque controller [66]. The developed model has the advantage that the d and q quantities become constant quantities at steady-state but the BDFM was considered as two subsystems.

In 1995, Boger et al. used the $d-q$ model of the BDFM of [65] to generalise it for any given pole-pairs configuration [67]. The model was validated experimentally but their starting point was an assumed configuration nevertheless.

In 1996 and 1997, Ferreira, and Williamson et al. contributed on the modelling of the BDFM in which they presented a mathematical model of the BDFM based on generalised harmonic analysis [68, 69]. This model is subsequently validated by experimentation for synchronous operation in another paper [70].

In 2004, Oliveria et al. presented a finite element model for the BDFM which allows to simulate it with different rotor bars configurations [71]. Meanwhile, Roberts presented in his PhD thesis a general study on the BDFM [72]. He gave a method to calculate the parameters of the equivalent circuit of the BDFM with a precious discussion, and he also presented several models for the BDFM and are: The coupled-circuit model; the $d-q$ model; the reduced $d-q$ model and the equivalent

circuit model. The main findings on the electrical equivalent circuit and parameter estimation were published a year later by Roberts et al. in [73].

In 2006, Poza et al. developed an interesting dynamic vector model of the BDFM [74]. Indeed, the work was part of the results of Poza's PhD thesis [75], which had been being published three years ago. The developed dynamic vector model was in a unified reference frame system and the rotor was nested loop rotor with both one loop per nest and multiple loops per nest. But no details were presented for the case of multiple loops per nest. Therefore, Barati et al. generalised the BDFM dynamic vector model of rotor of multiple loops per nest in 2011 in [76]. The model was verified by comparison with the coupled circuit model and experiments as well.

Two years later, Cárdenas et al. presented a mathematical model of the cascaded DFIM based on small signal approach. The model was good for control purposes, but no details were provided. In the meantime, Roberts et al. developed a model-reduction technique which allows to only one $d-q$ pair of rotor to be derived instead of the conventional multiple $d-q$ pairs [77].

In 2016, Han et al. developed a spiral vector model of the dual-stator brushless doubly-fed machine (DSBDFM) [78]. The method of modelling is generalised to well apply to any alternating current machine with arbitrary winding layout. The new DSBDFM consists of three parts: an outer stator with three-phase power windings, an inner stator with three-phase control windings, and a special rotor. The rotor consists of a non-magnetic support with dual-layer iron cores with balanced three-phase windings on each layer. The spiral vector model can be directly used to derive the vector model from the winding layout and symmetry of the machine, rather than from the coupled-circuit model using space vector and $d-q$ transformation. Experimental validation has been provided for the steady-state, and demonstrates the developed modelling method under all possible operation modes.

Other models of the BDFM which appear in the literature including models based on the magnetic equivalent circuit [38] and models based on the finite element approach [34] are not usable for control purposes, thus, they are not much sited in

this dissertation.

Along the line of research, it has been shown that the BDFM is having complex behaviour and hence linearisation is sought.

3.2 Small Signal Model of the BDFM

The principle of the use of the BDFM in electricity generation by variable speed wind turbines is shown in Fig. 3.1. In this variable speed configuration, the control winding is fed by a bidirectional converter while the power winding is directly connected to the power grid.

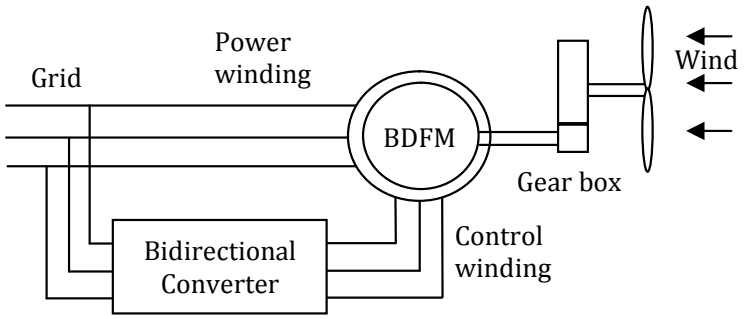

Fig. 3.1: Conceptual diagram of a BDFM-based wind turbine.

Based on the set of electromagnetic equations of the BDFM written in the natural reference frame $a-b-c$, the model of the BDFM aligned to the power winding flux and written in the $d-q$ reference frame is given by the following expressions:

$$\begin{bmatrix} v_{dp} \\ v_{qp} \end{bmatrix} = \begin{bmatrix} R_p & 0 \\ 0 & R_p \end{bmatrix} \begin{bmatrix} i_{dp} \\ i_{qp} \end{bmatrix} + \frac{d}{dt} \begin{bmatrix} \varphi_{dp} \\ \varphi_{qp} \end{bmatrix} + \begin{bmatrix} 0 & -\omega_p \\ \omega_p & 0 \end{bmatrix} \begin{bmatrix} \varphi_{dp} \\ \varphi_{qp} \end{bmatrix} \tag{3.1}$$

$$\begin{bmatrix} v_{dc} \\ v_{qc} \end{bmatrix} = \begin{bmatrix} R_c & 0 \\ 0 & R_c \end{bmatrix} \begin{bmatrix} i_{dc} \\ i_{qc} \end{bmatrix} + \frac{d}{dt} \begin{bmatrix} \varphi_{dc} \\ \varphi_{qc} \end{bmatrix} + \begin{bmatrix} 0 & -\alpha \\ \alpha & 0 \end{bmatrix} \begin{bmatrix} \varphi_{dc} \\ \varphi_{qc} \end{bmatrix} \tag{3.2}$$

$$\begin{bmatrix} v_{dr} \\ v_{qr} \end{bmatrix} = \begin{bmatrix} R_r & 0 \\ 0 & R_r \end{bmatrix} \begin{bmatrix} i_{dr} \\ i_{qr} \end{bmatrix} + \frac{d}{dt} \begin{bmatrix} \varphi_{dr} \\ \varphi_{qr} \end{bmatrix} + \begin{bmatrix} 0 & -\beta \\ \beta & 0 \end{bmatrix} \begin{bmatrix} \varphi_{dr} \\ \varphi_{qr} \end{bmatrix} \tag{3.3}$$

$$\begin{bmatrix} \varphi_{dp} \\ \varphi_{qp} \end{bmatrix} = \begin{bmatrix} L_p & 0 \\ 0 & L_p \end{bmatrix} \begin{bmatrix} i_{dp} \\ i_{qp} \end{bmatrix} + \begin{bmatrix} M_p & 0 \\ 0 & M_p \end{bmatrix} \begin{bmatrix} i_{dr} \\ i_{qr} \end{bmatrix} \tag{3.4}$$

$$\begin{bmatrix} \varphi_{dc} \\ \varphi_{qc} \end{bmatrix} = \begin{bmatrix} L_c & 0 \\ 0 & L_c \end{bmatrix} \begin{bmatrix} i_{dc} \\ i_{qc} \end{bmatrix} + \begin{bmatrix} M_c & 0 \\ 0 & M_c \end{bmatrix} \begin{bmatrix} i_{dr} \\ i_{qr} \end{bmatrix} \tag{3.5}$$

$$\begin{bmatrix} \varphi_{dr} \\ \varphi_{qr} \end{bmatrix} = \begin{bmatrix} L_r & 0 \\ 0 & L_r \end{bmatrix} \begin{bmatrix} i_{dr} \\ i_{qr} \end{bmatrix} + \begin{bmatrix} M_p & 0 \\ 0 & M_p \end{bmatrix} \begin{bmatrix} i_{dp} \\ i_{qp} \end{bmatrix} + \begin{bmatrix} M_c & 0 \\ 0 & M_c \end{bmatrix} \begin{bmatrix} i_{dc} \\ i_{qc} \end{bmatrix} \tag{3.6}$$

where

$$\alpha = \omega_p - (p_p + p_c)\,\omega_r \tag{3.7}$$

$$\beta = \omega_p - p_p \omega_r \tag{3.8}$$

where α represents the relative angular speed between the $d-q$ reference and the control winding reference in a p_c-type pole-pair distribution, and β represents the relative angular speed between the $d-q$ reference and the rotor reference in a p_p-type pole-pair distribution [74].

Now, substituting fluxes Eqs. (3.4), (3.5) and (3.6) into voltages Eqs. (3.1), (3.2) and (3.3), it results into:

$$\begin{bmatrix} v_{dp} \\ v_{qp} \end{bmatrix} = \begin{bmatrix} R_p + pL_p & -\omega_p L_p \\ \omega_p L_p & R_p + pL_p \end{bmatrix} \begin{bmatrix} i_{dp} \\ i_{qp} \end{bmatrix} + \begin{bmatrix} pM_p & -\omega_p M_p \\ \omega_p M_p & pM_p \end{bmatrix} \begin{bmatrix} i_{dr} \\ i_{qr} \end{bmatrix} \tag{3.9}$$

$$\begin{bmatrix} v_{dc} \\ v_{qc} \end{bmatrix} = \begin{bmatrix} R_c + pL_c & -\alpha L_c \\ \alpha L_c & R_c + pL_c \end{bmatrix} \begin{bmatrix} i_{dc} \\ i_{qc} \end{bmatrix} + \begin{bmatrix} pM_c & -\alpha M_c \\ \alpha M_c & pM_c \end{bmatrix} \begin{bmatrix} i_{dr} \\ i_{qr} \end{bmatrix} \tag{3.10}$$

$$\begin{bmatrix} v_{dr} \\ v_{qr} \end{bmatrix} = \begin{bmatrix} R_r + pL_r & -\beta L_r \\ \beta L_r & R_r + pL_r \end{bmatrix} \begin{bmatrix} i_{dr} \\ i_{qr} \end{bmatrix} + \begin{bmatrix} pM_p & -\beta M_p \\ \beta M_p & pM_p \end{bmatrix} \begin{bmatrix} i_{dp} \\ i_{qp} \end{bmatrix} + \begin{bmatrix} pM_c & -\beta M_c \\ \beta M_c & pM_c \end{bmatrix} \begin{bmatrix} i_{dc} \\ i_{qc} \end{bmatrix} \tag{3.11}$$

Seeing the non-linearity in the previous model, a small signal linearisation must be considered.

It is known that the derivative of a given function f at a point x_0 (we assume that f is defined in $\mathbb{R}$ and that the derivative of f exists at x_0) can be defined as a limit of difference quotients as follows:

$$f'(x_0) = \lim_{x \to x_0} \frac{f(x) - f(x_0)}{x - x_0} \tag{3.12}$$

By deleting the limit sign and x is near x_0, the relation between the left and right sides of the foregoing equation will be no more an equality but an approximation:

$$f'(x_0) \approx \frac{f(x) - f(x_0)}{x - x_0} \tag{3.13}$$

Solving for $f(x)$ from the previous approximation results in:

$$f(x) \approx f(x_0) + f'(x_0) \cdot (x - x_0) \tag{3.14}$$

This equation is the linearisation of f around the point x_0. In fact, Taylor series give the same approximation when higher order terms can be neglected.

By applying this linear approximation to the dynamic system $\dot{x} = f(x)$ yield:

$$\dot{x} = f(x) \approx f(x_0) + f'(x_0) \cdot (x - x_0) \tag{3.15}$$

where x_0 refers to the equilibrium point and it is also known as the critical point or stationary point.

The equilibrium solution is defined as:

$$\dot{x}_0 = f(x_0) \triangleq 0 \tag{3.16}$$

Rearranging Eq. (3.15) gives:

$$\dot{x} - \dot{x}_0 \approx f(x_0) + f'(x_0) \cdot (x - x_0) \tag{3.17}$$

Now supposing that the difference between x and x_0 is Δx, i.e. $x = x_0 + \Delta x$, so, Eq. (3.17) can be expressed as:

$$\Delta\dot{x} \approx f'(x_0) \cdot (\Delta x) \tag{3.18}$$

As can be seen from the last equation, the same signals turned to small signals and the non-linear dynamic model turned to a linear time-invariant model which is known as small signal model. For multivariable system, the component $f'(x_0)$ will be the Jacobian matrix and the component x contains the state vector and the input vector as well.

Now if we look at the set of Eqs. (3.9), (3.10) and (3.11) describing the BDFM non-linear model, we would observe that currents depend on constant electrical parameters. The only two variables which introduce non-linearity into the BDFM model are α and β, because they are related to the rotor angular speed as shown in Eqs. (3.7) and (3.8).

Commonly, the rotor angular speed is treated as a quasi-static value in the

phase of determination of the electrical variables dynamics. This assumption is typically valid since the mechanical dynamics is very slow compared to the electrical dynamics. However, it is possible that situations arise where the rotor speed has oscillations of small amplitude but relatively high frequency such as synchronism faults and mechanical vibrations. In this case the separation of mechanical and electrical dynamics will not be possible, and therefore, the dynamic system will remain non-linear. In this dissertation, such phenomena are not considered.

A simple solution exists in the literature to deal with this kind of non-linearities known as the 'small signal analysis' of the machine, that is to say considering changes of variables around a given operating point.

In case of wind energy conversion system working around an operating point, the angular speed of the rotor can be written as:

$$\omega_r = \omega_{r0} + \Delta\omega_r \tag{3.19}$$

As said before, mechanical variations can be neglected in front of electrical variations, thus, the following can be written:

$$\Delta\omega_r \approx 0 \tag{3.20}$$

The linearisation of the system of Eqs. (3.9), (3.10) and (3.11) around an operating point gives:

$$\begin{aligned}\begin{bmatrix} \Delta v_{dp} \\ \Delta v_{qp} \end{bmatrix} = &\begin{bmatrix} R_p + pL_p & -\omega_p L_p \\ \omega_p L_p & R_p + pL_p \end{bmatrix} \begin{bmatrix} \Delta i_{dp} \\ \Delta i_{qp} \end{bmatrix} \\ &+ \begin{bmatrix} pM_p & -\omega_p M_p \\ \omega_p M_p & pM_p \end{bmatrix} \begin{bmatrix} \Delta i_{dr} \\ \Delta i_{qr} \end{bmatrix}\end{aligned} \tag{3.21}$$

$$\begin{bmatrix} \Delta v_{dc} \\ \Delta v_{qc} \end{bmatrix} = \begin{bmatrix} R_c + pL_c & -\alpha L_c \\ \alpha L_c & R_c + pL_c \end{bmatrix} \begin{bmatrix} \Delta i_{dc} \\ \Delta i_{qc} \end{bmatrix} + \begin{bmatrix} pM_c & -\alpha M_c \\ \alpha M_c & pM_c \end{bmatrix} \begin{bmatrix} \Delta i_{dr} \\ \Delta i_{qr} \end{bmatrix} \tag{3.22}$$

$$\begin{bmatrix} \Delta v_{dr} \\ \Delta v_{qr} \end{bmatrix} = \begin{bmatrix} R_r + pL_r & -\beta L_r \\ \beta L_r & R_r + pL_r \end{bmatrix} \begin{bmatrix} \Delta i_{dr} \\ \Delta i_{qr} \end{bmatrix} + \begin{bmatrix} pM_p & -\beta M_p \\ \beta M_p & pM_p \end{bmatrix} \begin{bmatrix} \Delta i_{dp} \\ \Delta i_{qp} \end{bmatrix} + \begin{bmatrix} pM_c & -\beta M_c \\ \beta M_c & pM_c \end{bmatrix} \begin{bmatrix} \Delta i_{dc} \\ \Delta i_{qc} \end{bmatrix} \tag{3.23}$$

where

$$\alpha = \omega_p - (p_p + p_c)\,\omega_{r0} \tag{3.24}$$

$$\beta = \omega_p - p_p \omega_{r0} \tag{3.25}$$

In order to fulfil the linearisation in a correct way, we have treated Eqs. (3.9), (3.10) and (3.11) by considering the angular velocity ω_p of the rotating $d-q$ reference frame has a constant value independent of the rotor speed. In this study, the frequency of the grid is taken constant, 50 Hz. The Laplace transform of Eqs. (3.21), (3.22) and (3.23) is given as:

$$\begin{bmatrix} \Delta V_{dp} \\ \Delta V_{qp} \end{bmatrix} = [\boldsymbol{A}_p] \begin{bmatrix} \Delta I_{dp} \\ \Delta I_{qp} \end{bmatrix} + [\boldsymbol{B}_p] \begin{bmatrix} \Delta I_{dr} \\ \Delta I_{qr} \end{bmatrix} \tag{3.26}$$

$$\begin{bmatrix} \Delta V_{dc} \\ \Delta V_{qc} \end{bmatrix} = [\boldsymbol{A}_c] \begin{bmatrix} \Delta I_{dc} \\ \Delta I_{qc} \end{bmatrix} + [\boldsymbol{B}_c] \begin{bmatrix} \Delta I_{dr} \\ \Delta I_{qr} \end{bmatrix} \tag{3.27}$$

$$\begin{bmatrix} 0 \\ \\ 0 \end{bmatrix} = [\boldsymbol{A}_r] \begin{bmatrix} \Delta I_{dr} \\ \\ \Delta I_{qr} \end{bmatrix} + [\boldsymbol{A}_{rp}] \begin{bmatrix} \Delta I_{dp} \\ \\ \Delta I_{qp} \end{bmatrix} + [\boldsymbol{A}_{rc}] \begin{bmatrix} \Delta I_{dc} \\ \\ \Delta I_{qc} \end{bmatrix} \tag{3.28}$$

where

$$[\boldsymbol{A}_p] = \begin{bmatrix} R_p + sL_p & -\omega_p L_p \\ \\ \omega_p L_p & R_p + sL_p \end{bmatrix} \tag{3.29}$$

$$[\boldsymbol{B}_p] = \begin{bmatrix} sM_p & -\omega_p M_p \\ \\ \omega_p M_p & sM_p \end{bmatrix} \tag{3.30}$$

$$[\boldsymbol{A}_c] = \begin{bmatrix} R_c + sL_c & -\alpha L_c \\ \\ \alpha L_c & R_c + sL_c \end{bmatrix} \tag{3.31}$$

$$[\boldsymbol{B}_c] = \begin{bmatrix} sM_c & -\alpha M_c \\ \\ \alpha M_c & sM_c \end{bmatrix} \tag{3.32}$$

$$[\boldsymbol{A}_r] = \begin{bmatrix} R_r + sL_r & -\beta L_r \\ \\ \beta L_r & R_r + sL_r \end{bmatrix} \tag{3.33}$$

$$[\boldsymbol{A}_{rp}] = \begin{bmatrix} sM_p & -\beta M_p \\ \\ \beta M_p & sM_p \end{bmatrix} \tag{3.34}$$

$$[\boldsymbol{A}_{rc}] = \begin{bmatrix} sM_c & -\beta M_c \\ \\ \beta M_c & sM_c \end{bmatrix} \tag{3.35}$$

's' represents the Laplace variable. The rotor voltage of the BDFM is zero, as long as the BDFM's rotor is nested loop (squirrel cage), where cage voltage is zero

for all modes of operation.

Using Eq. (3.28), the variation of the control winding current can be expressed by:

$$\begin{bmatrix} \Delta I_{dc} \\ \Delta I_{qc} \end{bmatrix} = -[\boldsymbol{A}_{rc}]^{-1} \left([\boldsymbol{A}_r] \begin{bmatrix} \Delta I_{dr} \\ \Delta I_{qr} \end{bmatrix} + [\boldsymbol{A}_{rp}] \begin{bmatrix} \Delta I_{dp} \\ \Delta I_{qp} \end{bmatrix} \right) \tag{3.36}$$

By replacing Eq. (3.36) in Eq. (3.27), we may arrive to:

$$\begin{aligned} \begin{bmatrix} \Delta V_{dc} \\ \Delta V_{qc} \end{bmatrix} = & - [\boldsymbol{A}_c] [\boldsymbol{A}_{rc}]^{-1} [\boldsymbol{A}_{rp}] \begin{bmatrix} \Delta I_{dp} \\ \Delta I_{qp} \end{bmatrix} \\ & + \left([\boldsymbol{B}_c] - [\boldsymbol{A}_c] [\boldsymbol{A}_{rc}]^{-1} [\boldsymbol{A}_r] \right) \begin{bmatrix} \Delta I_{dr} \\ \Delta I_{qr} \end{bmatrix} \end{aligned} \tag{3.37}$$

Using Eq. (3.26), the variation of the rotor current can be written by:

$$\begin{bmatrix} \Delta I_{dr} \\ \Delta I_{qr} \end{bmatrix} = [\boldsymbol{B}_p]^{-1} \left(\begin{bmatrix} \Delta V_{dp} \\ \Delta V_{qp} \end{bmatrix} - [\boldsymbol{A}_p] \begin{bmatrix} \Delta I_{dp} \\ \Delta I_{qp} \end{bmatrix} \right) \tag{3.38}$$

Now the combination of Eqs. (3.37) and (3.38) allows writing the power winding current as a linear function of the control winding and power winding voltages as follows:

$$\begin{bmatrix} \Delta I_{dp} \\ \Delta I_{qp} \end{bmatrix} = [\boldsymbol{G}_c] \begin{bmatrix} \Delta V_{dc} \\ \Delta V_{qc} \end{bmatrix} + [\boldsymbol{G}_p] \begin{bmatrix} \Delta V_{dp} \\ \Delta V_{qp} \end{bmatrix} \tag{3.39}$$

where

$$[\boldsymbol{G}_c] = \left[[\boldsymbol{A}_c][\boldsymbol{A}_{rc}]^{-1} \left([\boldsymbol{A}_r][\boldsymbol{B}_p]^{-1}[\boldsymbol{A}_p] - [\boldsymbol{A}_{rp}] \right) - [\boldsymbol{B}_c][\boldsymbol{B}_p]^{-1}[\boldsymbol{A}_p] \right]^{-1} \tag{3.40}$$

$$[\boldsymbol{G}_p] = [\boldsymbol{G}_c] \left([\boldsymbol{A}_c][\boldsymbol{A}_{rc}]^{-1}[\boldsymbol{A}_r] - [\boldsymbol{B}_c] \right) [\boldsymbol{B}_p]^{-1} \tag{3.41}$$

$[\boldsymbol{G}_c]$ and $[\boldsymbol{G}_p]$ are transfer matrices which define the BDFM as a four-input-two-output multivariable linear system having the following structure:

$$\begin{bmatrix} \Delta I_{dp} \\ \Delta I_{qp} \end{bmatrix} = \begin{bmatrix} G_{c11}(s) & G_{c12}(s) & G_{p11}(s) & G_{p12}(s) \\ -G_{c12}(s) & G_{c11}(s) & -G_{p12}(s) & G_{p11}(s) \end{bmatrix} \cdot \begin{bmatrix} \Delta V_{dc} \\ \Delta V_{qc} \\ \Delta V_{dp} \\ \Delta V_{qp} \end{bmatrix} \tag{3.42}$$

where

$$[\boldsymbol{G}_c(s)] = \begin{bmatrix} G_{c11}(s) & G_{c12}(s) \\ -G_{c12}(s) & G_{c11}(s) \end{bmatrix} \tag{3.43}$$

$$[\boldsymbol{G}_p(s)] = \begin{bmatrix} G_{p11}(s) & G_{p12}(s) \\ -G_{p12}(s) & G_{p11}(s) \end{bmatrix} \tag{3.44}$$

Components $G_{c11}(s)$, $G_{c12}(s)$, $G_{p11}(s)$ and $G_{p12}(s)$ of the transfer matrices $[\boldsymbol{G}_c(s)]$ and $[\boldsymbol{G}_p(s)]$ depend on the nominal rotational speed of the rotor and the electrical parameters of the BDFM, and are given by:

$$G_{c11}(s) = \frac{b_{c1}(s)}{a(s)} \tag{3.45}$$

$$G_{c12}(s) = \frac{b_{c2}(s)}{a(s)} \tag{3.46}$$

$$G_{p11}(s) = \frac{b_{p1}(s)}{a(s)} \tag{3.47}$$

$$G_{p12}(s) = \frac{b_{p2}(s)}{a(s)} \tag{3.48}$$

where $a(s)$, $b_{c1}(s)$, $b_{c2}(s)$, $b_{p1}(s)$ and $b_{p2}(s)$ are polynomials of 's':

$$a(s) = a_6 s^6 + a_5 \cdot s^5 + a_4 \cdot s^4 + a_3 \cdot s^3 + a_2 \cdot s^2 + a_1 \cdot s + a_0 \tag{3.49}$$

$$b_{c1}(s) = b_{c15} \cdot s^5 + b_{c14} \cdot s^4 + b_{c13} \cdot s^3 + b_{c12} \cdot s^2 + b_{c11} \cdot s + b_{c10} \tag{3.50}$$

$$b_{c2}(s) = b_{c24} \cdot s^4 + b_{c23} \cdot s^3 + b_{c22} \cdot s^2 + b_{c21} \cdot s + b_{c20} \tag{3.51}$$

$$b_{p1}(s) = b_{p15} \cdot s^5 + b_{p14} \cdot s^4 + b_{p13} \cdot s^3 + b_{p12} \cdot s^2 + b_{p11} \cdot s + b_{p10} \tag{3.52}$$

$$b_{p2}(s) = b_{p24} \cdot s^4 + b_{p23} \cdot s^3 + b_{p22} \cdot s^2 + b_{p21} \cdot s + b_{p20} \tag{3.53}$$

Coefficients a_i, b_{x1j} and b_{x2k} where i go from 0 to 6, j go from 0 to 5, k go from 0 to 4, and x can be either c or p, are defined in the appendix as functions of the electrical parameters of the BDFM and the operating speed.

The functional diagram of the BDFM is illustrated in Fig 3.2.

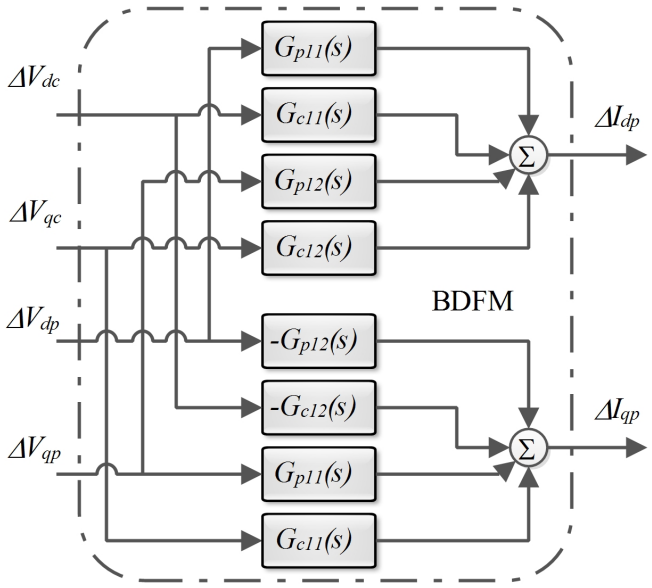

Fig. 3.2: Block diagram of the BDFM.

As can be seen, the BDFM model is multivariable four inputs and two outputs. The four inputs are the direct and quadrature components of the control and power winding voltages, and the two outputs are the direct and quadrature components of the power winding current. It is noteworthy to mention that the developed mathematical model of the BDFM is usable to well describe the dynamic of the

BDFM for wind power generation as well as for adjustable speed drive. For the latter case, i.e. adjustable speed drive, the primary winding of the BDFM (power winding) could be fed by converter providing variable voltage but, nevertheless, constant frequency.

3.3 Control Model of the BDFM

The small signal mathematical model of the BDFM given in the Eq. (3.42) defines a multivariable linear structure in the Laplace domain. However, because of the BDFM is considered as generator connected to the grid, the voltage comes in to the BDFM from the power winding side (the change in the power winding voltage) could be considered as a perturbation, and this could only happen under unbalanced grid voltage conditions. This model has been considered in the next chapter for stability analysis.

Assuming that the grid is balanced and has a constant voltage and constant frequency, changes in the power winding voltage can be neglected in the BDFM small signal model [79, 80]:

$$\begin{bmatrix} \Delta v_{dp} \\ \\ \Delta v_{qp} \end{bmatrix} \approx \begin{bmatrix} 0 \\ \\ 0 \end{bmatrix} \tag{3.54}$$

Thus, the small signal mathematical model of the BDFM represented in Eq. (3.42) can be expressed as:

$$\begin{bmatrix} \Delta I_{dp} \\ \\ \Delta I_{qp} \end{bmatrix} = \begin{bmatrix} G_{c11}(s) & G_{c12}(s) \\ \\ -G_{c12}(s) & G_{c11}(s) \end{bmatrix} \begin{bmatrix} \Delta V_{dc} \\ \\ \Delta V_{qc} \end{bmatrix} \tag{3.55}$$

The BDFM small signal mathematical model in (3.55) describes the behaviour of the BDFM in the vicinity of an operating point given by ω_{r0} and the derivative terms ΔV_{qc} and ΔV_{qc}, and allows the possibility of implementing all tools and

techniques made available by linear control theory for the design of convenient controller for the BDFM generator. For this reason, we call the model in Eq. (3.55), control model of the BDFM.

The functional diagram of the BDFM control model is illustrated by the following figure.

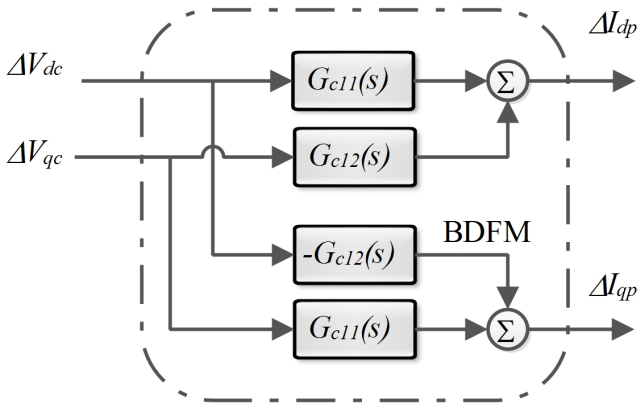

Fig. 3.3: Block diagram of the BDFM control model.

3.4 Simulation Results

Simulation of the model developed in the previous section was done by Matlab software. The electrical parameters used in the simulation are those of the prototype of [74]. All of which are given in the following Table:

Tab. 3.1: Electrical parameters of the BDFM

	Resistance (Ω)	Self inductance (H)	Mutual inductance (H)	Pole-pairs or Nests
Power winding	1.732	0.7148	0.2421	1
Control winding	1.079	0.1217	0.0598	3
Rotor	0.473	0.1326		4

To examine the performance of the BDFM in all possible operating points, we firstly started by calculating the static gains of the transfer matrix. These static gains represent the steady-state of the BDFM and can be easily calculated by:

$$gain_{c11} = \lim_{s\to 0} G_{c11}(s) = \lim_{s\to 0}\left(\frac{\sum_{i=0}^{5} b_{c1,i}\cdot s^i}{\sum_{i=0}^{6} a_i\cdot s^i}\right) = \frac{b_{c10}}{a_0} \tag{3.56}$$

$$gain_{c12} = \lim_{s\to 0} G_{c12}(s) = \lim_{s\to 0}\left(\frac{\sum_{i=0}^{4} b_{c2,i}\cdot s^i}{\sum_{i=0}^{6} a_i\cdot s^i}\right) = \frac{b_{c20}}{a_0} \tag{3.57}$$

By replacing the values of the electrical parameters of the BDFM prototype which are given in Table 3.1, it results into:

$$gain_{c11} = \frac{2668020 - 34522.8\omega_{r0} + 105.938\omega_{r0}^2 - 0.0734712\omega_{r0}^3}{6.21989 * 10^8 - 19628800\omega_{r0} + 204976\omega_{r0}^2 - 786.908\omega_{r0}^3 + \omega_{r0}^4} \tag{3.58}$$

$$gain_{c12} = \frac{1.51196 * 10^7 - 289537\omega_{r0} + 1383.61\omega_{r0}^2 - 1.95818\omega_{r0}^3}{6.21989 * 10^8 - 19628800\omega_{r0} + 204976\omega_{r0}^2 - 786.908\omega_{r0}^3 + \omega_{r0}^4} \tag{3.59}$$

The evolution of the static gains $gain_{c11}$ and $gain_{c12}$ depending on the rotational speed of the rotor is shown in Fig. 3.4.

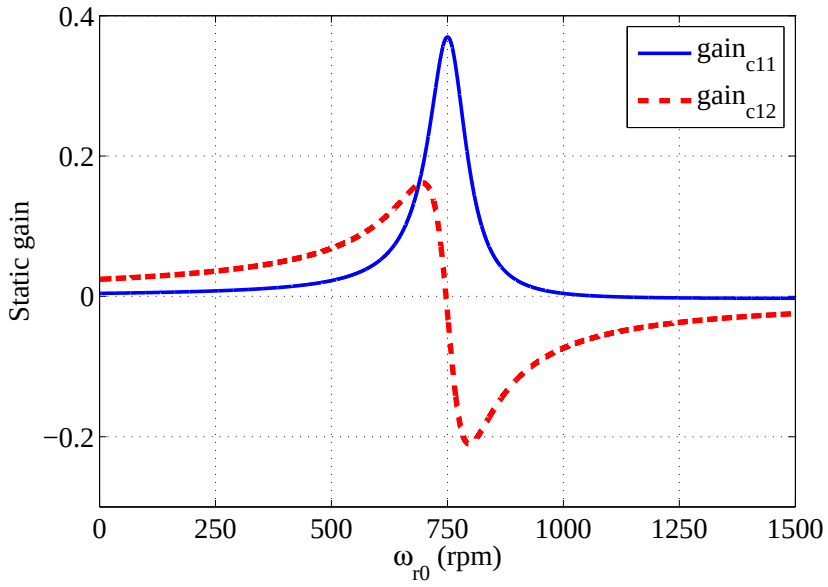

Fig. 3.4: Static gains of $\boldsymbol{G}_c(s)$ with respect to ω_{r0}.

$gain_{c11}$ and $gain_{c12}$ are both elements of $\boldsymbol{G}_c(0)$. In fact, $gain_{c11}$ is the gain between the direct components ΔV_{dp} and ΔI_{dp}, and between the quadrature components ΔV_{qp} and ΔI_{qp}, however, $gain_{c12}$ represents the coupling gain of $\boldsymbol{G}_c(0)$, i.e. influence of the direct component on the quadrature one, and vice versa.

As can be seen in Fig. 3.4, the static gain of the coupling action is close to zero around the synchronous speed, exactly at the speed 746.978 rpm which means that the coupling effect is weak around the synchronous speed.

Moreover, $gain_{c11}$ reaches its maximum value at 750.29 rpm with a gain of 0.37 which is very beneficial. However, $gain_{c11}$ falls down rapidly as much as the rotational speed of the rotor ω_{r0} is far from its synchronous value.

Figure 3.5 represents the direct and quadrature components of the power winding current with respect to the rotor speed. In this figure, we are supposing that both direct and quadrature components of the control winding voltage are 1 V.

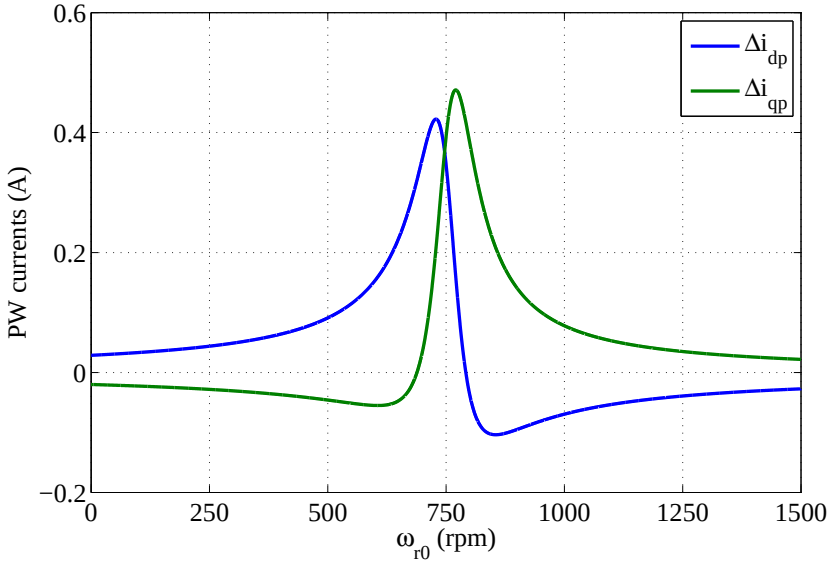

Fig. 3.5: Produced currents with respect to ω_{r0}.

As can be seen, the curves of Δi_{dp} and Δi_{qp} are quasi-axially symmetric at a speed near the synchronous one, 746.978 rpm, and having peaks around 750 rpm. Moreover, the range where both of current components are positive is extremely narrow starting from 688.56 rpm to 791.83 rpm, i.e. $[-8.192\%, 5.57733\%]$. This

means that the prototype is only effective in a narrow speed range which is actually less than 10%. Indeed, the prototype owner has noticed in several publications that this prototype is for validation of theoretical findings and not optimised.

Using Eq. (2.45), change in the produced power can be written by:

$$\Delta P_p = \frac{3}{2}\left(v_{dp0}\Delta i_{dp} + v_{qp0}\Delta i_{qp}\right) \tag{3.60}$$

Figure 3.6 represents the produced power by the BDFM where it is fed by 22 V on the control winding and the grid has a constant value of 220 V.

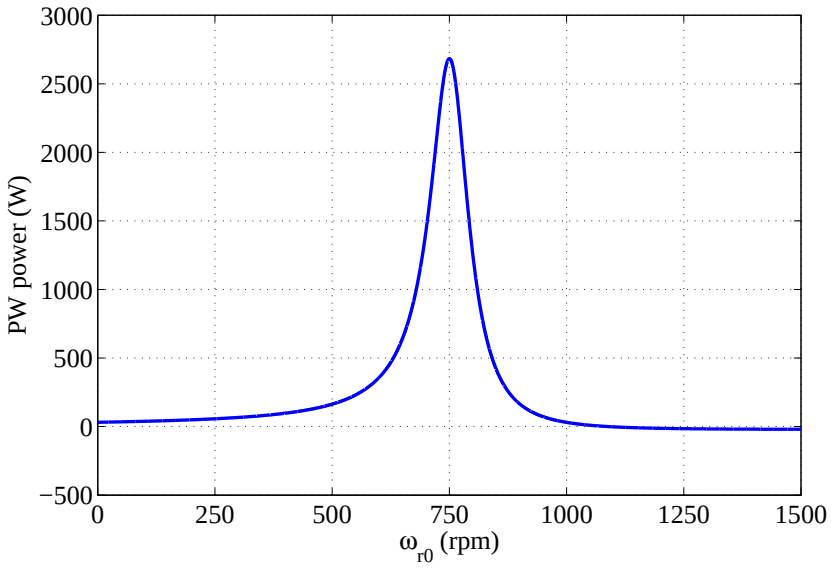

Fig. 3.6: Produced power with respect to ω_{r0}.

As shown in Fig. 3.6, the more the rotor speed is far from the synchronous speed, the more the produced power is of small magnitude. Moreover, the range of speed which is beneficial is narrow and less than 10% around the synchronous speed. This curve is similar to what we obtain using DFIM, but with less yield, this is why numerous studies are concerned with the optimisation of the BDFM design [81–86].

The step response of $\boldsymbol{G}(s)$ for different rotor speeds is mapped on Fig. 3.7.

In fact, the more the machine turns at a speed far from the synchronous speed,

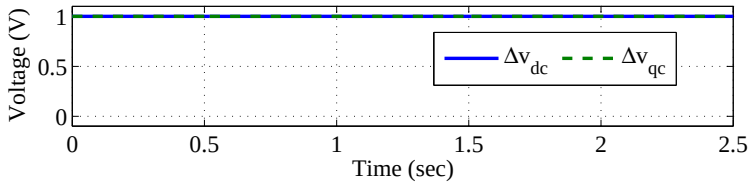

(a)

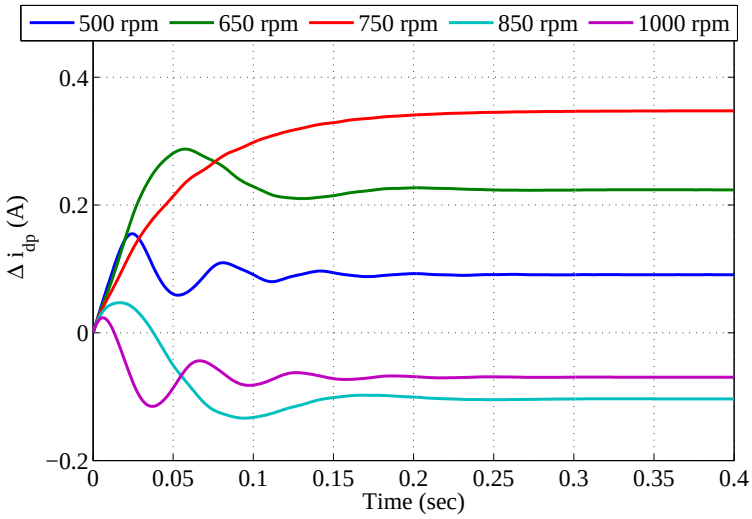

(b)

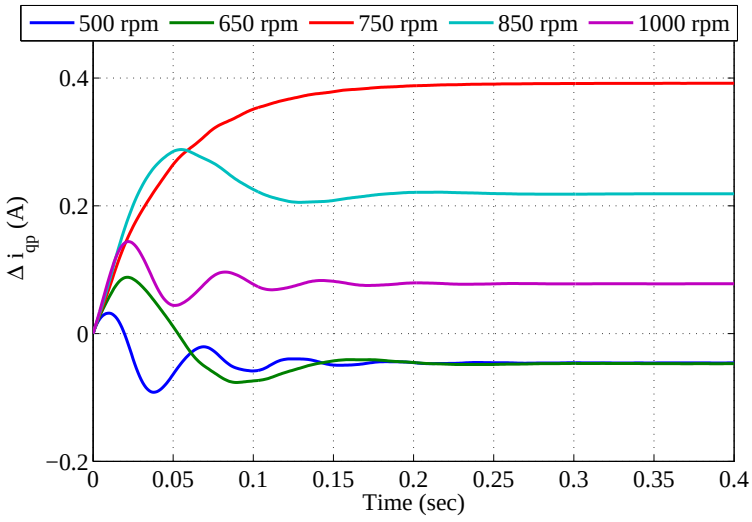

(c)

Fig. 3.7: Step response of the BDFM.

the more the amplitude of the produced current will be smaller. Moreover, we also note that the BDFM at the synchronous speed behaves like a synchronous machine

since the dynamic response of currents had the same shape as the step response of a first-order system.

Obviously, the previous figures (Fig. 3.7) do not reflect the coupling effect because the step of the input voltages start at the same time. In Fig. 3.8, the input voltages are considered shifted so that we reach several cases of overlap.

The coupling effect has become clear because even though the input Δv_{dc} (Δv_{qc}) keep the same value and the current Δi_{dc} (Δi_{qc}) reached its steady-state, a variation on Δv_{qc} (Δv_{dc}) causes a change in Δi_{dc} (Δi_{qc}) which is not preferred, therefore, control tasks of the BDFM will be difficult, and the use of a decoupling action will be considered.

3.5 Experimental Results

In order to validate the proposed model, a test bench consisting of a 2.2 kW BDFM driven by a direct current machine has been carried out in the Electrotechnical Laboratory of Constantine located at Mentouri University of Constantine as shown in Fig. 3.9. The power winding is connected to a local network and the control winding is supplied by an IGBT inverter operating at a switching frequency of 10 kHz. This inverter is controlled by a dSPACE 1104 in Pulse Width Modulation (PWM) mode. During our tests, the BDFM operates in open-loop.

Figures 3.10a and 3.10b show the measured power winding currents for a control winding voltage step when the rotor turns at 500 rpm and their filtering, respectively.

Figures 3.11a and 3.11b show the measured power winding currents for a control winding voltage step when the rotor turns at the synchronous speed and their filtering, respectively.

Figures 3.12a and 3.12b show the measured power winding currents for a control winding voltage step when the rotor turns at 1000 rpm and their filtering, respectively.

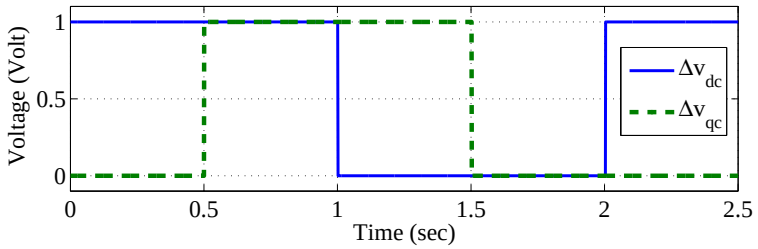

(a)

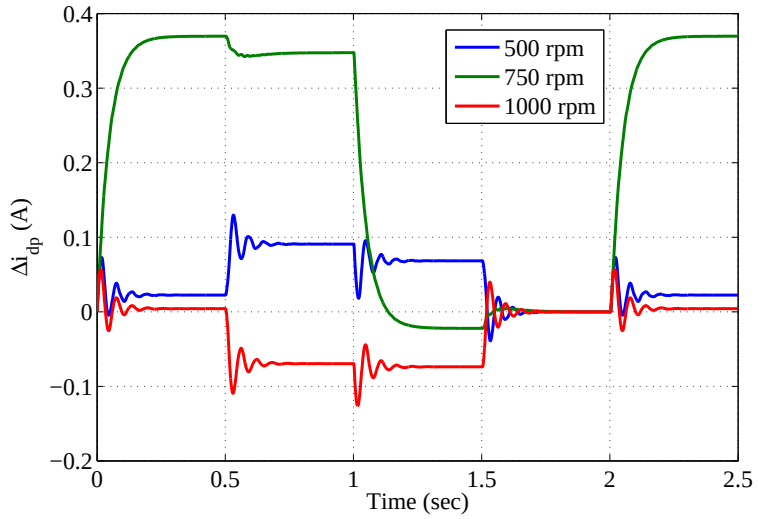

(b)

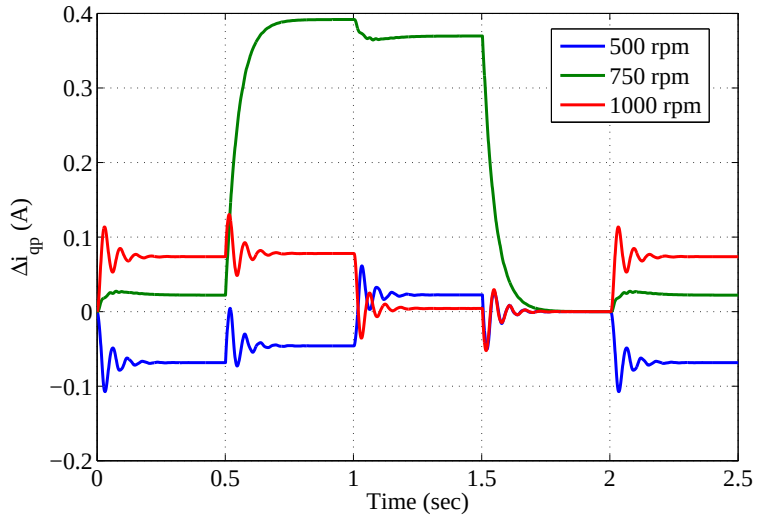

(c)

Fig. 3.8: Step response of the BDFM with shifted voltages.

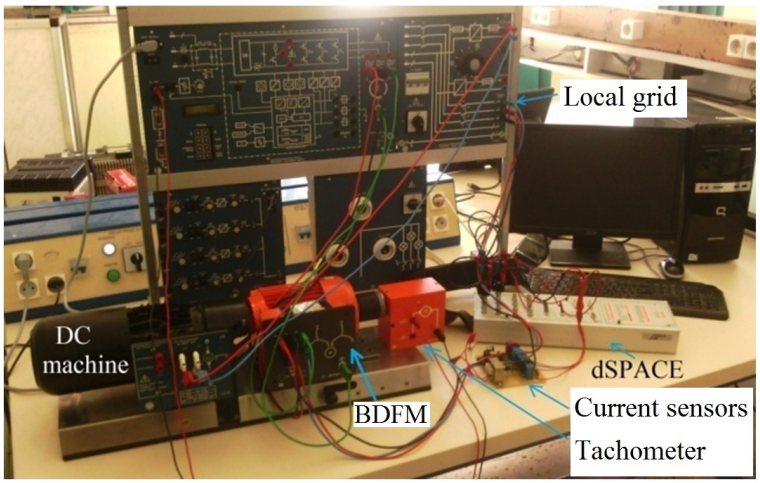

Fig. 3.9: Experimental test rig.

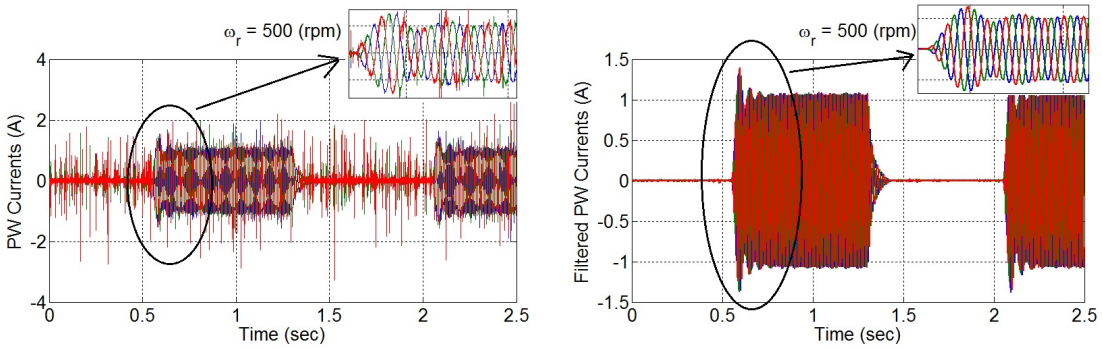

Fig. 3.10: Power winding currents when ω_{r0}=500 rpm.

At the right side in Figs. 3.10, 3.11 and 3.12 the currents are filtered by notch filters. The filters are chosen based on the knowledge of the output signals frequency which is 50 Hz.

Figure 3.13 represent the power winding current in the direct axis (Fig. 3.13a) and the quadrature axis (Fig. 3.13b). As we can conclude, these responses comply with those obtained by the proposed model. At the synchronous speed, the BDFM behave like a first-order system, and for other operating speeds other than the synchronous one, the BDFM behave like a second-order system or higher.

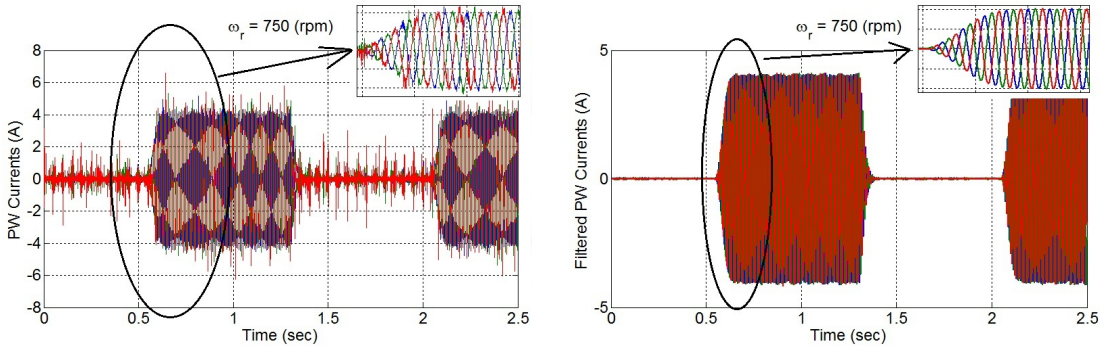

(a) (b)

Fig. 3.11: Power winding currents when ω_{r0}=750 rpm.

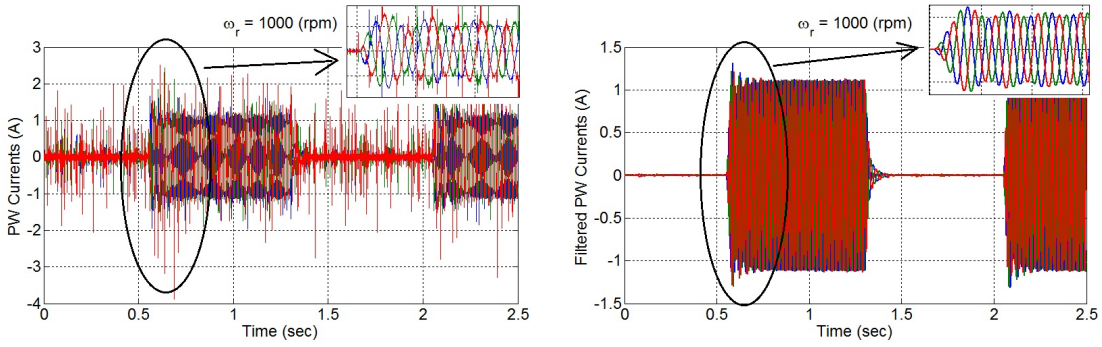

(a) (b)

Fig. 3.12: Power winding currents when ω_{r0}=1000 rpm.

3.6 Conclusions

In this chapter, we have proposed a new mathematical model $d-q$ complete for the BDFM. The BDFM is considered as a generator connected to the grid. The developed model is of multivariable structure connecting the outputs which are the currents of the power winding with the inputs which are the voltages of the control winding. The power generated by the BDFM is function of the nominal rotational speed of the rotor.

In order to validate the proposed model, some simulations and tests on laboratory prototypes were carried out. The obtained experimental and simulation results

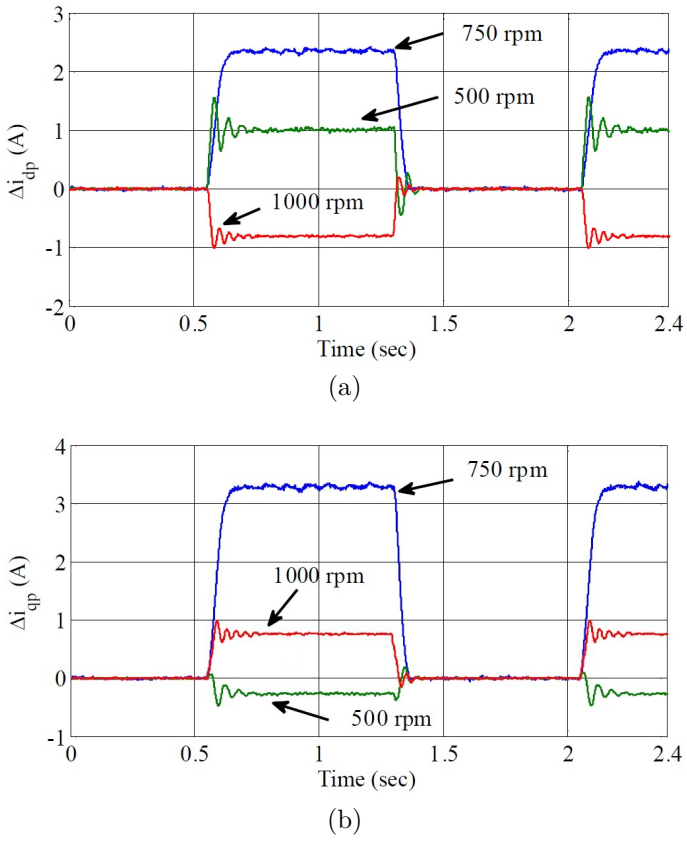

Fig. 3.13: Power winding currents in the reference $d-q$.

have shown that the dynamic and static behaviour of the BDFM depends on the rotational speed of the rotor. Thus, at 750 rpm, the machine acts as a simple first order system, while, at 500 and 1000 rpm, the machine acts as a higher order system, a sixth order. For this reason, the control strategies proposed in the literature cannot give good results. Based on the obtained results, we can conclude that:

- In closed-loop operation mode, when the rotor rotational speed is around 750 rpm, a simple PI controller is sufficient. But when the rotor rotational speed varies, a more sophisticated control structure will be needed;
- The proposed model allows the application and design of available linear control techniques, including robust control and optimal control;
- The BDFM must work on a range of speed of 10% or less around the syn-

chronous speed, outside this range the machine is less beneficial;

- The BDFM has a strong coupling between the quadrant axes, which will complicate its control tasks, and imposes the use of a decoupling action;
- The developed mathematical model is useful and usable during the design phase to optimise the BDFMs' efficiency.

Chapter 4

BDFM Stability Analysis

In Chapter 3 we have developed a new mathematical model of the BDFM, this model will be used in this Chapter to study the stability of the BDFM [59].

4.1 Definition and Basics of Stability

Consider a continuous finite-dimensional system described by a first-order non-linear vector differential equation:

$$\dot{\boldsymbol{x}} = f(\boldsymbol{x}) \qquad \boldsymbol{x} \in \mathbb{R}^n \tag{4.1}$$

Definition 4.1.1. (*Equilibrium point*) A vector $x_e \in \mathbb{R}^n$ is called an equilibrium point or equilibrium state if:

$$f(x_e) = 0 \tag{4.2}$$

Note any equilibrium point can be brought back to the origin by a simple change of variable $X \leftarrow x - x_e$. ß

Definition 4.1.2. (*Simple, asymptotic, marginal and global asymptotic stability*) The equilibrium point x_e of the system 4.1 is [52, 87]:

stable if, for all $\epsilon > 0$, there is $r = r(\epsilon)$, such as:

$$\|x(t=0)\| < r \implies \|x(t)\| < \epsilon \qquad \forall t > 0 \tag{4.3}$$

unstable, if not stable,
asymptotically stable, if stable and if r can be chosen such that:

$$\|x(t=0)\| < r \implies \lim_{t\to\infty} x(t) = 0 \tag{4.4}$$

marginally stable, if stable without being asymptotically stable:

$$\|x(t=0)\| < r \implies (\|x(t)\| < \epsilon) \wedge \left(\lim_{t\to\infty} x(t) \neq 0\right) \qquad \forall t > 0 \tag{4.5}$$

globally asymptotically stable, if asymptotically stable regardless of the initial state vector $x(t=0)$:

$$\|x(t=0)\| < \infty \implies \lim_{t\to\infty} x(t) = 0. \tag{4.6}$$

Practically, Lyapunov stability ensures that the trajectory will remain inside the loop $B(x_e, \epsilon)$ if the starting point belongs to a ball $B(x_e, r)$. Asymptotic stability includes this property, but further specifies that any initialised trajectory in the ball $B(x_e, r)$ converges to x_e.

Figures 4.1 and 4.2 represent the geometric interpretation of different stability definitions for a system of two state variables, x_1 and x_2.

In this chapter and by misuse of language, we speak about stability of the system instead of talking about stability of the equilibrium point.

If the system is linear:

$$\dot{x}(t) = A(t) \qquad x \in \mathbb{R}^n \tag{4.7}$$

then the system is globally asymptotically stable (the equilibrium point being at

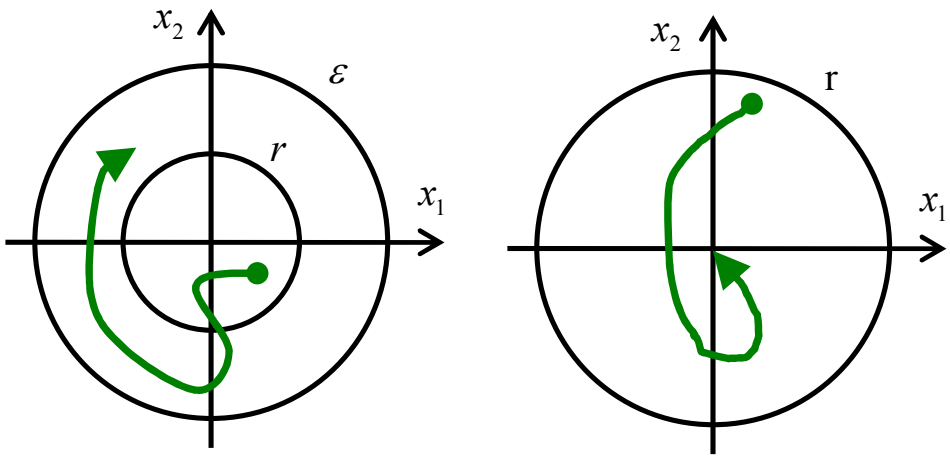

(a) Marginally stable (b) Asymptotically stable

Fig. 4.1: Geometric explanation of marginal and asymptotic stabilities.

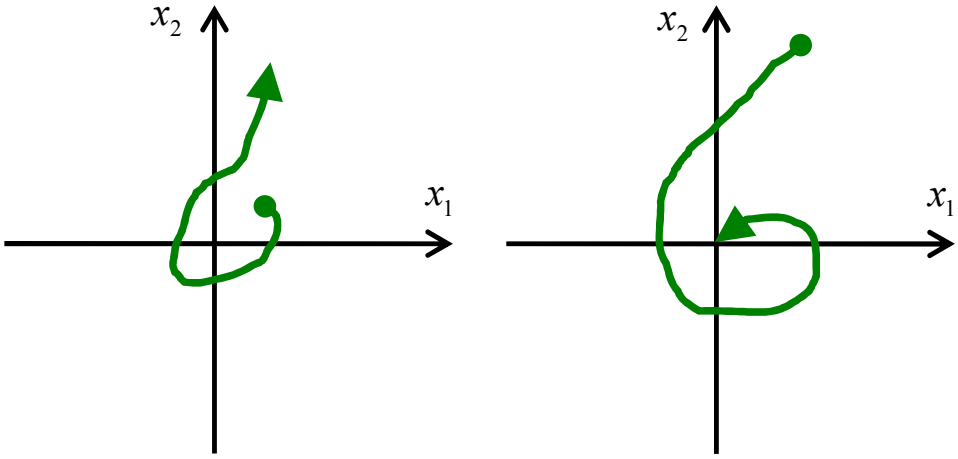

(a) Unstable (b) Globally asymptotically stable

Fig. 4.2: Geometric explanation of instability and global asymptotic stability.

the origin) if all the eigenvalues of A are strictly negative, that is:

$$Re\left(\lambda_i(A)\right) < 0 \qquad i = 1, ..., n \tag{4.8}$$

In fact, the eigenvalues of the state matrix A are the poles of the system transfer function. Therefore, the study in this chapter is based on the position of the

eigenvalues in the complex s-plane.

4.2 Review of the BDFM Stability Studies

In the published literature, the stability of the BDFM has been studied by many authors. In 1979, Cook and Smith studied the stability of the cascaded DFIM in synchronous operation using small signal analysis [88]. They concluded that the cascaded DFIM has certain regions of instability in open-loop operation. Four years later, the same authors used a linearised model of the cascaded DFIM to study the effect of parameters change on the stability of the cascaded DFIM. They demonstrated that the real part of the cascaded DFIM's dominating poles depends on the speed and the load [89].

In 1995, Li et al. analysed the stability characteristics of open-loop BDFM at equilibrium points based on Floquet's generalised theory [90]; They show by simulation results a possible instability when the frequency of the control winding is high, but their experimental results do not agree with those obtained by computer simulation.

In 2005, Poza et al. studied the open-loop stability of a small signal model of the BDFM in a unified reference frame [91], and showed that the stability zone depends on the parameters of the machine. One year later, Sarasola et al. studied the stability of the BDFM in closed-loop operation [92]. Their BDFM was operating under scalar current control, and their experiments showed a stable behaviour over the entire operating range.

It must be recognised that a contradiction arises between the arguments that the BDFM could reach a wide range of stable open-loop operation [90], and those the BDFM is conditionally stable in open-loop [88, 91]. From the view point of control theory, although the disagreement, however, the closed-loop control is always necessary to increase the stability margin and improve the dynamic performance. Therefore, many researchers have become focused on closed-loop control

schemes [79, 93, 94]. In these previous works, the absence of a clear mathematical model led to weak analysis of the BDFM stability in generation mode, where the analysis of the eigenvalues of the BDFM model cannot be carried out directly. In this chapter, a study of the stability of the open-loop BDFM is carried out with respect to the angular speed of the rotor on the one hand, and with respect to the electrical parameters on the other hand.

4.3 BDFM Stability Analysis with Respect to the Operating Point

The first step in the process of the stability analysis of the BDFM is the determination of the coefficients of the common denominator $a(s)$ of the transfer matrix $\mathbf{G}(s)$. The calculation's result of the polynomial $a(s)$ for a BDFM chosen according to the rotational speed of the rotor is given by:

$$\begin{aligned} a(s) = {} & 3.4067714 * 10^{-6} s^6 + 0.0003763 s^5 + s^4(0.0000579\omega_{r0}^2 \\ & - 0.0107027\omega_{r0} + 1.02172) + s^3(0.0039397\omega_{r0}^2 - 0.724582\omega_{r0} \\ & + 74.4223) + s^2(0.0000545\omega_{r0}^4 - 0.0428108\omega_{r0}^3 + 16.893\omega_{r0}^2 \\ & - 2130.75\omega_{r0} + 101607) + s(0.001285\omega_{r0}^4 - 1.00924\omega_{r0}^3 + 515.923\omega_{r0}^2 \\ & - 71585.9\omega_{r0} + 3.67863 \times 10^6) + 5.38733\omega_{r0}^4 - 4239.33\omega_{r0}^3 \\ & + 1.10427 \times 10^6 \omega_{r0}^2 - 1.05747 \times 10^8 \omega_{r0} + 3.35086 \times 10^9 \end{aligned} \tag{4.9}$$

Since the polynomial is of sixth order and some coefficients are a function of the rotor speed, so the position in the complex domain of the roots of $a(s)$ evolves accordingly and defines six different poles. Figure 4.3 shows the evolution of the real part of the poles for a rotor speed from 0 rpm up to 1500 rpm (1500 rpm represents the double of the synchronous speed), and Fig. 4.4 shows the evolution of the imaginary part of the poles for a rotor speed ranging from 0 rpm up to 1500 rpm

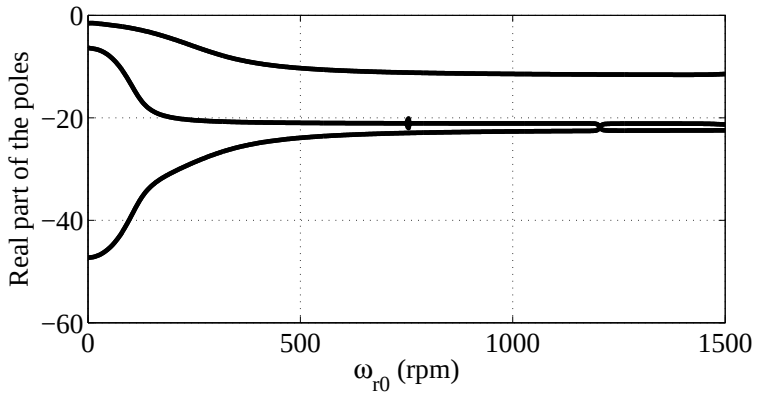

Fig. 4.3: Real part of the poles with respect to ω_{r0}.

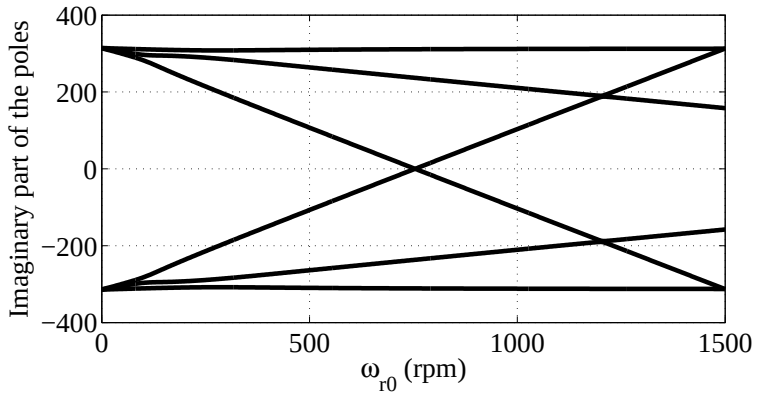

Fig. 4.4: Imaginary part of the poles with respect to ω_{r0}.

Indeed, for all possible values of the angular velocity of the rotor, the real part of the poles is strictly negative, which indicates that the BDFM is asymptotically stable in open-loop whatever the speed of operation ω_{r0}. In addition, the variation of the imaginary part of the poles indicates that the open-loop time response of the BDFM model varies with respect to the value of ω_{r0}.

4.4 BDFM Stability Analysis with Respect to Electric Parameters Change

In this section, other simulations have been conducted; this is to study the influence of electrical parameters change on the stability of the BDFM. Particular interest has

been given to the effect of variations in rotor resistance and self-inductance, as these parameters can undergo significant variations with rotor temperature increasing during machine operation. [95–97]. The variation of parameter, x can be expressed as:

$$x = x_0 + \Delta x \tag{4.10}$$

In the following we use the relative uncertainty which is defined in percent by:

$$\Delta x(\%) = \left(\frac{x}{x_0} - 1\right) 100\% \tag{4.11}$$

With the same manner, the eigenvalues variation can be mapped with respect to any parameter desired. Figures 4.5 and 4.6 mapped the real part of the BDFM poles in function of variations in R_r and L_r, respectively, when the BDFM turn at rated speed. Only $\pm$ 50% of variation in parameters is taken into account. As can be seen, the stability of the BDFM is not altered by any variations in R_r . However, if the stability is maintained for an increase of up to +50% in L_r , the machine becomes open-loop unstable for a decrease beyond -16% in the rotor self-inductance value.

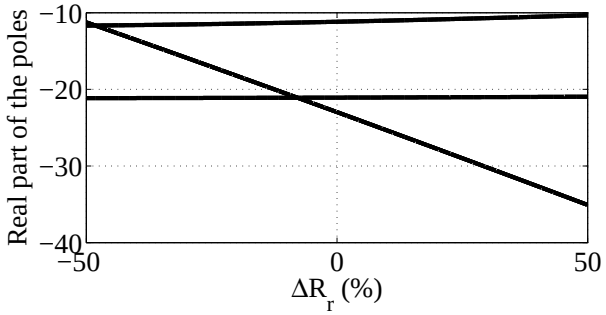

Fig. 4.5: Real part of the poles with respect to rotor resistance variations.

Figures 4.5 and 4.6 can be unified into one figure, Fig. 4.7, which represents the area of stability of the BDFM with respect to variations in both R_r and L_r. The plus mark, '+' indicates that the corresponding pair (R_r, L_r) has at least one pole with a positive real part, i.e. the BDFM is open-loop unstable. While the point mark, '·' indicates that all poles of the BDFM for the corresponding pair (R_r, L_r)

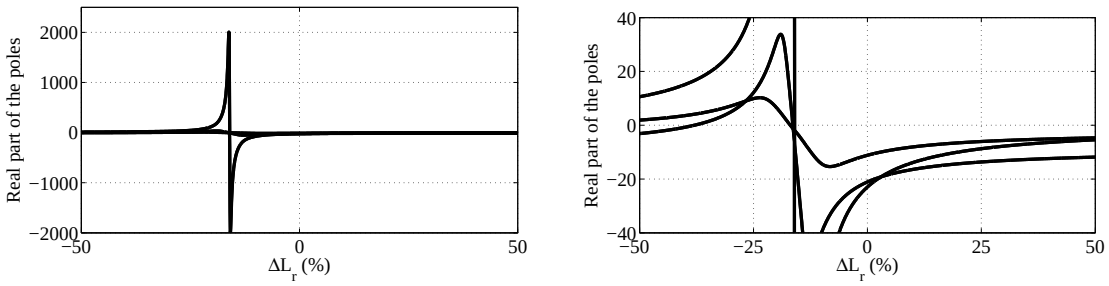

(a) (b) zoom of Fig. 4.6a

Fig. 4.6: Real part of the poles with respect to rotor inductance variations.

have a negative real part, i.e. the BDFM is open-loop stable.

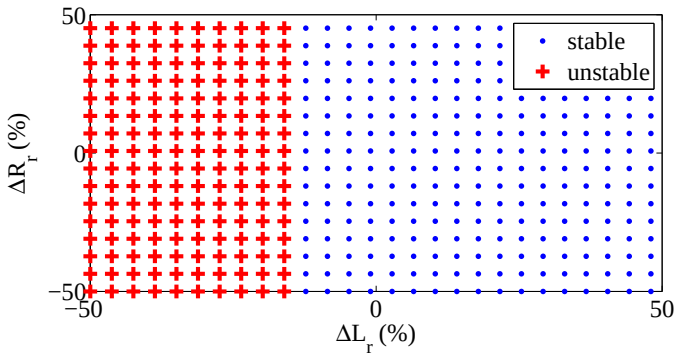

Fig. 4.7: Stability regions with respect to variations in the rotor self-inductance and resistance.

Figure 4.7 shows that the rotor resistance variations don't affect the stability of the BDFM. But variations in the rotor self-inductance can destabilise the BDFM. In order to make sure the BDFM stable, variations in L_r should not be under (-16%) of its nominal value. However, in fault conditions (rotor bars broken) the rotor electric parameters will decrease seriously, so the risk of being unstable will rise dramatically.

Figures 4.8 and 4.9 represent the area of stability for variations in resistance and self inductance of the stator power winding and stator control winding, respectively, when the rotor turns at the synchronous speed.

As can be seen, variations in R_p don't affect the stability of the BDFM, but a

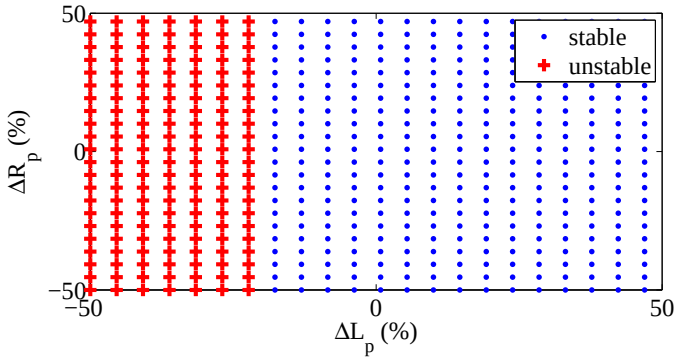

Fig. 4.8: Stability regions with respect to variations in the stator power winding self-inductance and resistance.

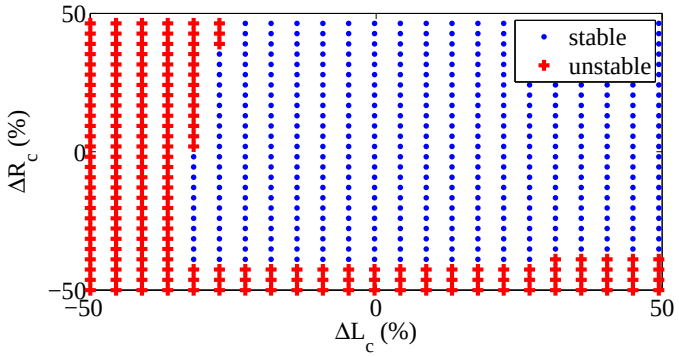

Fig. 4.9: Stability regions with respect to variations in the stator control winding self-inductance and resistance.

decrease in L_p by -20%, L_c by -30% or R_c by -40% from their nominal value can destabilise the BDFM. The decrease in stator electric parameters can be arrived not only due to temperature variation, but also due to fault conditions (short-circuit in electrical winding).

By knowing the position of the BDFM poles, the behaviour of any BDFM can be predicted on the one hand. On the other hand, this approach compared to other studies, gives the opportunity to the optimisation theory to take place, and contribute before the construction phase to get an optimal BDFM.

4.5 Conclusions

In this chapter, a stability analysis is achieved in open-loop operation of the BDFM. This study is done for wide operating rotor speed, and for stators and rotor electric parameters variation. The stability investigation of a selected benchmark BDFM is based on the calculation of the eigenvalues of the open-loop BDFM system. The obtained results indicate that the BDFM is stable over all speed range and, small variations in the electrical parameters do not affect its stability. However, it has also been shown that the BDFM can be unstable especially when one of the self-inductances decreases seriously. A serious diminution in electrical parameters can only happen in the case of short-circuit in the stator windings or, a break of some rotor bars.

Chapter 5

Control of the BDFM

5.1 History of the BDFM Control

In the mid of 90s, several papers have been published on the control aspects of the BDFM for both mode of operations generator and motor [25, 66, 90, 98–102]

In 1992, the first control algorithm for the BDFM was presented in a conference by Brassfield et al. where they proposed a direct torque control [103]. Later, they published their control strategy in [101].

In 1993, Zhou et al. improved the robustness of the direct torque controller by means of model reference adaptive control [104]. In 1996, Zhou et al. proposed rotor flux oriented control for the BDFM [99]. As an advantage they reduced the computational complexity, however, their algorithm needs more measurements compared to the field oriented control algorithm applied to conventional induction machines. In the same year, Zhou et al. proposed a simplified algorithm of control for the BDFM which is based on the field oriented control [100]. In 1997, Zhou et al. implemented a rotor flux oriented control for the BDFM over narrow speed and torque ranges [102].

Meanwhile Zhou's work, Spee et al. in 1995, implemented a maximum power point tracking control for the BDFM without the need of mechanical measurements

[98].

In 2000, Munoz et al. developed a vector model of the TSIM, and used it to perform two control structures, the scalar constant v/f and the vector control [105]. The stators had had dissimilar pole-pairs number, and both of them were feeding by an inverter.

In 2002, Shoudao et al. proposed a fuzzy logic control strategy for the BDFM using PID controller [106]. In the mean time, and using the $d-q$ model of the BDFM at that time, Poza et al. developed a vector control algorithm [107].

Later, a vector control for the BDFM is proposed by Poza in 2003 in [75] and by Poza et al. in 2009 in [94]. The BDFM model used was the same published in [74].

In the reference [75], the author proposed a cascade control structure of the BDFM. Moreover, he presented an analysis of the BDFM stability. These results have been validated by a prototype.

In 2008 and 2010, Shao et al. proposed a flux oriented control algorithm for the BDFM and showed good performance [51, 108].

In 2016, Chen et al. proposed an improved vector control for the BDFM under unbalanced grid conditions [109]. The vector control strategy was based on the proportional integral resonant controller (PI + R). The robustness of the proposed control scheme under parameters uncertainties and variations is discussed.

During the same year, Cheng et al. presented an improved voltage compensation method for DSBDFM-based standalone wind energy system to enhance the power winding voltage quality which mainly focuses on the suppression of the unbalanced fifth and seventh order harmonic voltages [110].

In 2017, Han et al. proposed a dual-electrical-port control scheme for cascaded DFIM fed by two inverters in all its four-quadrant operation [111]. The proposed control method is experimentally verified and demonstrates its effectiveness in reducing rotor slip frequency and related core losses.

In order to control the BDFM, we propose in this chapter the use of two different controllers with different structures: a PI controller; and a robust controller.

5.2 PI Control of the BDFM

As can be seen, the BDFM model is a Multiple-Input Multiple-Output (MIMO) system with high order transfer function matrix and highly coupled terms. Additionally, the model depends on the operating speed. To control this machine with simple PI controllers, we adopted the use of decoupling action.

5.2.1 Decoupling matrix calculation

To realise a perfect decoupling between the direct components and quadrature components, we propose the next decoupling matrix which has the following form [79, 80]:

$$H(s) = \begin{bmatrix} G_{c11}(s) & -G_{c12}(s) \\ G_{c12}(s) & G_{c11}(s) \end{bmatrix} = \begin{bmatrix} \dfrac{b_{c1}(s)}{a(s)} & -\dfrac{b_{c2}(s)}{a(s)} \\ \dfrac{b_{c2}(s)}{a(s)} & \dfrac{b_{c1}(s)}{a(s)} \end{bmatrix} \tag{5.1}$$

In this case, the set BDFM-Decoupling matrix is given by:

$$\begin{aligned} G_c(s) \cdot H(s) &= \begin{bmatrix} \dfrac{b_{c1}(s)}{a(s)} & \dfrac{b_{c2}(s)}{a(s)} \\ -\dfrac{b_{c2}(s)}{a(s)} & \dfrac{b_{c1}(s)}{a(s)} \end{bmatrix} \cdot \begin{bmatrix} \dfrac{b_{c1}(s)}{a(s)} & -\dfrac{b_{c2}(s)}{a(s)} \\ \dfrac{b_{c2}(s)}{a(s)} & \dfrac{b_{c1}(s)}{a(s)} \end{bmatrix} \\ &= \begin{bmatrix} \dfrac{b_{c1}^2(s) + b_{c2}^2(s)}{a^2(s)} & 0 \\ 0 & \dfrac{b_{c1}^2(s) + b_{c2}^2(s)}{a^2(s)} \end{bmatrix} \end{aligned} \tag{5.2}$$

The PI controller is much used in regulating electrical machines, and the PI coefficients calculation is available in different forms. However, the order of the obtained open-loop system is very high, twelfth order, consequently, we propose

order reduction of the set BDFM-Decoupling matrix at the synchronous speed [79].

5.2.2 Order reduction of the set BDFM-Decoupling action

Admittedly, complex systems so-called large-scale systems are difficult to manipulate either for studying their stability or for synthesising regulators which impose model order reduction and/or decomposition into subsystems [87, 112–118]. Even though the BDFM's model is linearised about an operating point, its linear model is of sixth order. Furthermore, the use of the decoupling transfer function increases the order of the set BDFM-Decoupling matrix into twelfth order. To reduce this set's order, we have used a frequency aggregation method which provides a reduced-order transfer function with a good approximation of the original one.

Consider a Single-Input Single-Output (SISO) linear time-invariant system having the following n-th-order transfer function:

$$G(s) = \frac{a_{2,n}s^{n-1} + \cdots + a_{23}s^2 + a_{22}s + a_{21}}{a_{1,n+1}s^n + \cdots + a_{13}s^2 + a_{12}s + a_{11}} \tag{5.3}$$

Using Maclaurin development, the transfer function $G(s)$ can be written as:

$$G(s) = \cfrac{1}{\gamma_1 + \cfrac{1}{\cfrac{\gamma_2}{s} + \cfrac{1}{\gamma_3 + \cfrac{1}{\cfrac{\gamma_4}{s} + \ddots \cfrac{1}{\cfrac{\gamma_{2n}}{s}}}}}} \tag{5.4}$$

The k-th-order transfer function approximant of $G(s)$ is given by the coming

relation:

$$G_k(s) = \cfrac{1}{\gamma_1 + \cfrac{1}{\cfrac{\gamma_2}{s} + \cfrac{1}{\gamma_3 + \cfrac{1}{\cfrac{\gamma_4}{s} + \ddots \cfrac{1}{\cfrac{\gamma_{2k}}{s}}}}}}} \tag{5.5}$$

where k is less than n, and coefficients γ_i are calculated according to the following Routh table.

Tab. 5.1: Routh table for model order reduction

	a_{11}	a_{12}	a_{13}	a_{14}	$\cdots$
	a_{21}	a_{22}	a_{23}	$\cdots$	
$\gamma_1 = \frac{a_{11}}{a_{21}}$	$a_{31} = a_{12} - \gamma_1 a_{22}$	$a_{32} = a_{13} - \gamma_1 a_{23}$	$a_{33} = a_{14} - \gamma_1 a_{24}$	$\cdots$	
$\gamma_2 = \frac{a_{21}}{a_{31}}$	$a_{41} = a_{22} - \gamma_2 a_{32}$	$a_{42} = a_{23} - \gamma_2 a_{33}$	$\cdots$		
$\gamma_3 = \frac{a_{31}}{a_{41}}$	$a_{51} = a_{32} - \gamma_3 a_{42}$	$a_{52} = a_{33} - \gamma_3 a_{43}$	$\cdots$		
$\gamma_4 = \frac{a_{41}}{a_{51}}$	$a_{61} = a_{42} - \gamma_4 a_{52}$	$\cdots$			
$\gamma_5 = \frac{a_{51}}{a_{61}}$	$a_{71} = a_{52} - \gamma_5 a_{62}$	$\cdots$			
$\gamma_6 = \frac{a_{61}}{a_{71}}$	$\cdots$				
$\vdots$					

The first and second rows of Table 5.1 contains coefficients of the original transfer function's denominator and numerator, respectively, whereas the remaining entries are computed using the following recursion:

$$a_{ij} = a_{i-2,j+1} - \gamma_{i-2} \cdot a_{i-1,j+1} \tag{5.6}$$

$$\gamma_l = \frac{a_{l,1}}{a_{l+1,1}} \tag{5.7}$$

where $3 \leq i \leq 2n+1, \quad 1 \leq j \leq n \quad \text{and} \quad 1 \leq l \leq 2n.$

The set of BDFM-Decoupling matrix is given by:

$$G(s) \cdot H(s) = \begin{bmatrix} sys(s) & 0 \\ 0 & sys(s) \end{bmatrix} \tag{5.8}$$

Writing $sys(s)$ of the BDFM prototype rotating at the synchronous speed gives:

$$\begin{aligned} sys(s) = &\Big(9.61319 \times 10^{12} + 9.17281 \times 10^{11}s + 2.30051 \times 10^{10}s^2 + 7.38402 \\ &\times 10^{7}s^3 + 1.25993 \times 10^{6}s^4 + 1951.16s^5 + 25.464s^6 + 0.020927s^7 \\ &+ 0.000222963s^8 + 7.88675 \times 10^{-8}s^9 + 7.1406 \times 10^{-10}s^{10}\Big) \\ &\div \Big(7.00659 \times 10^{13} + 1.33712 \times 10^{13}s + 9.69339 \times 10^{11}s^2 + 3.23222 \\ &\times 10^{10}s^3 + 4.67684 \times 10^{8}s^4 + 2.52188 \times 10^{6}s^5 + 23722.2s^6 \\ &+ 65.3655s^7 + 0.456208s^8 + 0.000690077s^9 + 3.8099 \times 10^{-6}s^{10} \\ &+ 2.56377 \times 10^{-9}s^{11} + 1.16061 \times 10^{-11}s^{12}\Big) \end{aligned} \tag{5.9}$$

By applying the aggregation to our system (BDFM-Decoupling matrix), the obtained reduced equivalent transfer function is:

$$sys_{reduced}(s) = \frac{61.1836 - 0.0604832s}{445.938 + 42.1101s + s^2} \tag{5.10}$$

Figure 5.1 shows the step responses of the original system and the reduced-order equivalent system while Fig. 5.2 presents their bode diagram.

It can be seen that the system and its approximant have identical step responses. Moreover, the frequency response demonstrates that a similarity is conducted in a wide frequency range. In conclusion, the original and reduced transfer functions have similar behaviours, thus, the reduced one can be used to calculate controllers

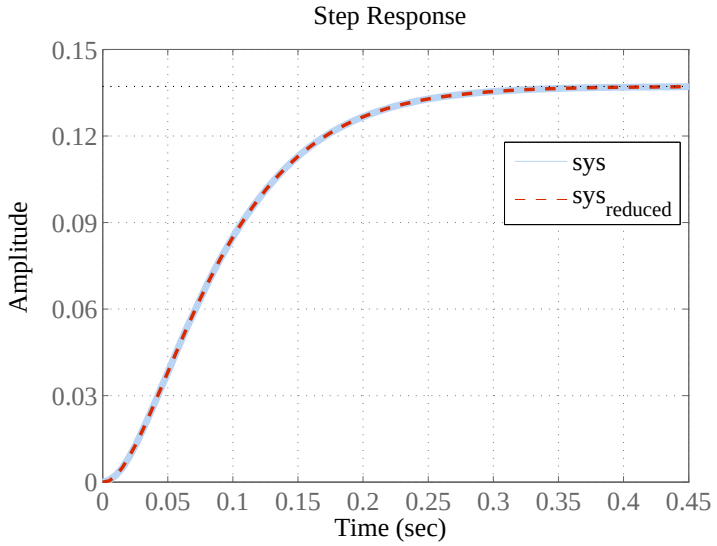

Fig. 5.1: Step response of $sys(s)$ and its reduced-order approximant.

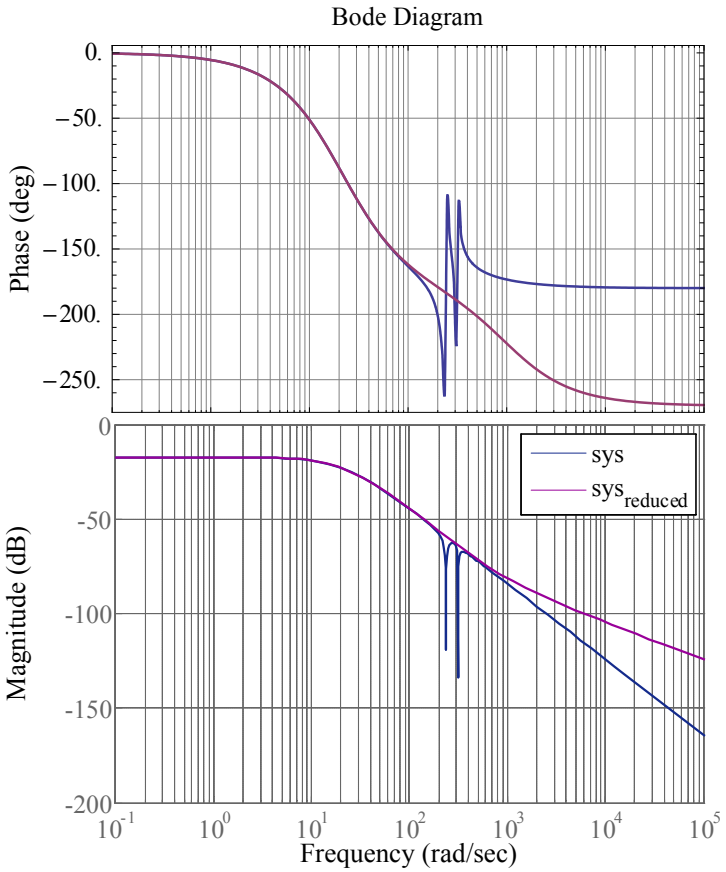

Fig. 5.2: Bode diagram of $sys(s)$ and its reduced-order approximant.

for the BDFM.

5.2.3 PI coefficients calculation: Naslin's method

The use of the decoupling matrix allows us to deal with the problem as being a SISO system rather than MIMO one. As mentioned earlier, the reduced-order system can be easily used to determine regulator coefficients based on available linear control techniques.

In most cases, PI coefficients are tuned based on experiences. In this dissertation, PI coefficients have been carefully calculated in an optimal way using Naslin polynomial technique [119–121].

Naslin's method is based on controlling the damping ratio of the step response of the controlled minimum phase system.

Let's consider that the closed-loop transfer function has the following denominator:

$$D(s) = a_0 + a_1 s + \cdots + a_n s^n \tag{5.11}$$

Using coefficients of the foregoing equation, characteristic pulsatances can be given as:

$$\omega_i = \frac{a_i}{a_{i+1}} \qquad i = 0, 1, 2, \cdots, (n-1) \tag{5.12}$$

Characteristic ratios between each two successive characteristic pulsatances are given by:

$$\alpha_i = \frac{\omega_i}{\omega_{i-1}} \qquad i = 0, 1, 2, \cdots, (n-1) \tag{5.13}$$

Writing the characteristic ratios as function of characteristic polynomial coefficients yields:

$$\alpha_i = \frac{a_i}{a_{i-1} \cdot a_{i+1}} \qquad i = 0, 1, 2, \cdots, (n-1) \tag{5.14}$$

Naslin advocated that these characteristic ratios must all be equal to a given coefficient who determines the overshoot of the step response of the controlled

system:

$$\alpha_1 = \alpha_2 = \cdots = \alpha_{n-1} = \alpha \tag{5.15}$$

Moreover, Naslin establishes experimentally that this coefficient must be two in order to obtain optimal damped response. Furthermore, for closed loop without much oscillations, α must be within the interval $1.8 \leq \alpha \leq 2.4$. In fact, for a second order system having the damping ratio ξ, the approximation of Naslin is exact, i.e. for a coefficient ratio $\alpha = 2$, the damping ratio will be $\xi = \frac{\sqrt{2}}{2}$.

Therefore, we need to find the PI coefficients which maintain the characteristic ratios of the closed-loop transfer function within the desired range. Without loss of generality, because the reduced order model described in Eq. (5.10) contains zero in the right-half plane, and the coefficient introducing this zero is of small value compared to the rest of the numerator coefficients (the zero can only influence in high frequencies), Naslin polynomial technique has been applied on Eq. (5.10) giving satisfactory results.

The PI regulator used is of parallel form:

$$PI(s) = K_p + \frac{K_i}{s} \tag{5.16}$$

where $K_p = 7.057$ and $K_i = 147.97$.

The control scheme of the produced currents by the BDFM is illustrated in Fig. 5.3.

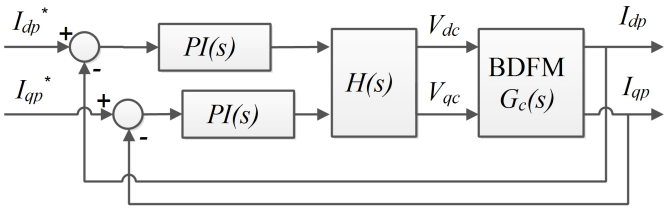

Fig. 5.3: Control diagram of the power winding currents using PI controller.

5.2.4 Results and discussion

In order to validate the proposed current control loop of the BDFM operating in generation mode for wind energy applications, a simulation is carried out using Matlab/Simulink environment.

As the proposed PI controller coefficients are calculated for the synchronous speed, and the BDFM effective speed range is less than 10% around the synchronous speed (750 rpm), thus, two operating points have been chosen outside this effective range of speed to evaluate the effectiveness of the proposed PI controller.

Results obtained for three different operating speeds, 650 rpm, 750 rpm and 850 rpm are presented in Fig 5.4.

It can be noticed that at synchronous speed, the response of the control system under the proposed PI control strategy is satisfactory; the steady-state errors have been eliminated and, both rise and settling times have been kept within small values which are comparable to those of the BDFM in open loop. For operating speeds other than the synchronous speed, the controller performances degrade with slower responses because the PI controller coefficients have been calculated in an optimal way $\left(\xi \approx \frac{\sqrt{2}}{2}\right)$, and any change in the BDFM dynamic may lead to weaker performances. Additionally, the voltage component v_{dc} is only effective on the current component i_{dp}, and has no significant effect on the current component i_{qp}, and the voltage component v_{qc} has no major influence on the current component i_{dp} but only effective on the current component i_{qp}, that is to say, the coupling effect is eliminated.

Table 5.2 summarises dynamic performances of the PI controller in digital form.

This table contains numerical values of the settling time, overshoot and steady-state error for different operating speeds. Results show that at the synchronous speed the settling time is a little bit bigger than its original settling time (two times or thereabouts). But at the operating speeds 650 rpm and 850 rpm the

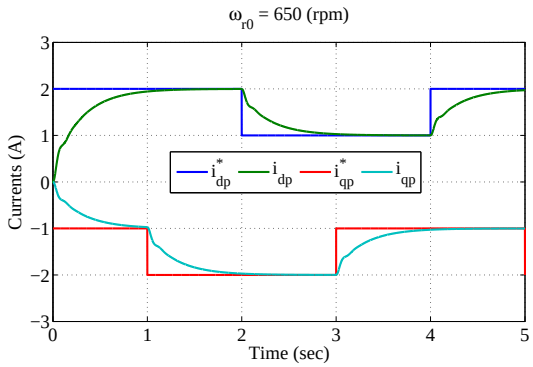

(a)

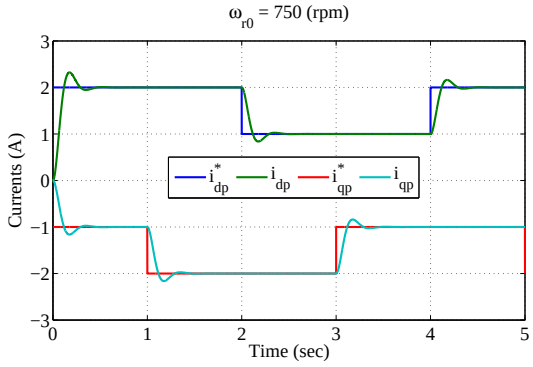

(b)

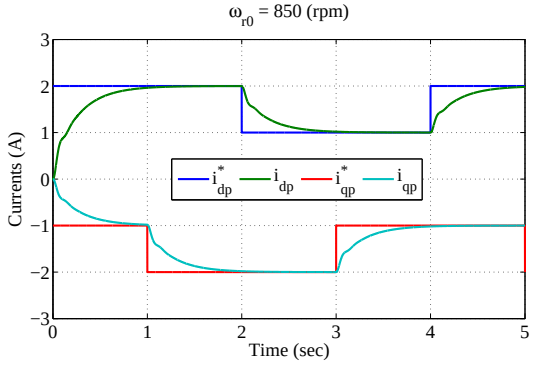

(c)

Fig. 5.4: Step response of the closed-loop for different operating points.

settling time is much bigger, thus, a robust controller is necessary.

Tab. 5.2: Dynamic performances of the PI controller

	Settling time (sec)	Overshoot %	Steady-state error (A)
650 (rpm)	0.83	Overdamped	0
750 (rpm)	0.25	16.2	0
850 (rpm)	0.75	Overdamped	0

5.3 Robust Control of the BDFM

Previously, the PI controller gives good performances in closed-loop only at the synchronous speed. However, the obtained results come from simulation, but in real application, more precautions should be taken into account. Actually, most of BDFM model parameters are not directly accessible and the identification task does not give good approximation. Besides that, simplifying hypotheses as well as linearisation lead to modelling errors. Thus, we propose in this section the use of robust controller [80].

5.3.1 H_∞ control theory

The robust control is a set of tools which allow [122]:

- Properties analysis of a closed-loop with a system to be regulated including uncertainties;
- The synthesis of a non-adaptive regulator (i.e. with fixed coefficients) for a family of systems to be controlled with uncertainties (parametric and non-parametric) such that a certain level of closed-loop performance is preserved for the whole family of systems.

Robust control can address the following problems which conventional controllers cannot perform:

- It works on paper and in simulation, but not in practice;

- The prototype and the preproduction of a product having a regulator work well, but the series show a high percentage of failures related to problems of stability or degradation of performance of the closed-loop.

The interaction between inputs and outputs leads to a number of characteristic transfer matrices. We note particularly:
the sensitivity function:

$$\boldsymbol{S}(s) = (I + \boldsymbol{G}(s) \cdot \boldsymbol{C}(s))^{-1} \tag{5.17}$$

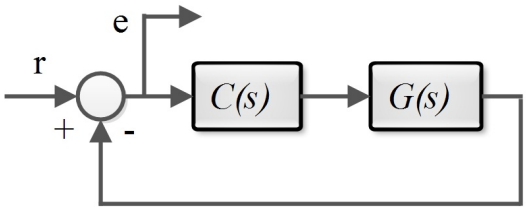

Fig. 5.5: Schematic block diagram of the sensitivity.

which represents perturbations influence on the measured outputs;
the complementary sensitivity function:

$$\boldsymbol{T}(s) = (I + \boldsymbol{G}(s) \cdot \boldsymbol{C}(s))^{-1} \cdot \boldsymbol{G}(s) \cdot \boldsymbol{C}(s) \tag{5.18}$$

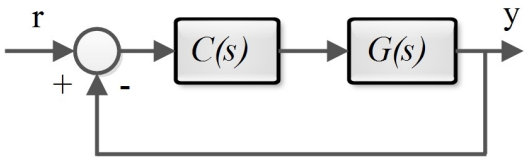

Fig. 5.6: Schematic block diagram of the complementary sensitivity.

which represents the influence of the noise on the measured outputs;
the function:

$$\boldsymbol{R}(s) = (I + \boldsymbol{C}(s) \cdot \boldsymbol{G}(s))^{-1} \cdot \boldsymbol{C}(s) \tag{5.19}$$

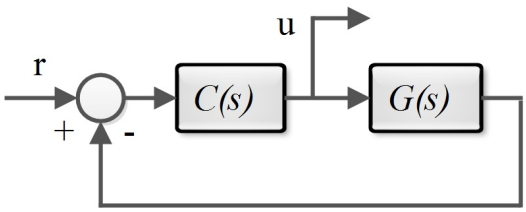

Fig. 5.7: Schematic block diagram of the control signal output.

which represents the impact of the perturbation on the control signals;
and the open-loop:

$$\boldsymbol{L}(s) = \boldsymbol{G}(s) \cdot \boldsymbol{C}(s) \tag{5.20}$$

Figure 5.8 presents typical curves of the open-loop, sensitivity and complementary sensitivity.

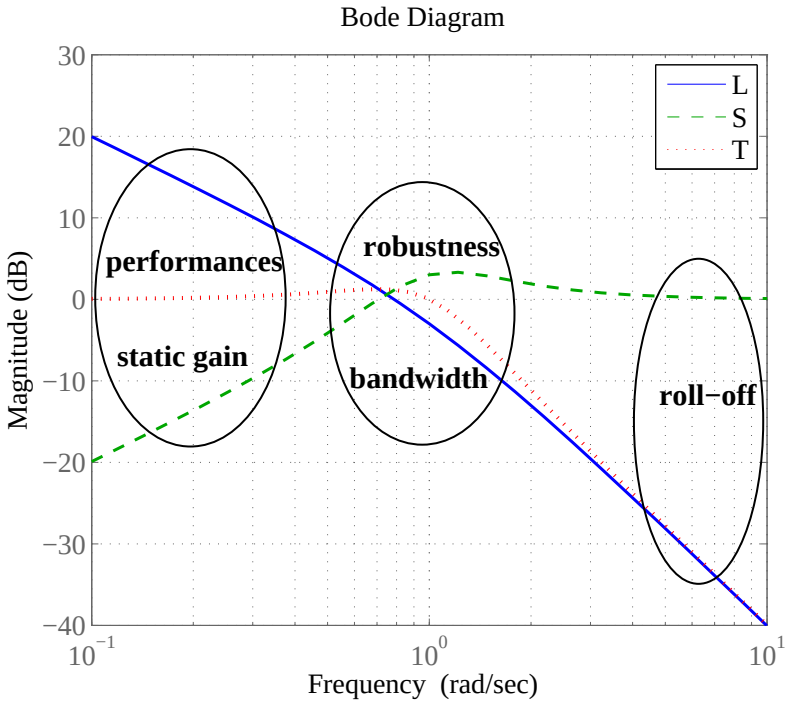

Fig. 5.8: Bode magnitude of a typically controlled system.

Generally, the regulator can compensate poles and/or zeros from the open-loop, the sensitivity or the complementary sensitivity. These poles and/or zeros disappear

from L(s), S(s) and T(s), but reappear in the following two transfer functions:

$$(I + \boldsymbol{C} \cdot \boldsymbol{G})^{-1} \cdot \boldsymbol{C}$$

$$(I + \boldsymbol{G} \cdot \boldsymbol{C})^{-1} \cdot \boldsymbol{G}$$

Consequently, automation engineers divided the complex s-plane into 3 sub-areas as shown in Fig. 5.9.

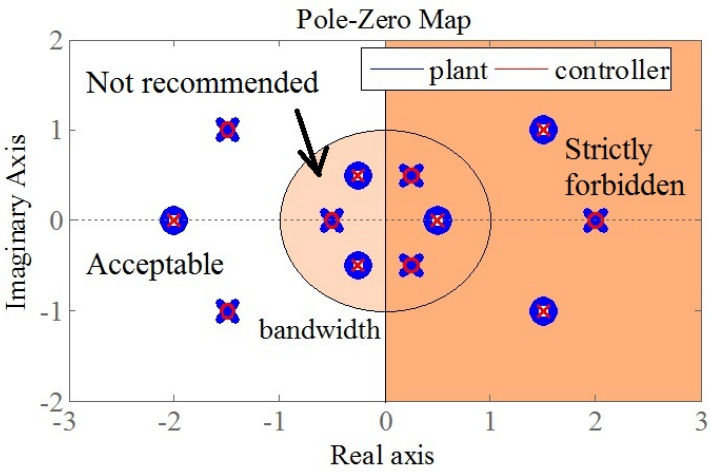

Fig. 5.9: Acceptability of compensation of poles and/or zeros.

As illustrated in the figure, it is not recommended to compensate poles and zeros in the shaded left half disk; meanwhile the darkly shaded right half-plane indicates that the compensation is prohibited.

In fact, for a given nominal plant and controller, it is possible to know if the closed-loop is stable or not. Indeed, the graphical technique of Nyquist is very useful which state that the closed-loop is stable if Nyquist locus of the open-loop keep the critical point $(-1 + \jmath \cdot 0)$ at its left side. Figure 5.10 shows the Nyquist plot of an open-loop system with uncertainty.

As can be seen, the Nyquist locus of the open-loop indicates that the closed-loop will be stable. Besides of that, the presence of uncertainty may cause the real system to be unstable in closed-loop, hence, it is preferred to have comfortable

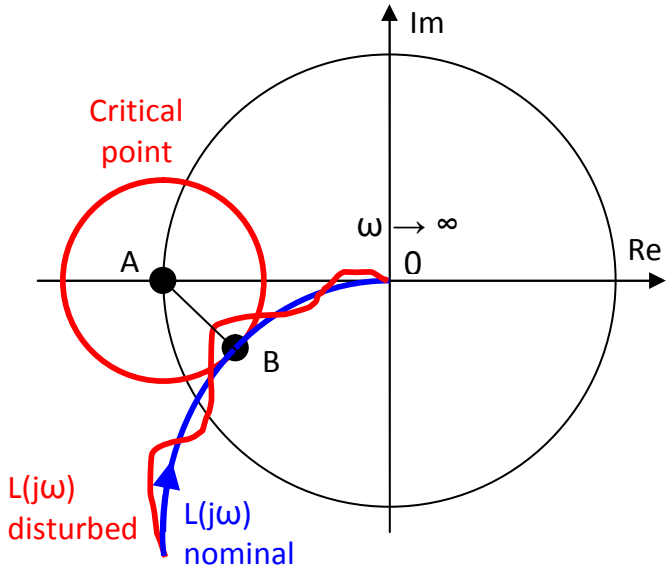

Fig. 5.10: Nyquist diagram of a given open-loop with uncertainty.

stability margins. Figure 5.11 shows Nyquist plot of a system have good phase and gain margin.

As shown in Fig. 5.11, the open-loop has good phase and gain margins. But, nevertheless, the robustness from the angle of stability is very weak since the minimum distance (critical distance) between the Nyquist plot and the critical point is very small. Accordingly, comfortable critic distance implies good gain and phase margin, but the opposite is not true.

Gain margin and phase margin are related to the critical distance by the following inequalities:

$$A_m > \frac{1}{1 - d_{crit}} \tag{5.21}$$

$$\phi_m > 2\arcsin(\frac{d_{crit}}{2}) \tag{5.22}$$

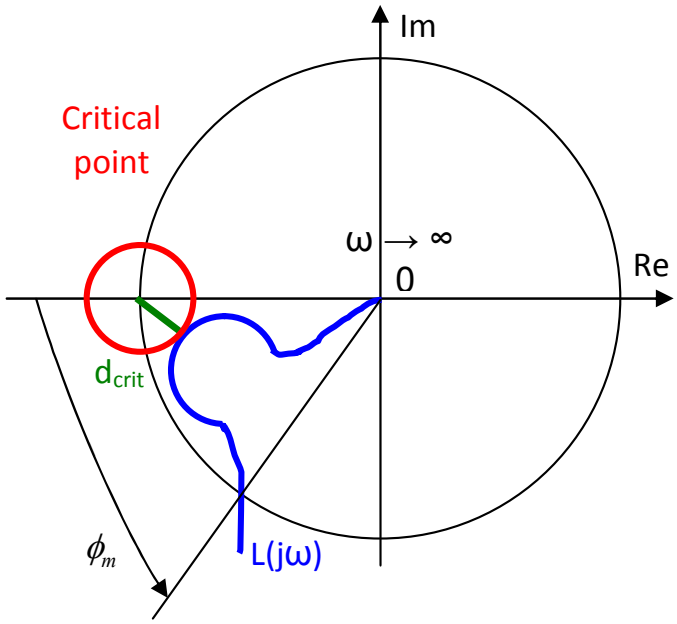

Fig. 5.11: Nyquist diagram of a system having small critical distance.

where:

$$\begin{aligned} d_{crit} &= \min_{\omega} \left(dist \left(L(j\omega), s_{crit} \right) \right) \\ &= \min_{\omega} |L(j\omega) - s_{crit}| \\ &= \min_{\omega} |L(j\omega) + 1| \\ &= \frac{1}{\max_{\omega} |\frac{1}{L(j\omega)+1}|} \\ &= \frac{1}{\|S\|_{\infty}} \end{aligned} \tag{5.23}$$

The H_{∞}-norm of a system proper and asymptotically stable is defined as:

$$\|G\|_{\infty} \triangleq \max_{\omega \in \mathbb{R}_0^+} |G(j\omega)| \tag{5.24}$$

In time-domain, the H_{∞}-norm can be expressed as:

$$\|G\|_{\infty} = \max_{u} \frac{\|y\|_2}{\|u\|_2} \tag{5.25}$$

In multivariable case, the H_∞-norm is defined as:

$$\|G\|_\infty \triangleq \max_{\omega \in \mathbb{R}_0^+} \bar{\sigma}\left(\boldsymbol{G}(j\omega)\right) \tag{5.26}$$

where $\bar{\sigma}$ is the maximal amplification, i.e. the biggest singular value.

The singular values decomposition of a given matrix G is defined as:

$$G = U \cdot S \cdot V^T \tag{5.27}$$

where columns of U are the left-singular vectors, S is diagonal (rectangular) matrix and its entries are positives and known as singular values and, columns of V are the right-singular vectors.

Figure 5.12 illustrates visualisation of the singular values decomposition of a given matrix 2×2. For numerical application the matrix chosen is the BDFM prototype in steady-state rotating at 750 rpm which is given by the following matrix:

$$G = \begin{bmatrix} 0.369745 & -0.0221483 \\ 0.0221483 & 0.369745 \end{bmatrix} \tag{5.28}$$

In this case, U, S and V are given by:

$$\begin{aligned} U &= \begin{bmatrix} -0.998211 & -0.059794 \\ -0.059794 & 0.998211 \end{bmatrix} \\ S &= \begin{bmatrix} 0.370408 & 0 \\ 0 & 0.370408 \end{bmatrix} \\ V &= \begin{bmatrix} -1 & 0 \\ 0 & 1 \end{bmatrix} \end{aligned} \tag{5.29}$$

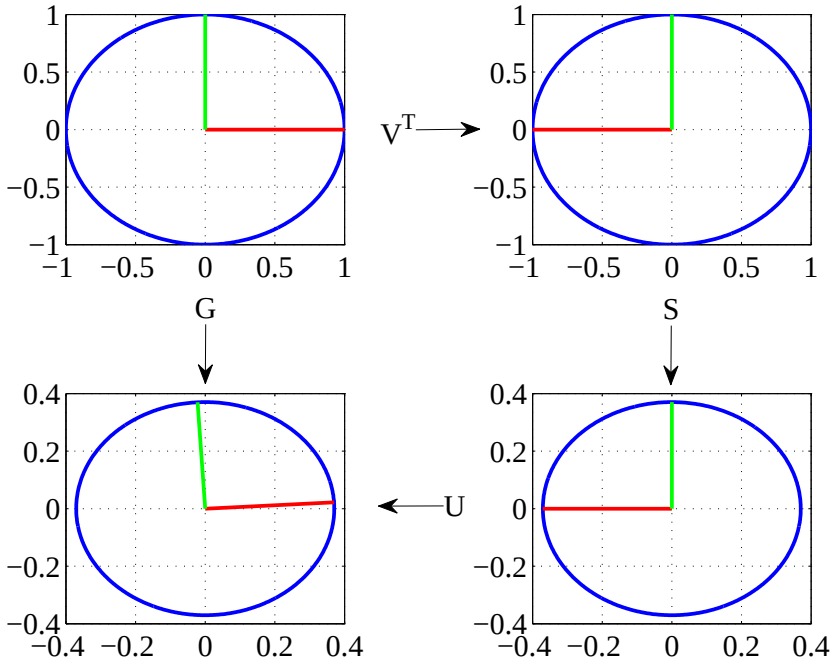

Fig. 5.12: Singular values decomposition.

As can be seen from Fig. 5.12, this figure is divided into 4 subfigures. The first one at the top-left represents the unit disc in blue together with the two canonical unit vectors in red and green. We can see the action of the matrix G on that unit disk and those unit vectors on subfigure bottom-left, which distorts it to an ellipse. The singular values decomposition decomposes the matrix G into three simple transformations: an initial rotation V^T which is presented on subfigure top-right, then a scaling S along the coordinate axes (subfigure bottom-right), and a final rotation U. The lengths of the semi-axes of the ellipse are the singular values of G which can be computed as the square roots of the non-zero eigenvalues of both $G^T \cdot G$ and $G \cdot G^T$.

Figure 5.13 represents the singular values of the BDFM for different operating points.

As illustrated, the dynamic behaviour and steady-state gain are greatly affected by changes in the rotor angular speed. Additionally, only at the synchronous speed the BDFM behave like a first order system. Moreover, two antiresonance frequencies appear clearly, one at a constant frequency, 313.3 rad/s, and the other frequency

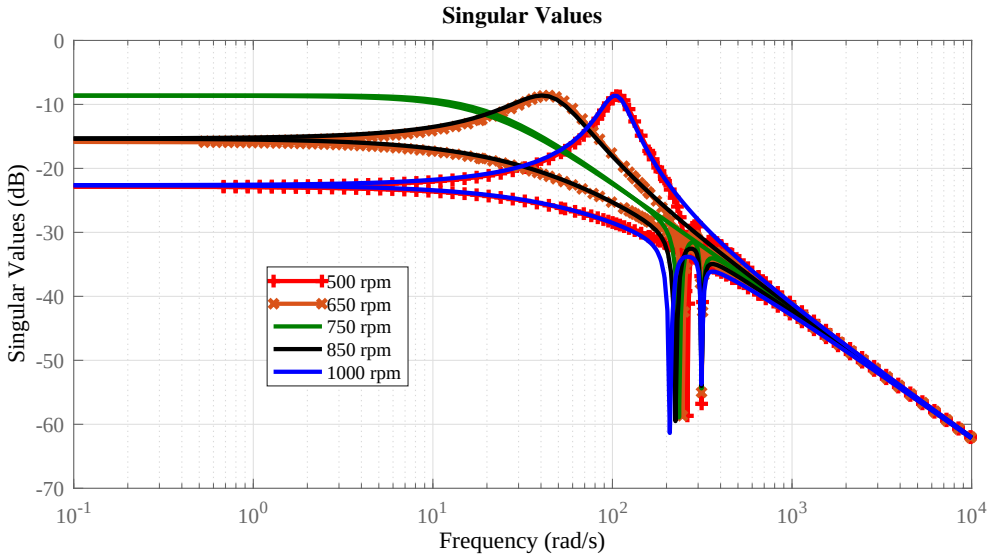

Fig. 5.13: Singular values of the BDFM.

is decreasing as the rotor speed increase, 261.3 rad/s for 500 rpm and 208.7 rad/s for 1000 rpm. These antiresonance frequencies are related to the angular speeds of the reference frames of the $d-q$ transform. The first 313.3 rad/s is approximately the frequency of the grid 50 Hz, and the second is not other than the angular speed $\omega_p - p_p\omega_r$. Indeed, the $d-q$ model is for converting sinusoidal quantities into constants ones, and any input in the $d-q$ model at those frequencies would implies on the output a maximum value in an axis and zero in the other axis as long as they rotate at exactly the same speed.

The standard configuration of the H_∞ control problem is given by Fig. 5.14 [123–125] where $\boldsymbol{P}(s)$ represents the generalised plant, $\boldsymbol{K}(s)$ is the controller, $\boldsymbol{w}$

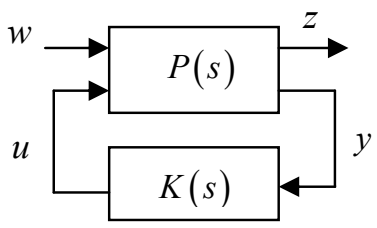

Fig. 5.14: General formulation of the H_∞ control problem.

is the exogenous inputs, $\boldsymbol{z}$ denotes the output signals to be minimised, $\boldsymbol{y}$ is the measurement outputs and $\boldsymbol{u}$ is the control signals.

The analysis results have proved that to obtain nominal performance and robust stability, the three matrices S, R and T have to be minimised. This synthesis may seem contradictory but it is not since these minimisations are imposed in different frequency ranges [123–126]. Henceforth, weighting matrices $\boldsymbol{W}_1(s)$, $\boldsymbol{W}_2(s)$ and $\boldsymbol{W}_3(s)$ are introduced.

The closed-loop of the uncertain plant is robust in stability and performance if and only if:

$$\begin{cases} \left\| \boldsymbol{W}_1 \cdot \boldsymbol{S} \right\|_\infty < 1 \\ \left\| \boldsymbol{W}_2 \cdot \boldsymbol{R} \right\|_\infty < 1 \\ \left\| \boldsymbol{W}_3 \cdot \boldsymbol{T} \right\|_\infty < 1 \end{cases} \tag{5.30}$$

Or more commonly:

$$\left\| \begin{array}{c} \boldsymbol{W}_1 \cdot \boldsymbol{S} \\ \boldsymbol{W}_2 \cdot \boldsymbol{R} \\ \boldsymbol{W}_3 \cdot \boldsymbol{T} \end{array} \right\|_\infty < 1 \tag{5.31}$$

This result is known as the mixed sensitivity problem. The H_∞ problem consists in minimising the effect of perturbation on the system, i.e. minimising the ratio $\left\| \frac{\boldsymbol{z}}{\boldsymbol{w}} \right\|_2$

However, in the worst case this ratio is equal to $\left\| F_1\left(\boldsymbol{P}, \boldsymbol{K}\right) \right\|_\infty$, where F_1 is the lower Redheffer product.

The problem can be formulated as follows: Given $\boldsymbol{P}(s)$ and $\gamma > 0$, finding $\boldsymbol{K}(s)$ which:

- stabilises the closed-loop system;
- ensures $\left\| F_1\left(\boldsymbol{P}, \boldsymbol{K}\right) \right\|_\infty < \gamma$.

Calculations prove that satisfying $\left\| F_1\left(\boldsymbol{P}, \boldsymbol{K}\right) \right\|_\infty < \gamma$ comes to satisfy $\left\| \begin{array}{c} \boldsymbol{W}_1 \cdot \boldsymbol{S} \\ \boldsymbol{W}_2 \cdot \boldsymbol{R} \\ \boldsymbol{W}_3 \cdot \boldsymbol{T} \end{array} \right\|_\infty <$ 1 which is the condition obtained in Eq. (5.31).

The mixed sensitivity structure is given in Fig. 5.15.

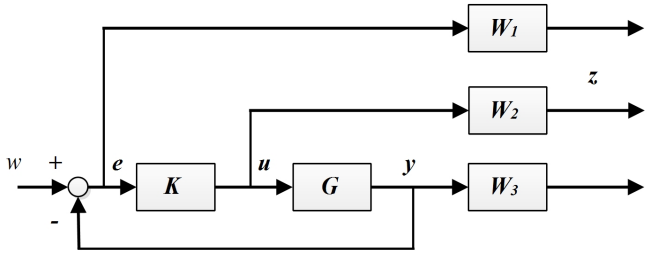

Fig. 5.15: Mixed sensitivity structure for H_∞ controller design.

The good choice of weighting functions allows us to achieve good dynamic response with good robustness in stability. The weighting functions W_1 and W_3 chosen for our BDFM prototype model are calculated according to a practical formula described in Matlab help which is given by:

$$W_1 = \frac{\frac{s}{m} + w_0}{s + w_0 \cdot a} \tag{5.32}$$

$$W_3 = \frac{s + \frac{w_0}{m}}{a \cdot s + w_0} \tag{5.33}$$

where m is the desired bound on $\|S\|_\infty$ and $\|T\|_\infty$, w_0 is the desired bandwidth of the closed-loop and, a is the maximum steady-state error.

In our study, the control weight is not considered and chosen small enough, m is chosen 2 for better robustness in stability, w_0 is chosen 50 rad/s and therefore any real wind profile can be tracked easily and, a is chosen 1/1000. Thus, the weighting functions are as follows:

$$W_1 = \frac{100 + s}{0.1 + 2s} \tag{5.34}$$

$$W_2 = 10^{-4} \tag{5.35}$$

$$W_3 = \frac{25+s}{50+0.001s} \tag{5.36}$$

Numerical results of the controller $\boldsymbol{K}(s)$ are obtained using the function syntax 'mixsyn' of the Robust Control Toolbox of Matlab, which minimises the H_∞-norm of the weighted mixed sensitivity. The H_∞ controller calculated for the BDFM prototype at the synchronous speed can be expressed as a transfer function matrix 2×2 where each entry is written as a ratio of two polynomials of s:

$$\boldsymbol{K}(s) = \begin{bmatrix} \dfrac{num_{K11}(s)}{den_K(s)} & \dfrac{num_{K12}(s)}{den_K(s)} \\ -\dfrac{num_{K12}(s)}{den_K(s)} & \dfrac{num_{K11}(s)}{den_K(s)} \end{bmatrix} \tag{5.37}$$

$$\begin{aligned} num_{K11} = {} & 3.65741 \times 10^6 s^9 + 2.87427 \times 10^{13} s^8 + 1.53506 \times 10^{18} s^7 \\ & + 5.37688 \times 10^{21} s^6 + 5.3055 \times 10^{23} s^5 + 8.27093 \times 10^{26} s^4 \\ & + 4.08968 \times 10^{28} s^3 + 2.92789 \times 10^{31} s^2 + 6.13191 \times 10^{32} s \\ & + 1.4058 \times 10^{31} \end{aligned} \tag{5.38}$$

$$\begin{aligned} num_{K12} = {} & 3679.74 s^9 + 2.89166 \times 10^{10} s^8 + 1.53271 \times 10^{15} s^7 + 5.0865 \\ & \times 10^{18} s^6 + 1.44272 \times 10^{22} s^5 + 4.80005 \times 10^{25} s^4 + 1.78633 \\ & \times 10^{27} s^3 + 3.84257 \times 10^{30} s^2 + 3.67997 \times 10^{31} s + 8.42571 \times 10^{29} \end{aligned} \tag{5.39}$$

$$\begin{aligned} den_K = {} & s^{10} + 1.56174 \times 10^7 s^9 + 6.10338 \times 10^{13} s^8 + 4.51672 \times 10^{17} s^7 \\ & + 8.45942 \times 10^{20} s^6 + 7.00688 \times 10^{22} s^5 + 1.29347 \times 10^{26} s^4 + 2.51222 \\ & \times 10^{27} s^3 + 4.58439 \times 10^{30} s^2 + 2.1043 \times 10^{29} s + 2.4148 \times 10^{27} \end{aligned} \tag{5.40}$$

Indeed, the H_∞ control theory provides us controllers with good robustness in performances and stability. However, the order of the obtained controllers is very high. Hence, the controller can only be implemented by computation rather than what have been long-established physically constructed.

Seeing the high order of the obtained controller and its huge coefficients, see Eqs.

(5.37), (5.38)-(5.40), it seems clearly that its implementation in case of electrical machines costs too much. In order to simplify this controller, we opted for the reduction of the controller's order.

Each element of $\boldsymbol{K}(s)$ have been aggregated separately using the aggregation method described in Section 5.2.2. Numerical results of the final H_∞ controller are given by:

$$\boldsymbol{K}_{new}(s) = \begin{bmatrix} K_{new11}(s) & K_{new12}(s) \\ -K_{new12}(s) & K_{new11}(s) \end{bmatrix} \tag{5.41}$$

$$K_{new11}(s) = \frac{33.87s^2 + 717.6s + 16.45}{5.364s^2 + 0.2463s + 0.002827} \tag{5.42}$$

$$K_{new12}(s) = \frac{8.861s^2 + 85.32s + 1.954}{10.62s^2 + 0.4879s + 0.0056} \tag{5.43}$$

Singular values of the reduced-order robust controller are mapped together with those of the original robust controller in Fig. 5.16.

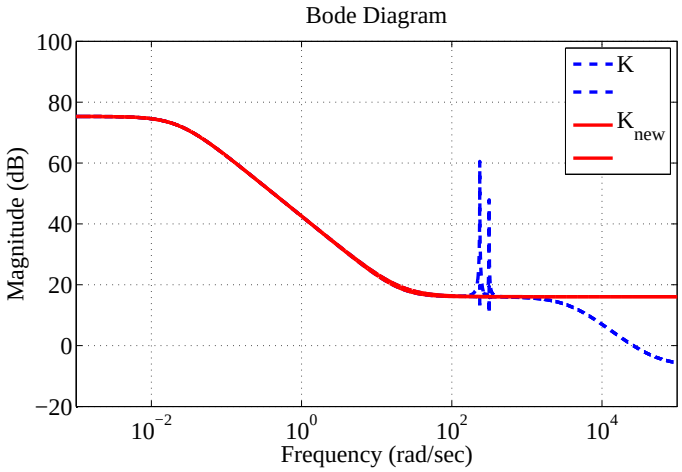

Fig. 5.16: Bode diagram of the regulator.

As shown in this figure, the new controller has the same performances in low-mid frequencies. In high frequencies, the controller increases the noise magnitude, but this may not make a problem in the control procedure since the BDFM is a good noise filter as illustrated in its singular values loci in Fig. 5.13

The proposed H_∞ control structure is presented in Fig. 5.17.

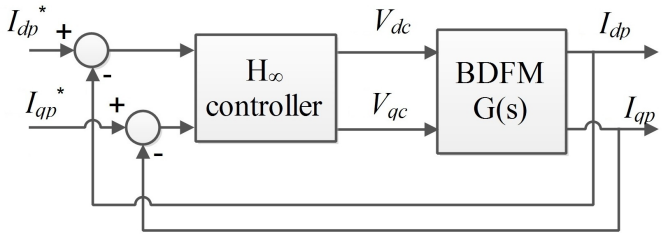

Fig. 5.17: Control diagram of the power winding currents.

5.3.2 Results and discussion

In order to validate the proposed current control loop of the BDFM operating in generation mode for wind energy applications, a simulation is carried out using Matlab/Simulink environment.

Analogously to what has been done in the previous section with the PI controller. The proposed H_∞ controller is calculated for the synchronous speed. Therefore, two other operating speeds (650 rpm and 850 rpm) have been chosen outside of the BDFM effective speed range to evaluate the effectiveness of the proposed H_∞ controller.

Results obtained for the three different operating speeds are presented in Fig. 5.18.

As follows from the left side of Fig. 5.18 which represents from the top to the bottom the singular values loci of the sensitivity function for the three different operating points, 650 rpm, 750 rpm and 850 rpm, respectively. The magnitude of the sensitivity function at 750 rpm is always less than the dashed red piecewise function which implies robustness in dynamic performances and stability. Moreover, the transition frequency at which the sensitivity changes from attenuating to amplifying disturbances known also as the 'sensitivity crossover frequency' is within the interval from 143.5 rad/s to 381.2 rad/s (in our MIMO model we have two singular values), which is sufficient to attenuate disturbances and track a real wind

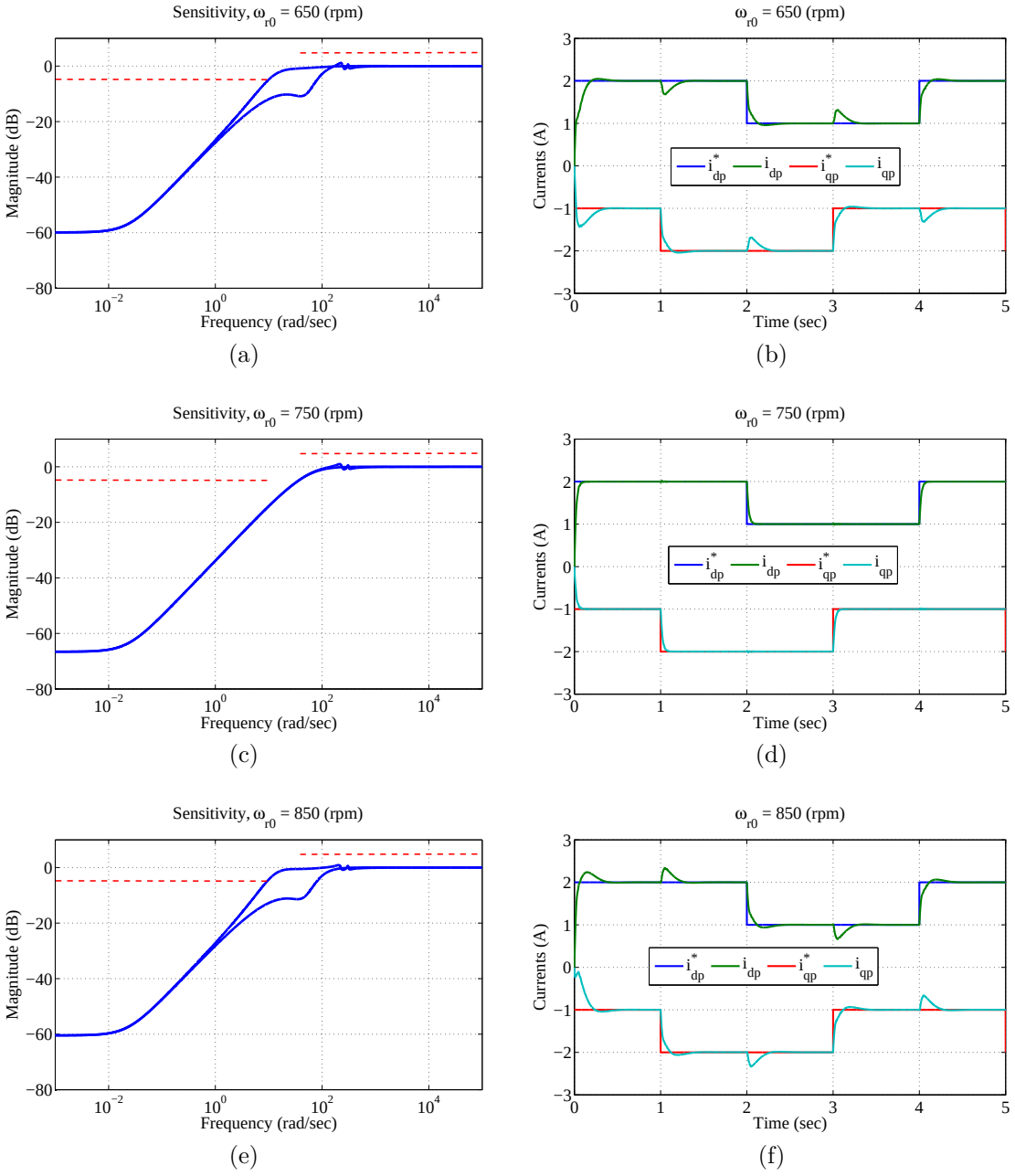

Fig. 5.18: Frequency and time responses of the mixed sensitivity structure-based BDFM.

profile [127,128]. Furthermore, for the two operating speeds 650 rpm and 850 rpm, performances may degrade with slower tracking abilities compared to those at the synchronous speed.

Tab. 5.3: Dynamic performances of the H_∞ controller

	Settling time (ms)	Overshoot %	Steady-state error (A)
650 (rpm)	0.1	3.9	0.0014
750 (rpm)	0.057	0.06	$5 \cdot 10^{-4}$
850 (rpm)	0.26	6.6	$5 \cdot 10^{-4}$

Generally speaking, in the low frequencies, the magnitude of the sensitivities is less than or equal to -60 dB, thus indicates steady-state error is less than or equal a thousandth of the input, whereas in the high frequencies, the sensitivities gain is held to zero, so, we can conclude good disturbance rejection.

On the right side where the step response of the complementary sensitivity is presented for the three operating speeds, 650 rpm, 750 rpm and 850 rpm, it can be seen that performances of the H_∞ controller are satisfactory including fast settling and rise times, and steady-state error very small, about one per mille. In addition to the good performances in time response, the coupling effect is greatly minimised, but not eliminated as may a decoupling action do. In fact, some performances (settling time and steady-state error) of the H_∞ controller deteriorate when the operating speed is other than the synchronous one in view of the fact that the dynamic of the BDFM changes brusquely with respect to variation in the shaft speed.

Table 5.3 summarises the dynamic performances of the H_∞ controller in digital form.

5.4 Application to Wind Turbine based on BDFM

5.4.1 Wind turbine model

The mechanical power of the wind turbine on the BDFM rotor shaft can be represented by [56]:

$$P_w = \frac{1}{2} C_p(\lambda, \theta) \rho \pi R^2 V_w^3 \tag{5.44}$$

where C_p is the power coefficient, V_w is the wind velocity, ρ is the air density and R is the radius of the turbine planes.

The produced turbine torque is given by the ratio below:

$$T_t = \frac{P_w}{\omega_t} \tag{5.45}$$

The mechanical coupling between the turbine and the rotor of the BDFM is provided through the gearbox. The mechanical torque of the wind turbine referred to the BDFM side is given by:

$$T_m = \frac{T_t}{GB} \tag{5.46}$$

where GB is the gear ratio which maintains the BDFM shaft speed within a desired speed range. Likewise, the turbine shaft speed can be expressed as a function of the BDFM shaft speed and the gear ratio as follows:

$$\omega_t = \frac{\omega_r}{GB} \tag{5.47}$$

Based on Eq. (5.44), only certain percentage of the available wind power can be transformed into mechanical power. This percentage is related to the power coefficient and is unique for each wind turbine. The power coefficient can be approximated as:

$$C_p(\lambda, \theta) = 0.22 \left(\frac{116}{\lambda_i} - 0.4\theta - 5 \right) e^{\frac{-12.5}{\lambda_i}} \tag{5.48}$$

$$\frac{1}{\lambda_i} = \frac{1}{\lambda + 0.08\theta} - \frac{0.035}{1 + \theta^3} \tag{5.49}$$

where λ is the tip-speed ratio and is given by:

$$\lambda = \frac{\omega_t R}{V_w} \tag{5.50}$$

Table 5.4 complete the parameters used for simulation implementation of wind turbine based on the BDFM whose electric parameters have been given in Table 3.1.

Tab. 5.4: Wind turbine and BDFM mechanical parameters

Parameter	Symbol	Value
Blade length	R	2.5 (m)
Air density	ρ	1.25 (kg/m^3)
Gearbox ratio	GB	1.25
Total inertia	J	0.1 $(kg \cdot m^2)$
Viscous friction	B	0.0005 $(N \cdot m \cdot s)$

Given that the selected $d-q$ reference frame is aligned with the power winding flux, therefore, the direct component of the grid voltage equals to zero and the quadrature component equals to the voltage maximum magnitude [93, 129–131]:

$$\begin{cases} v_{dp} = 0 \\ v_{qp} = v_p \end{cases} \tag{5.51}$$

Using Eq. 5.51, the relationship between powers (active and reactive) of the power winding and currents (direct and quadrature) of the power winding can be written by:

$$P_p = \frac{3}{2} v_{qp} i_{qp} \tag{5.52}$$

$$Q_p = \frac{3}{2} v_{qp} i_{dp} \tag{5.53}$$

Therefore, references of the power winding currents can be obtained by:

$$\begin{cases} i_{qp}^{*} = \dfrac{2}{3v_{qp}} P_{p}^{*} \\ i_{dp}^{*} = \dfrac{2}{3v_{qp}} Q_{p}^{*} \end{cases} \tag{5.54}$$

Control structures of the BDFM-based wind turbine using PI and H_∞ controllers are represented schematically in Figs. 5.19 and 5.20, respectively.

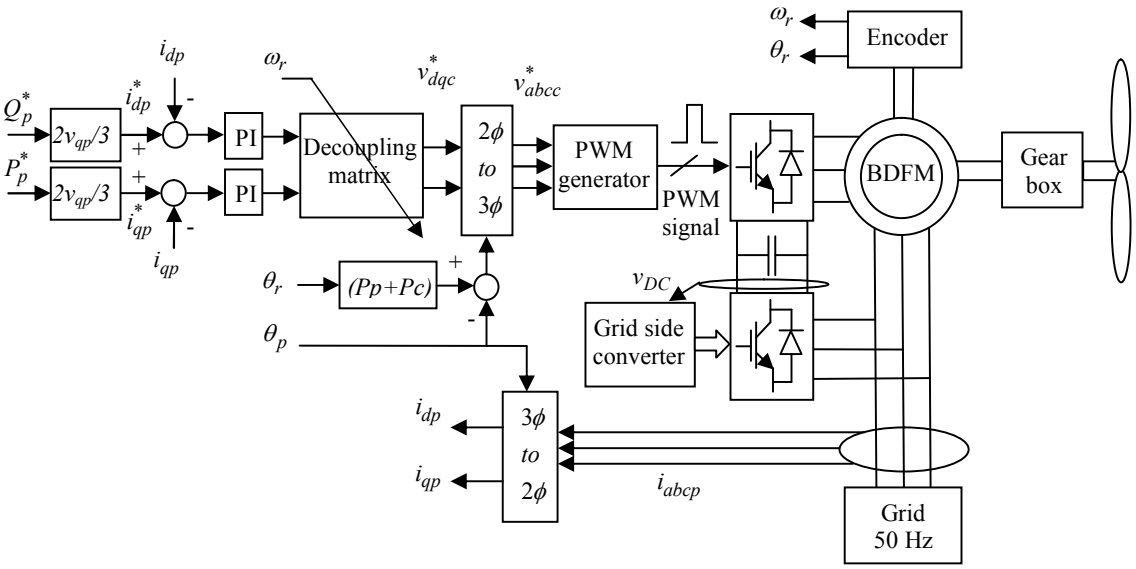

Fig. 5.19: Schematic representation of the BDFM PI control structure.

The Matlab/Simulink model of wind turbine based on BDFM is shown in Fig. 5.21, where we were using a fixed-step simulation time of 5×10^{-5}sec. The output of the decoupling matrix/H_∞ controller go through saturation of $\pm$ 12v.

The turbine block contains the turbine model and the shaft speed equation as illustrated in Fig. 5.22.

It is worth pointing out that the control strategies developed in this Chapter either with PI or H_∞ controllers are mainly focusing on the validation of the proposed mathematical model of the BDFM for control in Chapter 3, and are not focusing on the maximisation of the produced power as long as the maximum power point tracking requires both pitch angle and shaft speed controls which are

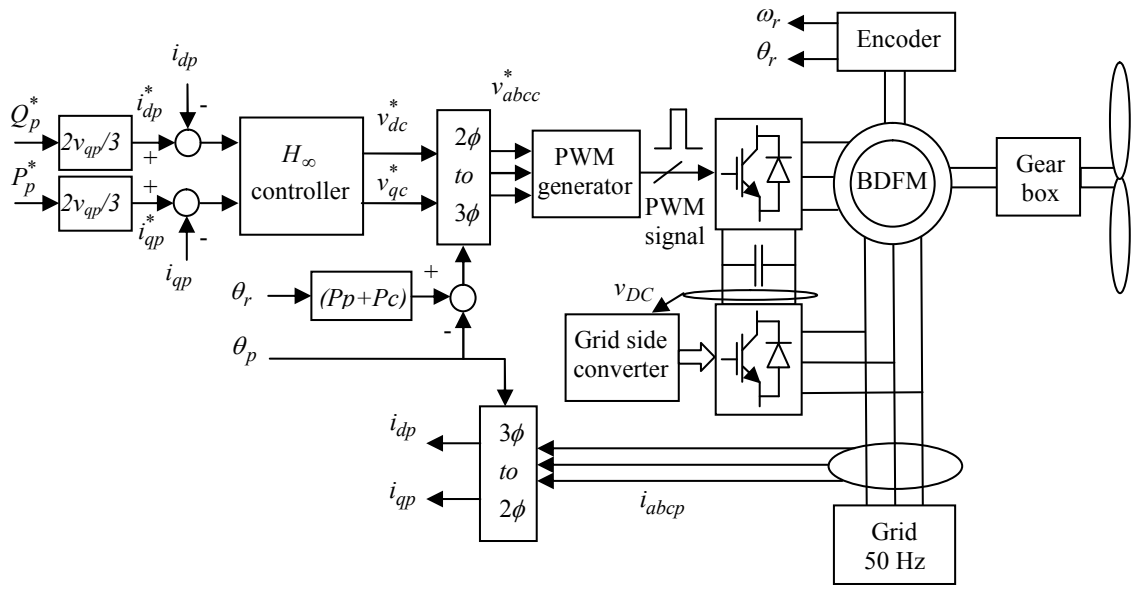

Fig. 5.20: Schematic representation of the BDFM H_∞ control structure.

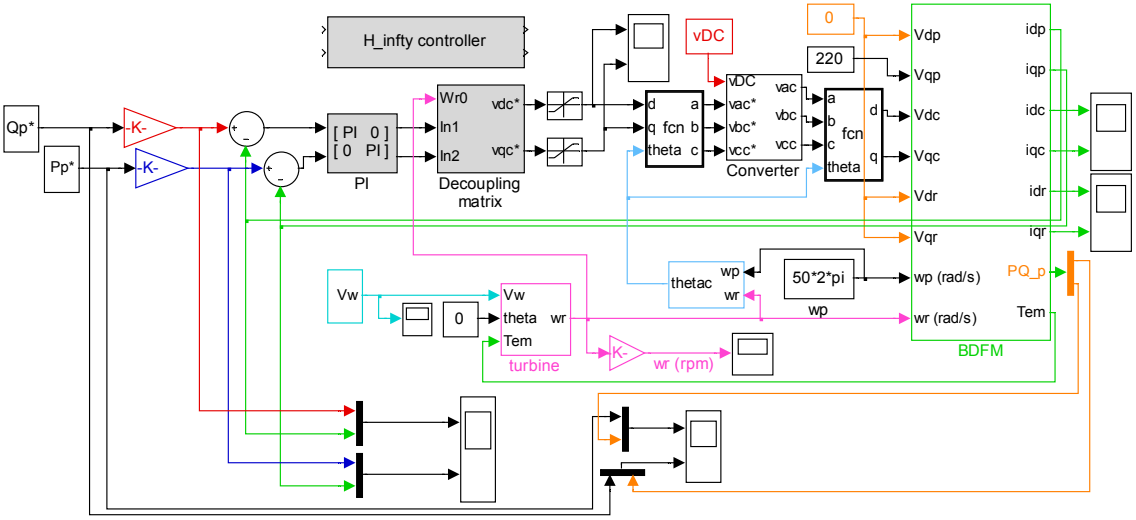

Fig. 5.21: Matlab/Simulink model.

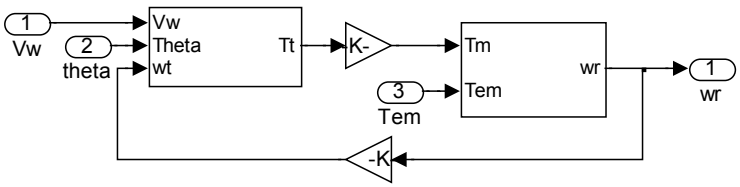

Fig. 5.22: Turbine Simulink model.

outside the scope of the dissertation.

The power winding active power reference, P_p^*, is generally come from the electricity demand forecast [132, 133], or from the wind speed sensor. In the following, the active power reference chosen is steps at different rotor speeds, and the reactive power reference is always 0.

5.4.2 Control without parameters uncertainty

In order to validate the proposed control schemes, the obtained controllers will be applied on the non-linear model of the BDFM-based wind turbine.

Constant wind speed

In Fig. 5.23, the dynamic response of steps of wind speed is presented. The steps of the wind speed are chosen long enough to reach the steady-state, then, steps on the active power reference P_p^* appear which expose the transient-state at different operating speeds.

Figure 5.24 represents the zoom of the active and reactive powers of Fig. 5.23.

As can be seen form Fig. 5.23a the wind speeds are 14 m/s, 8.5 m/s, 12.5 m/s, 7 m/s and 11 m/s, which correspond to the changing times t = 6 s, t = 12 s, t = 18 s and t = 24 s, respectively. For steps of the active power reference of ± 600 Watt at t = 4 s, t = 9 s, t = 15 s, t = 21 s and t = 27 s, the steady-state errors of the active and reactive powers are ± 20 Watt and ± 30 VAR, and the BDFM works in the sub-synchronous mode and the super-synchronous mode with a satisfactory dynamic response with the H_∞ control method. However, the response with PI controller is slower, and has a large oscillations in all speed range (± 200 Watt) due to the converter whose switching frequency is relatively small, 2 KHz. Moreover, the overshoot in the case of H_∞ controller is very small, for instance 5% at the step of 9 s and 2.7% at the step of 21 s, but at any rate, the overshoot will not impact the system negatively because the BFDM inherits strong ability to handle

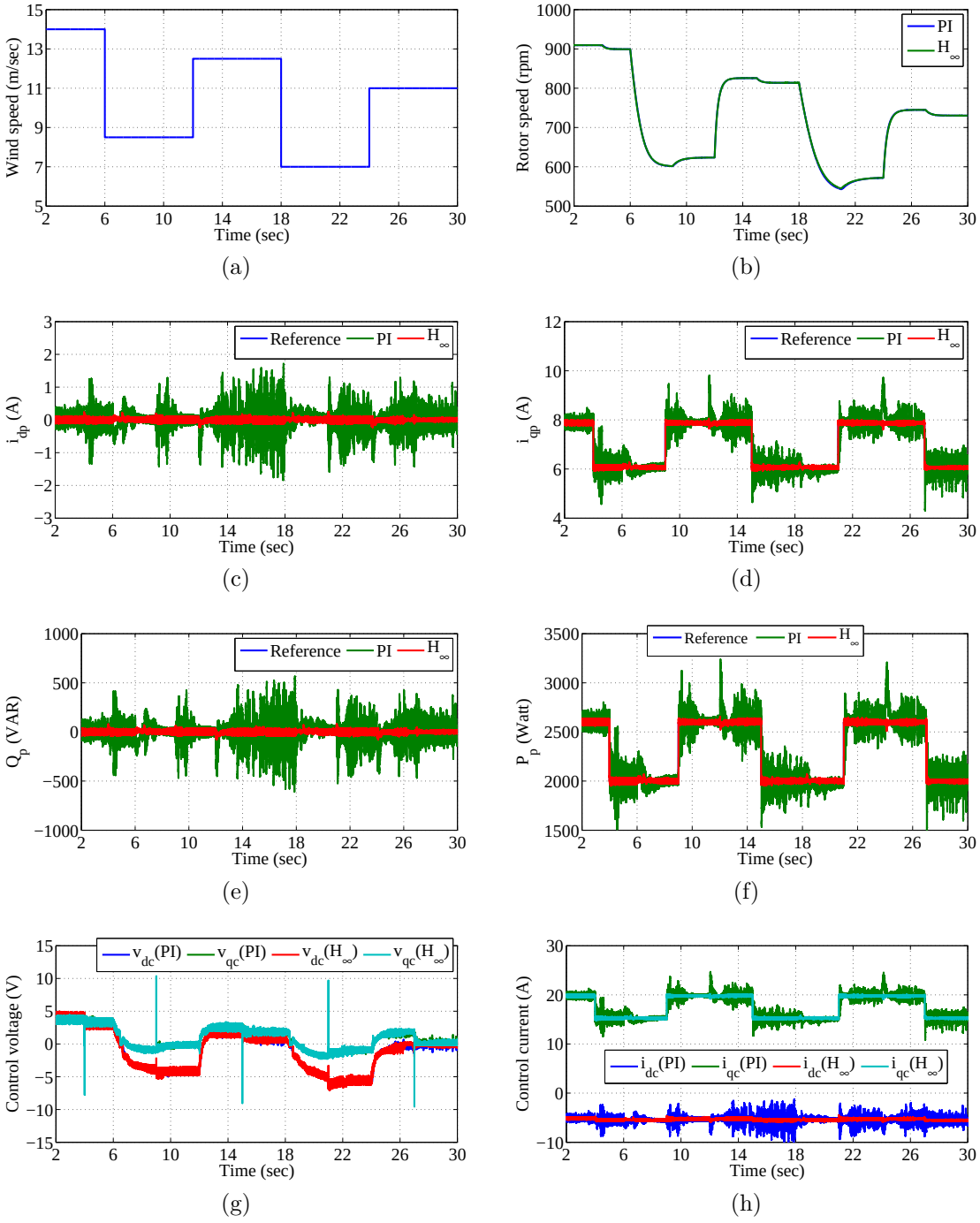

Fig. 5.23: Dynamic response of constant wind speed.

the current overshoot, additionally, the stepping of the active power reference in this test is an extreme condition, which would not happen in practice since P_p^*

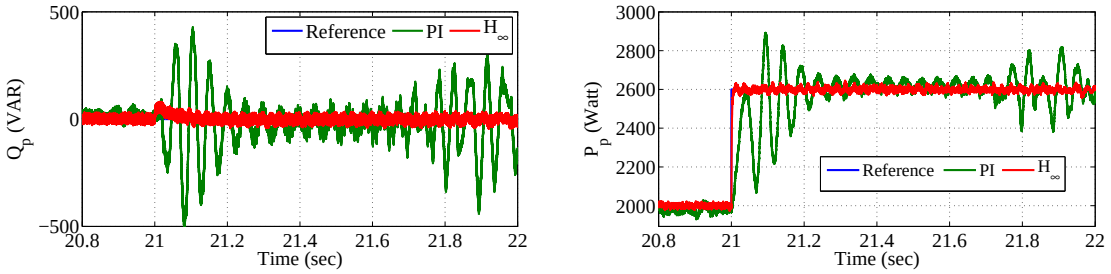

(a) (b)

Fig. 5.24: Zoom of the dynamic response of constant wind speed.

would be generated by an outer loop of control for maximisation of the produced power.

Variable wind speed

In general, the rotor speed is variable in practical applications, so, we consider in the following that the wind turbine is subject to a variable wind velocity. The wind speed profile used in this study is given by:

$$\begin{aligned} V_w = 10 + 2.2\sin(0.2t) + 0.6\sin(4t) + 0.4\sin(3t) \\ + 1.2\sin(1.3t) + 0.1\sin(100t) + 0.1\sin(8t) \end{aligned} \tag{5.55}$$

Figure 5.25 represents the dynamic response of the wind turbine based on the BDFM for a variable wind speed.

Figure 5.26 represents the zoom of the active and reactive powers of Fig. 5.25.

As can be seen from the curves presented in Fig. 5.25, performances of the PI controller are limited as long as the desired active and reactive power are not reached perfectly, the curves in steady-state are not centred around the desired value, i.e. the reference signal, but, alter around their reference as the wind speed change instead. Moreover, the H_∞ controller shows good steady-state and transient performances, where the settling time, rise time and the overshoot are almost exactly the same for constants wind speed.

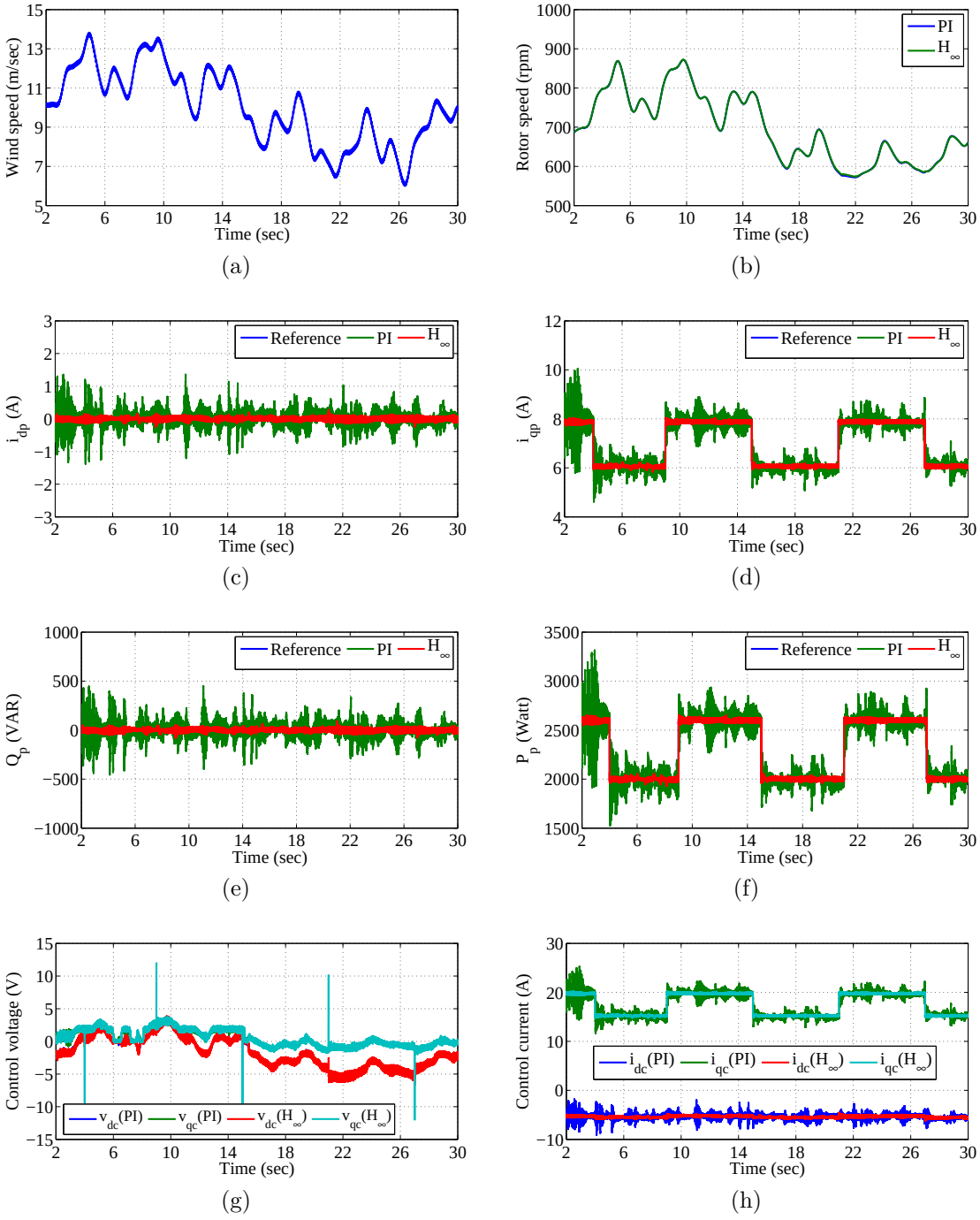

Fig. 5.25: Dynamic response of variable wind speed.

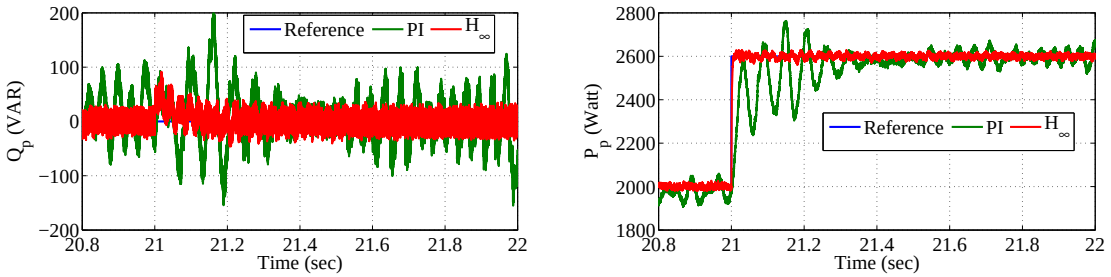

(a) (b)

Fig. 5.26: Zoom of the dynamic response of variable wind speed.

5.4.3 Control in the presence of parameters uncertainty

To study the obtained controllers' robustness, dynamic responses of steps in the active power, meanwhile the reactive power is regulated to zero are given considering the parameters imprecise.

We suppose in the following that the electrical parameters of the BDFM have been inaccurately identified. To do so, we assume that the indentified rotor parameters are different by 5% from the real rotor parameters, and the identified stator parameters are different by 10% from the real stator parameters. The assumed real parameters of the BDFM are given in Table 5.5.

Tab. 5.5: The assumed BDFM real parameters

	Resistance (Ω)	Self inductance (H)	Mutual inductance (H)
Power winding	1.5588	0.6433	0.2179
Control winding	1.1869	0.1339	0.0658
Rotor	0.4966	0.1392	

Constant wind speed

Figure 5.27 represents the dynamic response of the BDFM driven by a wind turbine to steps of wind speed in the presence of parameters uncertainty.

Figure 5.28 represents the zoom of the active and reactive powers of Fig. 5.27.

As can be seen, the PI controller provides in the presence of uncertain parameters similar performances to those obtained in certain parameters. This does not demonstrate the effectiveness of the PI controller for the BDFM since the active and reactive powers are centred around their references and the tracking error is within about ± 200 Watt and ± 300 VAR, respectively.

Besides of that, it can also be seen that the H_∞ method achieves a good control performance in a wide rotor speed range and under parameters uncertain. In fact, with parameters uncertain, the control performance of the BDFM system slightly decreases. The settling time increases, for example 4.5 ms in certain parameters and 7 ms in the presence of uncertainties at the step of the 21^{st} s, moreover, the coupled terms have bigger effect compared to the case using nominal parameters where the reactive power reach its maximum value 72 VAR to the active power step at 9 s meanwhile its maximum value for that step in certain parameters is just 55 VAR. In spite of this degradation in some performances, these results prove the robustness of the H_∞ method with respect to BDFM parameters uncertainty.

Variable wind speed

Figure 5.29 represents the dynamic response of the BDFM driven by a wind turbine for a variable wind speed and under parameters uncertainty.

Figure 5.30 represents the zoom of the active and reactive powers of Fig. 5.29.

The previous wind profile has been used. As can be seen, the proposed control structure using the H_∞ controller adjusts the active and reactive powers independently (a small coupling for a bit), and it achieves a good steady state performance as fast as in constants wind speed. However, the maximum value of the coupling

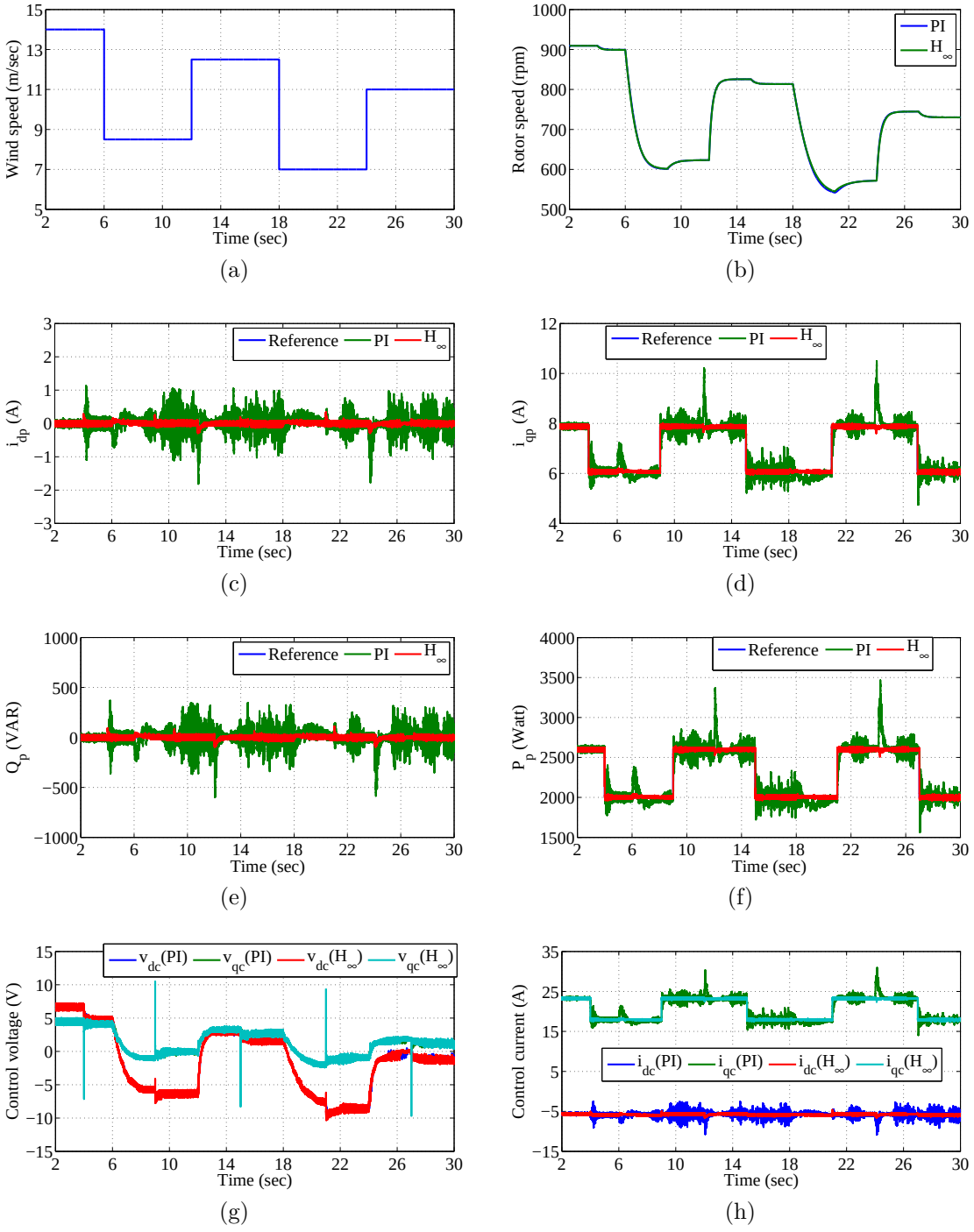

Fig. 5.27: Dynamic response under constant wind speed in the presence of parameters uncertainty.

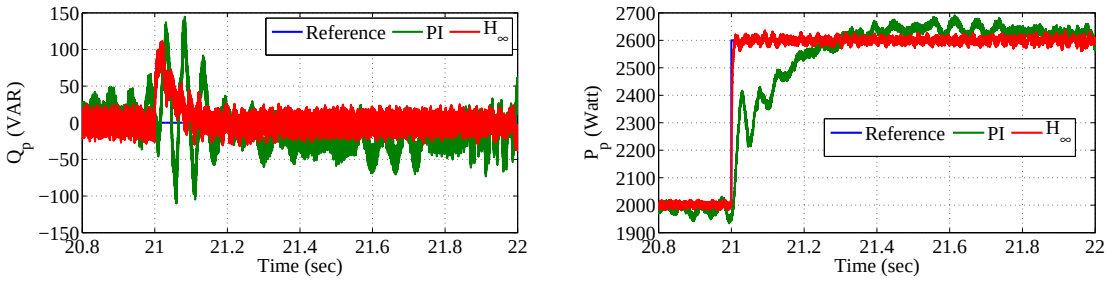

(a) (b)

Fig. 5.28: Zoom of the dynamic response for constant wind speed in the presence of parameters uncertainty.

effect is slightly bigger compared to the case of certain parameters, 80 VAR in uncertain parameters and 65 VAR in certain parameters at t = 21 s.

In spite of the inaccurate electrical parameters used for the calculation of the controller, the dynamic response is as good as in case of precise identification, which demonstrates the robustness of the H_∞ controller.

However, for the PI controller, the regulator cannot track the powers references. Indeed, the wind velocity changes affecting with it the dynamic of the BDFM. Additionally, the rise time is bigger compared to the case of certain parameters, 19 ms at 9 s and 28 ms at 21 s become 27 ms and 160 ms, respectively. In fact this study demonstrates the limit of one loop PI controller for such complex application. The commonly used PI control structures for the BDFM requires multi-PI controllers to perform cascade control loop structure [94, 109, 134–137].

5.5 Conclusions

In this Chapter we have proposed two control strategies, both of which have been validated by simulation. These modest contributions are for the BDFM working as generator connected to the grid. The BDFM is modelled as a MIMO system with a high order transfer function matrix and highly coupled terms.

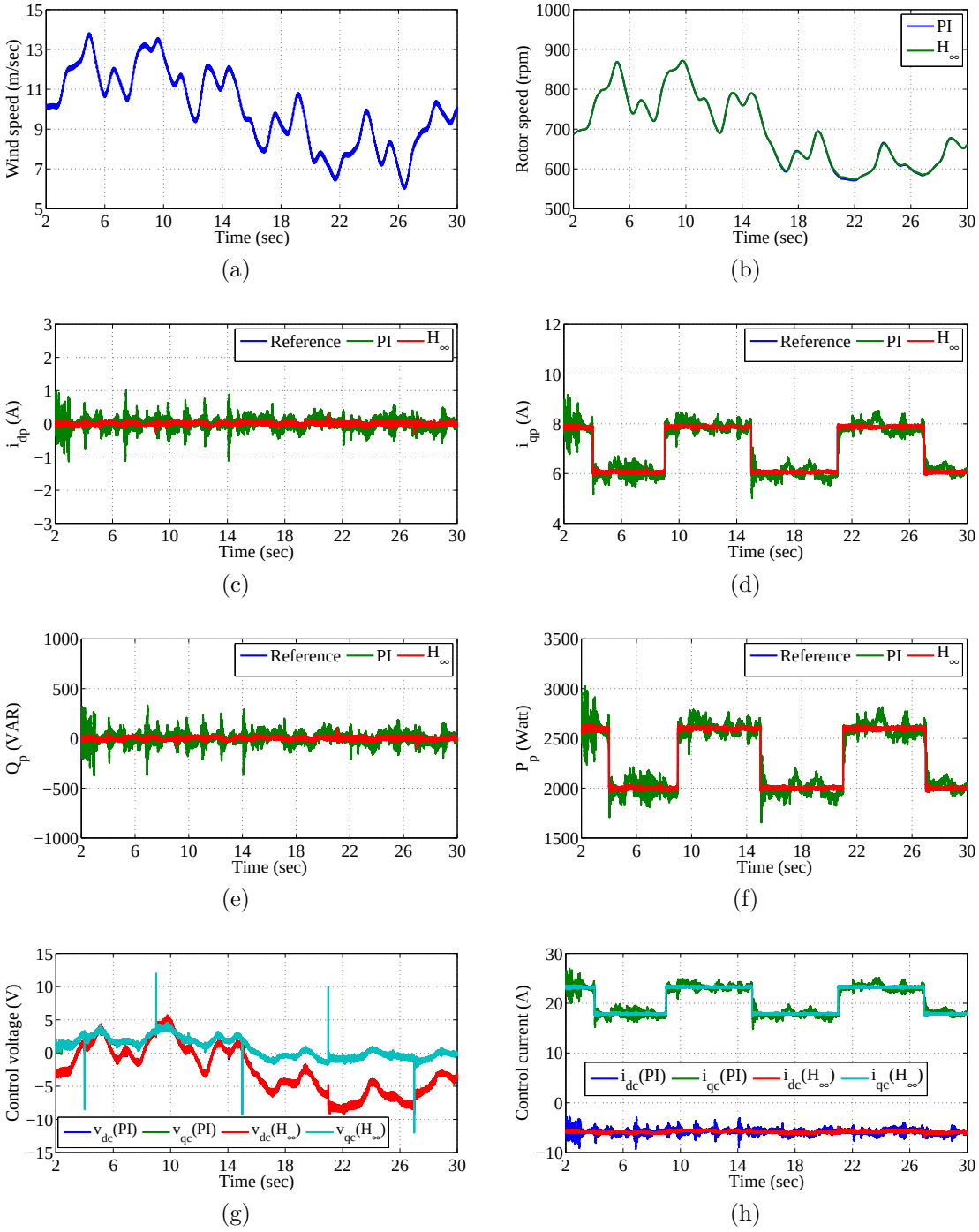

Fig. 5.29: Dynamic response under variable wind speed in the presence of parameters uncertainty.

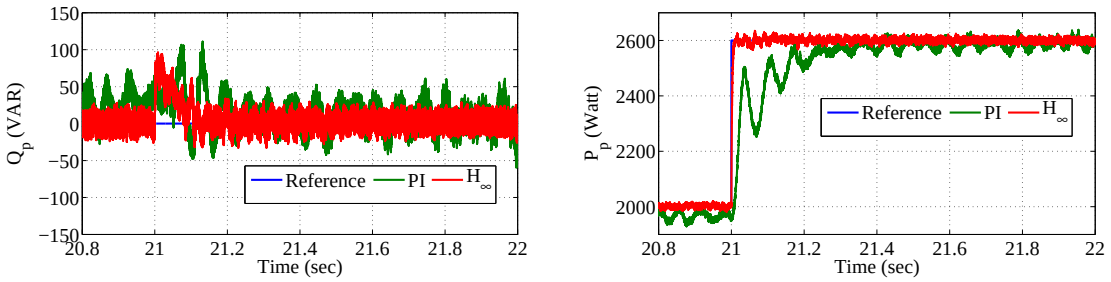

Fig. 5.30: Zoom of the dynamic response for variable wind speed in the presence of parameters uncertainty.

To calculate the coefficients of the PI controllers, firstly, we proposed to decouple between the direct and quadrature axes. To do so, a decoupling matrix is calculated. But, nonetheless, the set of BDFM-Decoupling matrix is having a very high order. Thus, to facilitate the task of calculating the PI coefficients for the enormous transfer function matrix, we performed an aggregation method. This aggregation method in the frequency-domain provides low order transfer functions with similar performances to the high order one. The approximant low order transfer function is used then to calculate the PI coefficients using Naslin polynomial technique.

On the other hand, seeing the complexity of the BDFM small signal model, a robust control structure is proposed where the minimisation of the H_∞-norm of the weighted mixed sensitivity is performed. Unfortunately, the resulted H_∞ controller is expensive for implementation especially for electrical systems where the step time needed is very small. Therefore, simplification of the resulted controller has been done.

The proposed control schemes have been validated by simulation results on the non-linear dynamic model of a wind turbine based on BDFM. It has been shown that the decoupling action has a great effect and compensated the coupled terms with acceptable performances. Furthermore, with the proposed control structures, the BDFM is always stable in all operating speeds.

For constant wind speed, the robust controller showed better waveforms in all operating speeds including fast response and low oscillations in transient state. Besides of that, responses with the PI controller match well the references but with tracking error relatively large due to the small switching frequency of the converter.

Moreover, for variable wind speed, dynamic performances of both controllers degrade especially in the case of the PI controller where the tracking objective is not achieved which may shed light on the limit of having just one control loop using the PI controller.

Furthermore, the performances under parameters variation are also tested. The results show the validity of the H_∞ controller which gives the best dynamic performance with smaller oscillation, which is practically important for the grid connection.

In fact, the more the parameters are imprecise, the more the control algorithms provide low dynamic performances.

Eventually, the achieved performances by the mixed sensitivity synthesis which include fast response time, very good tracking and comfortable robustness margin in dynamic and stability, demonstrates a rigorous controller for future works on the BDFM.

Chapter 6

Conclusions and Future Work

6.1 Conclusions

The objectives of this dissertation have been: to develop a new mathematical model for the BDFM as generator in wind turbines by describing a direct relationship between the control winding as input and the power winding as output; to analyse the stability of the BDFM with respect to parameters variations and shaft speed change; and to propose optimal control structure of wind turbines based on BDFM. The specific contributions of this dissertation will now be summarised.

Firstly, the coupled circuit model of the BDFM was presented. After that, some preliminaries about space vector and $d-q$ transformation was presented to introduce the $d-q$ vector model of the BDFM.

Then, linearisation of the BDFM $d-q$ vector model around an operating point was performed. This has conducted us to derive two new mathematical models for the BDFM:

- The first mathematical model proposed is a transfer function matrix describing the direct relation between the inputs which are the voltages of the power and control windings, and the outputs which are the currents of the power windings. This mathematical model is qualified to represent the dynamic of

the BDFM in generation/motion mode;

- The second mathematical model proposed was derived from the first one assuming balanced grid voltage conditions and is, a transfer function matrix representing the relationship between the control windings voltages as inputs and the power winding currents as outputs. In fact, this mathematical model was been for control purposes, and was validated by simulation and experimental results which implies the validation of the first mathematical model as well. The obtained model of the grid-connected BDFM is mathematically of high order, multivariable, highly coupled, non-minimum-phase as it contains unstable zeros, and may considered as linear parameter-varying since the rotor speed is not constant and involves in the model. Therefore, control tasks would be difficult.

Next, the first mathematical model was used to examine the stability of the BDFM under unbalanced grid voltage conditions and under parameters variations. Moreover, this study was done in an extremely wide speed range, and valid for both of operation modes, motor and generator. This stability study was achieved by checking the position of the poles of the BDFM in the complex s-plane whether they are located in the left half-plane or not. In point of fact, the first and second mathematical models of the BDFM share the same denominator which indicates that the stability analysis is valid for both models. Generally speaking, in normal (faultless) conditions, the BDFM is stable along all the possible rotor speed range. Moreover, small change in the BDFM electric parameters do not alter its stability, however, considerable change, like short circuits in electrical windings may destabilise it. Besides that, the stability analysis allows us to define a centred orthotope in which the BDFM is stable.

Lastly, the BDFM control model was used to propose two control structures for the BDFM operating as generator connected to the grid:

- The first control structure was based on PI controllers. Perceiving the complexity of the obtained model of the BDFM, the use of a decoupling matrix

was proposed. The order of the resulted set BDFM-Decoupling action was very high, thus, order reduction was used allowing the calculation of PI coefficients in an optimal way using Naslin's method. In fact, simulation results for this control structure were only satisfactory for constants wind speed ignoring noises resulted from the converter. For variable wind speed the PI cannot track the desired power perfectly. Thus, the conclusion that one PI control loop is powerless in front of such complex systems;

- The second control structure was based on robust control theory where minimisation of the H_∞-norm of the weighted mixed sensitivity is performed. The resulted weighted mixed sensitivity based-H_∞ controller is high-order causing its practical application very costly; therefore, simplification of the controller was carried out. The proposed control strategy was validated by simulation results. The effectiveness of the control scheme was proved over wide operating speed and under parameters uncertainties demonstrating rigorous controller for future works on the BDFM. In spite of the achieved performances by the mixed sensitivity synthesis which include fast response, very good tracking and comfortable robustness margin in dynamics and stability with respect to parameters uncertainties and operating speed change, unfortunately, the more the parameters are imprecise the more the controller provides weaker effect.

6.2 Future Work

The work of this thesis suggests and open the way for a number of possible directions of research:

- Generalise the developed mathematical model for unbalanced grid voltage conditions;
- Optimise the design of the BDFM for better stability areas and better efficiency;

- Identify the parameters of the BDFM with high accuracy;
- Application of non-linear methods on the BDFM to achieve better closed-loop performances and study its stability;
- Employment of the estimation theory to perform sensorless control schemes for the BDFM.
- Development of new approaches to control the BDFM under unbalanced grid conditions.

Appendix A

Coefficients of the Transfer Matrix

Description of the coefficients of the common denominator of the BDFM transfer function matrix model as a function of the electrical parameters:

$$a_6 = \Big(L_p(M_c^2 - L_r L_c) + M_p^2 L_c\Big)^2 \tag{A.1}$$

$$\begin{aligned} a_5 = 2\Big(L_p(M_c^2 - L_r L_c) + M_p^2 L_c\Big) \cdot \Big(M_c^2 R_p \\ + R_c(M_p^2 - L_r L_p) - L_c(L_r R_p + L_p R_r)\Big) \end{aligned} \tag{A.2}$$

$$\begin{aligned} a_4 = {} & M_c^4\Big(L_p^2(\alpha^2 + \beta^2 + \omega_p^2) + R_p^2\Big) + 2M_p^2\Big(M_c^2\Big(L_c L_p(\alpha^2 + \beta^2 + \omega_p^2) \\ & + R_c R_p\Big) - L_r\Big(L_c^2 L_p(\alpha^2 + \beta^2 + \omega_p^2) + 2L_c R_c R_p + L_p R_c^2\Big) \\ & - L_c R_r(L_c R_p + 2L_p R_c)\Big) - 2M_c^2\Bigg(L_r\Big(L_c\Big(L_p^2(\alpha^2 + \beta^2 + \omega_p^2) + R_p^2\Big) \\ & + 2L_p R_c R_p\Big) + L_p R_r(2L_c R_p + L_p R_c)\Bigg) + M_p^4\Big(L_c^2(\alpha^2 + \beta^2 + \omega_p^2) \\ & + R_c^2\Big) + L_r^2 L_c^2 L_p^2(\alpha^2 + \beta^2 + \omega_p^2) + L_r^2 L_c^2 R_p^2 + 4L_r^2 L_c L_p R_c R_p \\ & + L_r^2 L_p^2 R_c^2 + 4L_r L_c^2 L_p R_r R_p + 4L_r L_c L_p^2 R_r R_c + L_c^2 L_p^2 R_r^2 \end{aligned} \tag{A.3}$$

$$
\begin{aligned}
a_3 = 2\Bigg(& M_c^4 L_p R_p(\alpha^2+\beta^2) + M_p^2\Bigg(L_c\Big(R_p\Big(M_c^2(\alpha^2+\beta^2) - 2R_rR_c\Big) \\
& - 2L_rL_pR_c(\beta^2+\omega_p^2)\Big) + R_c\Big(M_c^2L_p(\beta^2+\omega_p^2) - R_c(L_rR_p + L_pR_r)\Big) \\
& - L_c^2\Big(L_rR_p(\alpha^2+\beta^2) + L_pR_r(\alpha^2+\omega_p^2)\Big)\Bigg) - M_c^2L_p^2(\beta^2L_rR_c \\
& + \alpha^2L_cR_r) + L_p^2\omega_p^2(L_rL_c - M_c^2)\cdot(L_rR_c + L_cR_r) \\
& - 2M_c^2L_pR_p\Big(L_rL_c(\alpha^2+\beta^2) + R_rR_c\Big) - M_c^2R_p^2(L_rR_c + L_cR_r) \\
& + M_p^4L_cR_c(\beta^2+\omega_p^2) + \alpha^2L_r^2L_c^2L_pR_p + L_rL_c^2R_rR_p^2 + L_r^2L_cR_cR_p^2 \\
& + L_r^2L_pR_c^2R_p + \alpha^2L_rL_c^2L_p^2R_r + \beta^2L_r^2L_cL_p^2R_c + \beta^2L_r^2L_c^2L_pR_p \\
& + 4L_rL_cL_pR_rR_cR_p + L_rL_p^2R_rR_c^2 + L_c^2L_pR_r^2R_p + L_cL_p^2R_r^2R_c\Bigg)
\end{aligned}
\tag{A.4}
$$

$$
\begin{aligned}
a_2 = & \Big(\big(\alpha^2\beta^2 + (\alpha^2+\beta^2)\omega_p^2\big)L_p^2 + (\alpha^2+\beta^2)R_p^2\Big)M_c^4 + 2\Bigg(L_r\Bigg(L_c\Big(\\
& - \big(\alpha^2\beta^2 + (\alpha^2+\beta^2)\omega_p^2\big)L_p^2 - (\alpha^2+\beta^2)R_p^2\Big) - 2\beta^2L_pR_cR_p\Bigg) \\
& - R_r\Big(2L_cL_pR_p\alpha^2 + R_cR_p^2 + L_p^2R_c(\omega_p^2 - \alpha\beta)\Big)\Bigg)M_c^2 + \alpha^2\beta^2L_r^2L_c^2L_p^2 \\
& + \alpha^2L_c^2L_p^2R_r^2 + \beta^2L_r^2L_p^2R_c^2 + L_p^2R_r^2R_c^2 + \alpha^2L_r^2L_c^2R_p^2 + \beta^2L_r^2L_c^2R_p^2 \\
& + R_p^2(L_c^2R_r^2 + L_r^2R_c^2 + 4L_rL_cR_rR_c) + L_p^2\Bigg(\Big((\alpha^2+\beta^2)L_c^2 + R_c^2\Big)L_r^2 \\
& + 4L_cR_rR_cL_r + L_c^2R_r^2\Bigg)\omega_p^2 + 4L_rL_pR_rR_c^2R_p + 4\alpha^2L_rL_c^2L_pR_rR_p \\
& + L_cL_pR_cR_p(4R_r^2 + 4\beta^2L_r^2) + M_p^4\Bigg(\big(\alpha^2\beta^2 + (\alpha^2+\beta^2)\omega_p^2\big)L_c^2 + R_c^2 \\
& \times(\beta^2+\omega_p^2)\Bigg) + 2M_p^2\Bigg(\Big(R_cR_p(\beta^2+\alpha\omega_p) + L_cL_p\Big(\alpha^2\beta^2 + (\alpha^2+\beta^2) \\
& \times\omega_p^2\Big)\Big)M_c^2 - R_r\Big(R_p(\alpha^2-\beta\omega_p)L_c^2 + R_c^2R_p + 2L_pR_c\omega_p^2L_c\Big) + L_r\Big(\\
& - 2L_cR_cR_p\beta^2 - L_pR_c^2(\beta^2+\omega_p^2 - L_c^2L_p\big(\alpha^2\beta^2 + (\alpha^2+\beta^2)\omega_p^2\big)\Big)\Bigg)\Bigg)
\end{aligned}
\tag{A.5}
$$

$$
\begin{aligned}
a_1 = 2\Bigg(&\alpha^2\beta^2 M_c^4 L_p R_p + M_c^2\Bigg(R_p\Big(\alpha\beta\Big(\alpha\beta L_c(M_p^2 - 2L_r L_p) \\
&+ 2L_p R_r R_c\Big) - R_p(\beta^2 L_r R_c + \alpha^2 L_c R_r)\Big) - L_p\omega_p^2\Big(\beta^2 R_c(L_r L_p \\
&- M_p^2) + \alpha^2 L_c L_p R_r\Big)\Bigg) + R_p\Big(R_p\Big(\beta^2 L_r^2 L_c R_c + L_r R_r(\alpha^2 L_c^2 + R_c^2) \\
&+ L_c R_r^2 R_c\Big) - (\alpha^2 L_c^2 + R_c^2)\cdot\Big(\beta^2 M_p^2 L_r - L_p(\beta^2 L_r^2 + R_r^2)\Big)\Big) \\
&+ \omega_p^2\Big(\alpha^2 L_c^2 L_p R_r(L_r L_p - M_p^2) + L_c R_c\Big(\beta^2(M_p^2 - L_r L_p)^2 \\
&+ L_p^2 R_r^2\Big) + L_p R_r R_c^2(L_r L_p - M_p^2)\Big) + 2\beta M_p^2 L_c R_r R_c R_p\omega_p\Bigg)
\end{aligned}
\tag{A.6}
$$

$$
\begin{aligned}
a_0 = {}&\alpha^2\beta^2 M_c^4(L_p^2\omega_p^2 + R_p^2) + 2\alpha\beta M_c^2\Big(\beta M_p^2\omega_p(\alpha L_c L_p\omega_p + R_c R_p) \\
&- \alpha\beta L_r L_c(L_p^2\omega_p^2 + R_p^2) + R_r R_c(L_p^2\omega_p^2 + R_p^2)\Big) + (\alpha^2 L_c^2 + R_c^2) \\
&\times\Big(\omega_p^2\Big(\beta^2(M_p^2 - L_r L_p)^2 + L_p^2 R_r^2\Big) + 2\beta M_p^2 R_r R_p\omega_p + R_p^2(\beta^2 L_r^2 + R_r^2)\Big)
\end{aligned}
\tag{A.7}
$$

Description of the coefficients of the BDFM control transfer matrix numerators as a function of the electrical parameters:

$$
b_{c15} = -M_c M_p\Big(L_p(M_c^2 - L_r L_c) + M_p^2 L_c\Big) \tag{A.8}
$$

$$
b_{c14} = -M_c M_p\Big(M_c^2 R_p + R_c(M_p^2 - L_r L_p) - L_c(L_r R_p + L_p R_r)\Big) \tag{A.9}
$$

$$
\begin{aligned}
b_{c13} = -M_c M_p\Big(&M_c^2 L_p(\beta^2 + \omega_p^2) + M_p^2 L_c(\beta^2 + \omega_p^2) - \beta^2 L_r L_c L_p \\
&- L_r L_c L_p\omega_p^2 - L_r R_c R_p - L_c R_r R_p - L_p R_r R_c\Big)
\end{aligned}
\tag{A.10}
$$

$$
\begin{aligned}
b_{c12} = -M_c M_p\Big(&\alpha M_c^2 R_p\omega_p + \beta^2 M_c^2 R_p + M_p^2 R_c(\beta^2 + \omega_p^2) - L_c\Big(L_r R_p \\
&\times(\alpha\omega_p + \beta^2) + L_p R_r(\alpha\beta + \omega_p^2)\Big) - L_r L_p R_c(\beta^2 + \omega_p^2) - R_r R_c R_p\Big)
\end{aligned}
\tag{A.11}
$$

$$
\begin{aligned}
b_{c11} = -M_c M_p\Bigg(&L_p\omega_p^2(\beta^2 M_c^2 - R_r R_c) + L_c\Big(\beta^2\omega_p^2(M_p^2 - L_r L_p) \\
&- R_r R_p\Big(\omega_p(\alpha - \beta) + \alpha\beta\Big)\Big) - \beta^2 L_r R_c R_p\Bigg)
\end{aligned}
\tag{A.12}
$$

$$b_{c10} = -\beta M_c M_p \omega_p \Big(R_p \Big(\alpha\beta (M_c^2 - L_r L_c) + R_r R_c \Big) - \omega_p \Big(\beta R_c (L_r L_p - M_p^2) + \alpha L_c L_p R_r \Big) \Big) \tag{A.13}$$

$$b_{c24} = -\alpha M_c M_p \Big(L_p (M_c^2 - L_r L_c) + M_p^2 L_c \Big) \tag{A.14}$$

$$b_{c23} = -M_c M_p \Big(M_c^2 R_p (\alpha - \omega_p) + L_c \Big(L_r R_p (\omega_p - \alpha) + L_p R_r (\beta - \alpha) \Big) \Big) \tag{A.15}$$

$$b_{c22} = -M_c M_p \Big(\alpha M_c^2 L_p (\beta^2 + \omega_p^2) + \alpha M_p^2 L_c (\beta^2 + \omega_p^2) + L_c R_r R_p (\beta - \alpha) - \alpha L_r L_c L_p \omega_p^2 + R_p \omega_p (L_r R_c + L_c R_r) - \alpha\beta^2 L_r L_c L_p + \beta L_p R_r R_c \Big) \tag{A.16}$$

$$b_{c21} = -M_c M_p \Big(\beta^2 M_c^2 R_p (\alpha - \omega_p) + \beta^2 L_r L_c R_p (\omega_p - \alpha) + R_r \Big(L_c L_p \omega_p^2 (\beta - \alpha) + R_c R_p (\beta + \omega_p) \Big) \Big) \tag{A.17}$$

$$b_{c20} = -\beta M_c M_p \omega_p \Big(\omega_p \Big(L_p \Big(\alpha\beta (M_c^2 - L_r L_c) + R_r R_c \Big) + \alpha\beta M_p^2 L_c \Big) + R_p (\beta L_r R_c + \alpha L_c R_r) \Big) \tag{A.18}$$

Description of the coefficients of the BDFM power transfer matrix numerators as a function of the electrical parameters:

$$b_{p15} = (L_c L_r - M_c^2)(L_c L_p L_r - L_p M_c^2 - L_c M_p^2) \tag{A.19}$$

$$b_{p14} = 2L_c L_r (L_p L_r R_c - M_p^2 R_c - M_c^2 R_p) + M_c^2 (-2L_p L_r R_c + M_p^2 R_c + M_c^2 R_p) - 2L_c L_p M_c^2 R_r + L_c^2 (L_r^2 R_p + 2L_p L_r R_r - M_p^2 R_r) \tag{A.20}$$

$$\begin{aligned} b_{p13} = {} & 2L_c L_r^2 R_c R_p - L_r \Big(2R_p (M_c^2 R_c - L_c^2 R_r) + M_p^2 \Big(R_c^2 + L_c^2 (\alpha^2 + \beta^2) \Big) \Big) \\ & + L_p \Big(-2M_c^2 R_c R_r + L_c^2 R_r^2 + M_c^4 (\alpha^2 + \beta^2) + L_r^2 \Big(R_c^2 + L_c^2 (\alpha^2 + \beta^2) \Big) \\ & + 2L_c L_r \Big(2R_c R_r - M_c^2 (\alpha^2 + \beta^2) \Big) \Big) + L_c \Big(-2M_c^2 R_p R_r \\ & + M_p^2 \Big(-2R_c R_r + M_c^2 (\alpha^2 + \beta^2) \Big) \Big) \end{aligned} \tag{A.21}$$

$$\begin{aligned} b_{p12} = &-2M_c^2R_cR_pR_r + 2L_cL_pR_cR_r^2 + L_c^2R_pR_r^2 + M_c^4R_p\alpha^2 \\ &- 2L_cL_pM_c^2R_r\alpha^2 + M_c^4R_p\beta^2 + 2L_r\Big(L_pR_c^2R_r + 2L_cR_cR_pR_r \\ &- L_cM_c^2R_p\alpha^2 + L_c^2L_pR_r\alpha^2 - (L_pM_c^2R_c + L_cM_p^2R_c + L_cM_c^2R_p)\beta^2\Big) \\ &+ L_r^2\Big(R_c^2R_p + 2L_cL_pR_c\beta^2 + L_c^2R_p(\alpha^2+\beta^2)\Big) + M_p^2\Big(-R_c^2R_r \\ &+ M_c^2R_c(\beta^2+\alpha\omega_p) + L_c^2R_r(-\alpha^2+\beta\omega_p)\Big) \end{aligned} \tag{A.22}$$

$$\begin{aligned} b_{p11} = &\,2L_rR_pR_r(R_c^2 + L_c^2\alpha^2) + L_r^2\Big(2L_cR_cR_p + L_p(R_c^2+L_c^2\alpha^2)\Big)\beta^2 \\ &- L_r\Big(M_p^2(R_c^2+L_c^2\alpha^2) + 2M_c^2(R_cR_p + L_cL_p\alpha^2)\Big)\beta^2 \\ &+ L_p\Big(R_r^2(R_c^2+L_c^2\alpha^2) + 2M_c^2R_cR_r\alpha\beta + M_c^4\alpha^2\beta^2\Big) \\ &+ L_c\Big(M_c^2\alpha^2(-2R_pR_r + M_p^2\beta^2) + 2R_cR_r(R_pR_r + M_p^2\beta\omega_p)\Big) \end{aligned} \tag{A.23}$$

$$\begin{aligned} b_{p10} = R_p\Big(&2M_c^2R_cR_r\alpha\beta + \alpha^2\Big(L_c^2R_r^2 + (-L_cL_r + M_c^2)^2\beta^2\Big) \\ &+ R_c^2(R_r^2 + L_r^2\beta^2)\Big) + M_p^2\beta(R_c^2R_r + L_c^2R_r\alpha^2 + M_c^2R_c\alpha\beta)\omega_p \end{aligned} \tag{A.24}$$

$$b_{p24} = (L_cL_r - M_c^2)(L_cL_pL_r - L_pM_c^2 - L_cM_p^2)\omega_p \tag{A.25}$$

$$\begin{aligned} b_{p23} = &-M_c^2\Big(M_p^2R_c(\alpha-\omega_p) + 2L_p(L_rR_c + L_cR_r)\omega_p\Big) \\ &- L_c\Big(2L_r(-L_pL_r + M_p^2)R_c\omega_p + L_cR_r\Big(-2L_pL_r\omega_p + M_p^2(\beta+\omega_p)\Big)\Big) \end{aligned} \tag{A.26}$$

$$\begin{aligned} b_{p22} = &-2L_cM_p^2R_cR_r\beta + L_c(2L_pL_r - M_p^2)\Big(2R_cR_r - M_c^2(\alpha^2+\beta^2)\Big)\omega_p \\ &+ L_c^2\Big(-L_rM_p^2(\alpha^2+\beta^2) + L_p\Big(R_r^2 + L_r^2(\alpha^2+\beta^2)\Big)\Big)\omega_p + \Big(-L_rM_p^2R_c^2 \\ &+ L_p\Big(L_r^2R_c^2 - 2M_c^2R_cR_r + M_c^4(\alpha^2+\beta^2)\Big)\Big)\omega_p \end{aligned} \tag{A.27}$$

$$\begin{aligned} b_{p21} = &\,2L_p\Big(R_cR_r(L_rR_c + L_cR_r) + L_c(L_cL_r - M_c^2)R_r\alpha^2 \\ &+ L_r(L_cL_r - M_c^2)R_c\beta^2\Big)\omega_p - M_p^2\Big(R_c^2R_r(\beta+\omega_p) + L_c^2R_r\alpha^2(\beta+\omega_p) \\ &+ R_c\beta^2\Big(M_c^2(\alpha-\omega_p) + 2L_cL_r\omega_p\Big)\Big) \end{aligned} \tag{A.28}$$

$$\begin{aligned} b_{p20} = \Big(&L_pR_r^2(R_c^2 + L_c^2\alpha^2) + 2L_pM_c^2R_cR_r\alpha\beta + \Big(L_r(L_pL_r - M_p^2)R_c^2 \\ &+ (L_cL_r - M_c^2)(L_cL_pL_r - L_pM_c^2 - L_cM_p^2)\alpha^2\Big)\beta^2\Big)\omega_p \end{aligned} \tag{A.29}$$

Bibliography

[1] A. Abdelbaset, Y. S. Mohamed, A.-H. M. El-Sayed, and A. E. H. A. Ahmed, *Wind Driven Doubly Fed Induction Generator: Grid Synchronization and Control*. Springer, 2018.

[2] A. Beddar, *Adaptabilité des régulateurs d'ordre fractionnaire à la commande vectorielle des machines électriques : Application à une éolienne utilisant une machine synchrone à aimant permanent*. PhD thesis, University 20 August 1955 – Skikda, 2018.

[3] J. Fortmann, *Modeling of wind turbines with doubly fed generator system*. Springer, 2015.

[4] C. Carunaiselvane and T. R. Chelliah, "Present trends and future prospects of asynchronous machines in renewable energy systems," *Renewable and Sustainable Energy Reviews*, vol. 74, pp. 1028–1041, 2017.

[5] X. Wang, *Modeling and Design of Brushless Doubly-Fed Induction Machines*. PhD thesis, Delft University of Technology, 2017.

[6] T. D. Strous, *Brushless Doubly-Fed Induction Machines for Wind Turbine Drive-Train Applications*. PhD thesis, Delft University of Technology, 2016.

[7] L. J. Hunt, "A new type of induction motor," *Electrical Engineers, Journal of the Institution of*, vol. 39, no. 186, pp. 648–667, 1907.

[8] L. J. Hunt, "The cascade induction motor," *J. IEE*, vol. 52, no. 230, pp. 406–426, 1914.

[9] F. Creedy, "Some developments in multi-speed cascade induction motors," *Electrical Engineers, Journal of the Institution of*, vol. 59, no. 301, pp. 511–532, 1920.

[10] A. Broadway and L. Burbridge, "Self-cascaded machine: a low-speed motor or high-frequency brushless alternator," *Electrical Engineers, Proceedings of the Institution of*, vol. 117, no. 7, pp. 1277–1290, 1970.

[11] A. Broadway, "Cageless induction machine," in *Proceedings of the Institution of Electrical Engineers*, vol. 118, no. 11, pp. 1593–1600, IET, 1971.

[12] A. Broadway, B. Cook, and P. Neal, "Brushless cascade alternator," in *Proceedings of the Institution of Electrical Engineers*, vol. 121, no. 12, pp. 1529–1535, IET, 1974.

[13] A. Kusko and C. B. Somuah, "Speed control of a single-frame cascade induction motor with slip-power pump back," *Industry Applications, IEEE Transactions on*, vol. IA-14, no. 2, pp. 97–105, 1978.

[14] F. Shibata and T. Kohrin, "A brushless, self-excited polyphase synchronous generator," *Power Apparatus and Systems, IEEE Transactions on*, vol. PAS-102, no. 8, pp. 2413–2419, 1983.

[15] F. Shibata and K. Taka, "speed control system for brushless cascade induction motors in control range of slips s1> 1 and s2> 1," *Energy Conversion, IEEE Transactions on*, vol. EC-2, no. 2, pp. 246–253, 1987.

[16] A. K. Wallace, R. Spée, and H. K. Lauw, "Dynamic modeling of brushless doubly-fed machines," in *Industry Applications Society Annual Meeting, 1989., Conference Record of the 1989 IEEE*, vol. 1, pp. 329–334, IEEE, 1989.

[17] R. Spee, A. K. Wallace, and H. K. Lauw, "Performance simulation of brushless doubly-fed adjustable speed drives," in *Industry Applications Society Annual Meeting, 1989., Conference Record of the 1989 IEEE*, vol. 1, pp. 738–743, IEEE, 1989.

[18] P. Rochelle, R. Spee, and A. K. Wallace, "The effect of stator winding configuration on the performance of brushless doubly-fed machines in adjustable speed drives," in *Industry Applications Society Annual Meeting, 1990., Conference Record of the 1990 IEEE*, vol. 1, pp. 331–337, IEEE, 1990.

[19] A. Ramchandran, G. C. Alexander, and R. Spée, "Off-line parameter estimation for the doubly-fed machine," in *Industrial Electronics, Control, Instrumentation, and Automation, 1992. Power Electronics and Motion Control., Proceedings of the 1992 International Conference on*, vol. 3, pp. 1294–1298, IEEE, 1992.

[20] A. Ramchandran and G. C. Alexander, "Frequency-domain parameter estimation for the brushless doubly-fed machine," in *Power Conversion Conference, 1993. Yokohama 1993., Conference Record of the*, pp. 346–351, IEEE, 1993.

[21] A. K. Wallace, R. Spee, and G. Alexander, "The brushless doubly-fed machine: its advantages, applications and design methods," in *Electrical Machines and Drives, 1993. Sixth International Conference on (Conf. Publ. No. 376)*, pp. 511–517, IET, 1993.

[22] H. K. Lauw, "Brushless doubly-fed motor control system," Aug. 24 1993. US Patent 5,239,251.

[23] A. Wallace, P. Rochelle, and R. Spée, "Rotor modeling and development for brushless doubly-fed machines," *Electric machines and power systems*, vol. 23, no. 6, pp. 703–715, 1995.

[24] M. Boger and A. Wallace, "Performance capability analysis of the brushless doubly-fed machine as a wind generator," in *Electrical Machines and Drives, 1995. Seventh International Conference on (Conf. Publ. No. 412)*, pp. 458–461, IET, 1995.

[25] B. Gorti, G. Alexander, and R. Spée, "Power balance considerations for brushless doubly-fed machines," *Energy Conversion, IEEE Transactions on*, vol. 11, no. 4, pp. 687–692, 1996.

[26] Y. Liao, "Design of a brushless doubly-fed induction motor for adjustable speed drive applications," in *Industry Applications Conference, 1996. Thirty-First IAS Annual Meeting, IAS'96., Conference Record of the 1996 IEEE*, vol. 2, pp. 850–855, IEEE, 1996.

[27] M. S. Boger, *Aspects of brushless doubly-fed induction machines.* PhD thesis, University of Cambridge, 1997.

[28] S. Williamson and M. S. Boger, "Impact of inter-bar currents on the performance of the brushless doubly fed motor," *Industry Applications, IEEE Transactions on*, vol. 35, no. 2, pp. 453–460, 1999.

[29] A. C. Ferreira and S. Williamson, "Time-stepping finite-element analysis of brushless doubly fed machine taking iron loss and saturation into account," *Industry Applications, IEEE Transactions on*, vol. 35, no. 3, pp. 583–588, 1999.

[30] B. Koch, R. Spee, and B. Clever, "A comparison of stack preparation methods for bar insulation in diecast rotors," in *Industry Applications Conference, 1997. Thirty-Second IAS Annual Meeting, IAS'97., Conference Record of the 1997 IEEE*, vol. 1, pp. 182–187, IEEE, 1997.

[31] F. Wang, F. Zhang, and L. Xu, "Parameter and performance comparison of doubly fed brushless machine with cage and reluctance rotors," *Industry Applications, IEEE Transactions on*, vol. 38, no. 5, pp. 1237–1243, 2002.

[32] R. McMahon, P. Roberts, X. Wang, and P. Tavner, "Performance of BDFM as generator and motor," in *Electric Power Applications, IEE Proceedings*, vol. 153, no. 2, pp. 289–299, IET, 2006.

[33] F. Blazquez, C. Veganzones, D. Ramirez, and C. Platero, "Characterization of the rotor magnetic field in a brushless doubly-fed induction machine," *Energy Conversion, IEEE Transactions on*, vol. 24, no. 3, pp. 599–607, 2009.

[34] H. Gorginpour, B. Jandaghi, and H. Oraee, "Finite element analysis of brushless doubly-fed machine under stator winding faults," in *2011 2nd Power Electronics, Drive Systems and Technologies Conference*, 2011.

[35] H. Gorginpour, P. Sotoodeh, and H. Oraee, "Dynamic model for brushless doubly-fed machine with stator winding faults," in *Power Electronic & Drive Systems & Technologies Conference (PEDSTC), 2010 1st*, pp. 316–322, IEEE, 2010.

[36] H. Gorginpour, H. Oraee, and R. A. McMahon, "Performance description of brushless doubly-fed induction machine in its asynchronous and variable speed synchronous modes," *Journal of Electromagnetic Analysis and Applications*, vol. 3, no. 12, p. 490, 2011.

[37] H. Gorginpour, H. Oraee, and R. A. McMahon, "A novel modeling approach for design studies of brushless doubly fed induction generator based on magnetic equivalent circuit," *Energy Conversion, IEEE Transactions on*, vol. 28, no. 4, pp. 902–912, 2013.

[38] H. Gorginpour, B. Jandaghi, H. Oraee, and E. Abdi, "Magnetic equivalent circuit modelling of brushless doubly fed induction generator," *Renewable Power Generation, IET*, vol. 8, no. 3, pp. 334–346, 2014.

[39] H. Gorginpour, H. Oraee, and R. A. McMahon, "Electromagnetic-thermal design optimization of the brushless doubly fed induction generator," *Industrial Electronics, IEEE Transactions on*, vol. 61, no. 4, pp. 1710–1721, 2014.

[40] H. Gorginpour, H. Oraee, and E. Abdi, "Calculation of core and stray load losses in brushless doubly fed induction generators," *Industrial Electronics, IEEE Transactions on*, vol. 61, no. 7, pp. 3167–3177, 2014.

[41] M. El Achkar, R. Mbayed, G. Salloum, N. Patin, S. Le Ballois, and E. Monmasson, "Power operating domain of a cascaded doubly fed induction machine," *Mathematics and Computers in Simulation*, vol. 130, pp. 142–154, 2015.

[42] M. El Achkar, R. Mbayed, G. Salloum, S. Le Ballois, and E. Monmasson, "Generic study of the power capability of a cascaded doubly fed induction machine," *International Journal of Electrical Power & Energy Systems*, vol. 86, pp. 61–70, 2017.

[43] Y. Cheng, P. Yuan, C. Kan, L. Chen, and Y. He, "Design and simulation of a new brushless doubly-fed pulsed alternator for high-energy pulsed lasers," *Plasma Science, IEEE Transactions on*, vol. 45, no. 7, pp. 1115–1121, 2017.

[44] H. Djadi, K. Yazid, and M. Menaa, "Parameters identification of a brushless doubly fed induction machine using pseudo-random binary signal excitation signal for recursive least squares method," *Electric Power Applications, IET*, vol. 11, no. 9, pp. 1585–1595, 2017.

[45] M. Gholizadeh, A. Oraee, S. Tohidi, H. Oraee, and R. A. McMahon, "An analytical study for low voltage ride through of the brushless doubly-fed induction generator during asymmetrical voltage dips," *Renewable Energy*, vol. 115, pp. 64–75, 2018.

[46] M. Gholizadeh, S. Tohidi, A. Oraee, and H. Oraee, "Appropriate crowbar protection for improvement of brushless DFIG LVRT during asymmetrical voltage dips," *International Journal of Electrical Power & Energy Systems*, vol. 95, pp. 1–10, 2018.

[47] S. Tohidi, "Analysis and simplified modelling of brushless doubly-fed induction machine in synchronous mode of operation," *Electric Power Applications, IET*, vol. 10, no. 2, pp. 110–116, 2016.

[48] B. Guan, *Design and control of a high-efficiency doubly-fed brushless machine for power generation applications*. PhD thesis, Ohio State University, 2014.

[49] N. U. R. MALIK, *Modelling, Analysis, and Control Aspects of a Rotating Power Electronic Brushless Doubly-Fed Induction Generator*. PhD thesis, KTH Royal Institute of Technology, 2015.

[50] U. Shipurkar, T. D. Strous, H. Polinder, J. Ferreira, and A. Veltman, "Achieving sensorless control for the brushless doubly fed induction machine," *Energy Conversion, IEEE Transactions on*, vol. 32, no. 4, pp. 1611–1619, 2017.

[51] S. Shao, *Control of brushless doubly-fed (induction) machines*. PhD thesis, University of Cambridge, 2010.

[52] J. A. Melkebeek, *Electrical Machines and Drives: Fundamentals and Advanced Modelling*. Springer, 2018.

[53] D. Gerling, *Electrical Machines*. Springer, 2015.

[54] S. N. Vukosavic, *Electrical machines*. Springer Science & Business Media, 2013.

[55] P. C. Krause, O. Wasynczuk, and S. D. Sudhoff, *Analysis of electric machinery and drive systems*. John Wiley & Sons, 2002.

[56] H. Altun and S. Sünter, "Modeling, simulation and control of wind turbine driven doubly-fed induction generator with matrix converter on the rotor side," *Electrical Engineering*, vol. 95, no. 2, pp. 157–170, 2013.

[57] R. Sadeghi, S. M. Madani, and M. Ataei, "A new smooth synchronization of brushless doubly-fed induction generator by applying a proposed machine model," *Sustainable Energy, IEEE Transactions on*, vol. 9, no. 1, pp. 371–380, 2018.

[58] L. Sun, Y. Chen, L. Peng, and Y. Kang, "Numerical-based frequency domain controller design for stand-alone brushless doubly fed induction generator power system," *IET Power Electronics*, vol. 10, no. 5, pp. 588–598, 2016.

[59] A. **Ganouche**, H. Bouzekri, and A. Beddar, "Modelling and stability analysis of brushless doubly fed generators," *TELKOMNIKA (Telecommunication Computing Electronics and Control)*, vol. 15, no. 4, pp. 1741–1749, 2017.

[60] B. H. Smith, "Theory and performance of a twin stator induction machine," *Power Apparatus and Systems, IEEE Transactions on*, vol. 2, no. PAS-85, pp. 123–131, 1966.

[61] B. H. Smith, "Synchronous behavior of doubly fed twin stator induction machine," *Power Apparatus and Systems, IEEE Transactions on*, vol. PAS-86, no. 10, pp. 1227–1236, 1967.

[62] R. Li, A. Wallace, R. Spee, and Y. Wang, "Two-axis model development of cage-rotor brushless doubly fed machines," *Energy Conversion, IEEE Transactions on*, vol. 6, no. 3, pp. 453–460, 1991.

[63] R. Li, A. Wallace, R. Spee, and Y. Wang, "Dynamic simulation of brushless doubly-fed machines," *Energy Conversion, IEEE Transactions on*, vol. 6, no. 3, pp. 445–452, 1991.

[64] R. Li, *Dynamic modeling, simulation and stability analysis of brushless doubly fed machines.* PhD thesis, Oregon State University, 1991.

[65] R. Li, R. Spée, A. K. Wallace, and G. Alexander, "Synchronous drive performance of brushless doubly-fed motors," *Industry Applications, IEEE Transactions on*, vol. 30, no. 4, pp. 963–970, 1994.

[66] D. Zhou and R. Spee, "Synchronous frame model and decoupled control development for doubly fed machines," in *Power Electronics Specialists Conference, PESC'94 Record., 25th Annual IEEE*, pp. 1229–1236, IEEE, 1994.

[67] M. S. Boger, A. K. Wallace, R. Spee, and R. Li, "General pole number model of the brushless doubly fed machine," *Industry Applications, IEEE Transactions on*, vol. 31, no. 5, pp. 1022–1028, 1995.

[68] A. C. Ferreira, *Analysis of brushless doubly-fed induction machines.* PhD thesis, University of Cambridge, 1996.

[69] S. Williamson, A. Ferreira, and A. Wallace, "Generalised theory of the brushless doubly fed machine. part 1: Analysis," in *Electric Power Applications, IEE Proceedings*, vol. 144, no. 2, pp. 111–122, IET, 1997.

[70] S. Williamson and A. Ferreira, "Generalised theory of the brushless doubly-fed machine. part 2: Model verification and performance," in *Electric Power Applications, IEE Proceedings*, vol. 144, no. 2, pp. 123–129, IET, 1997.

[71] A. M. Oliveira, P. Kuo-Peng, N. Sadowski, F. Rüncos, R. Carlson, and P. Dular, "Finite-element analysis of a double-winding induction motor with a special rotor bars topology," *Magnetics, IEEE Transactions on*, vol. 40, no. 2, pp. 770–773, 2004.

[72] P. C. Roberts, *A study of brushless doubly fed (induction) machines.* PhD thesis, University of Cambridge, Cambridge, 2004.

[73] P. C. Roberts, R. McMahon, P. Tavner, J. Maciejowski, and T. Flack, "Equivalent circuit for the brushless doubly fed machine (BDFM) including parameter estimation and experimental

verification," in *Electric Power Applications, IEE Proceedings*, vol. 152, no. 4, pp. 933–942, IET, 2005.

[74] J. Poza, E. Oyarbide, D. Roye, and M. Rodriguez, "Unified reference frame dq model of the brushless doubly fed machine," in *Electric Power Applications, IEE Proceedings*, vol. 153, no. 5, pp. 726–734, IET, 2006.

[75] F. J. Poza Lobo, *Modélisation, conception et commande d'une machine asynchrone sans balais doublement alimentée pour la génération à vitesse variable.* PhD thesis, Grenoble, INPG, 2003.

[76] F. Barati, S. Shao, E. Abdi, H. Oraee, and R. McMahon, "Generalized vector model for the brushless doubly fed machine with a nested-loop rotor," *Industrial Electronics, IEEE Transactions on*, vol. 58, no. 6, pp. 2313–2321, 2011.

[77] P. C. Roberts, T. Long, R. A. McMahon, S. Shao, E. Abdi, and J. M. Maciejowski, "Dynamic modelling of the brushless doubly fed machine," *Electric Power Applications, IET*, vol. 7, no. 7, pp. 544–556, 2013.

[78] P. Han, M. Cheng, X. Wei, and N. Li, "Modeling and performance analysis of a dual-stator brushless doubly fed induction machine based on spiral vector theory," *Industry Applications, IEEE Transactions on*, vol. 52, no. 2, pp. 1380–1389, 2016.

[79] H. Bouzekri, A. **Ganouche**, and Z. Ahmida, "Investigation into control performance of brushless doubly fed asynchronous machines in wind energy conversion systems," in *Environment and Electrical Engineering (EEEIC), 2015 IEEE 15th International Conference on*, pp. 1099–1103, IEEE, 2015.

[80] A. **Ganouche**, H. Bouzekri, and A. Beddar, "Robust control of brushless doubly fed induction generator," in *International Conference on Technological Advances in Electrical Engineering (ICTAEE'16)*, pp. 1–5, 2016.

[81] X. Wang, T. D. Strous, D. Lahaye, H. Polinder, and J. A. Ferreira, "Modeling and optimization of brushless doubly-fed induction machines using computationally efficient finite-element analysis," *Industry Applications, IEEE Transactions on*, vol. 52, no. 6, pp. 4525–4534, 2016.

[82] R. A. McMahon, M. E. Mathekga, X. Wang, and M. R. Tatlow, "Design considerations for the brushless doubly-fed (induction) machine," *Electric Power Applications, IET*, vol. 10, no. 5, pp. 394–402, 2016.

[83] P. Han, M. Cheng, Y. Jiang, and Z. Chen, "Torque/power density optimization of a dual-stator brushless doubly-fed induction generator for wind power application," *Industrial Electronics, IEEE Transactions on*, vol. 64, no. 12, pp. 9864–9875, 2017.

[84] L. Han, X. Ou, J. Du, X. Han, and Y. Guo, "Study of direct coupling in stator dual windings of a brushless doubly fed machine," *Energy Conversion, IEEE Transactions on*, vol. 32, no. 3, pp. 974–982, 2017.

[85] F. Zhang, S. Yu, Y. Wang, S. Jin, and M. G. Jovanovic, "Design and performance comparisons of brushless doubly-fed generators with different rotor structures," *Industrial Electronics, IEEE Transactions on*, vol. PP, no. 99, pp. 1–1, 2018.

[86] P. Han, M. Cheng, X. Wei, and Y. Jiang, "Steady-state characteristics of the dual-stator brushless doubly fed induction generator," *Industrial Electronics, IEEE Transactions on*, vol. 65, no. 1, pp. 200–210, 2018.

[87] M. Kidouche, *calcul généré de la fonction de Lyapunov des systèmes non linéaires de grande dimension*. PhD thesis, Mentouri University of Constantine, 2006.

[88] C. Cook and B. H. Smith, "Stability and stabilisation of doubly-fed single-frame cascade induction machines," in *Proceedings of the Institution of Electrical Engineers*, vol. 126, no. 11, pp. 1168–1174, IET, 1979.

[89] C. Cook and B. H. Smith, "Effects of machine parameter values on dynamic response and stability regions of doubly-fed cascade induction machines," in *IEE Proceedings B-Electric Power Applications*, vol. 130, no. 2, pp. 137–142, IET, 1983.

[90] R. Li, A. Wallace, and R. Spéé, "Determination of converter control algorithms for brushless doubly-fed induction motor drives using floquet and lyapunov techniques," *Power Electronics, IEEE Transactions on*, vol. 10, no. 1, pp. 78–85, 1995.

[91] J. Poza, E. Oarbide, D. Roye, and I. Sarasola, "Stability analysis of a BDFM under open-loop voltage control," in *Power Electronics and Applications, 2005 European Conference on*, pp. 10–pp, IEEE, 2005.

[92] I. Sarasola, J. Poza, E. Oyarbide, and M. Á. Rodríguez, "Stability analysis of a brushless doubly-fed machine under closed loop scalar current control," in *IEEE Industrial Electronics, IECON 2006-32nd Annual Conference on*, pp. 1527–1532, IEEE, 2006.

[93] R. Cárdenas, R. Peña, P. Wheeler, J. Clare, A. Muñoz, and A. Sureda, "Control of a wind generation system based on a brushless doubly fed induction generator fed by a matrix converter," *Electric Power Systems Research*, vol. 103, pp. 49–60, 2013.

[94] J. Poza, E. Oyarbide, I. Sarasola, and M. Rodriguez, "Vector control design and experimental evaluation for the brushless doubly fed machine," *Electric Power Applications, IET*, vol. 3, no. 4, pp. 247–256, 2009.

[95] O. Agbaje, D. Kavanagh, M. Sumisławska, D. Howey, M. McCulloch, and K. Burnham, "Estimation of temperature dependent equivalent circuit parameters for traction-based electric machines," *Coventry University*, 2013.

[96] M. Sumisławska, O. Agbaje, D. F. Kavanagh, and K. J. Bumham, "Equivalent circuit model estimation of induction machines under elevated temperature conditions," in *Control (CONTROL), 2014 UKACC International Conference on*, pp. 413–418, IEEE, 2014.

[97] M. Sumislawska, K. N. Gyftakis, D. F. Kavanagh, M. D. McCulloch, K. J. Burnham, and D. A. Howey, "The impact of thermal degradation on properties of electrical machine winding insulation material," *Industry Applications, IEEE Transactions on*, vol. 52, no. 4, pp. 2951–2960, 2016.

[98] R. Spée, S. Bhowmik, and J. H. Enslin, "Novel control strategies for variable-speed doubly fed wind power generation systems," *Renewable Energy*, vol. 6, no. 8, pp. 907–915, 1995.

[99] D. Zhou and R. Spee, "Field oriented control development for brushless doubly-fed machines," in *Industry Applications Conference, 1996. Thirty-First IAS Annual Meeting, IAS'96., Conference Record of the 1996 IEEE*, vol. 1, pp. 304–310, IEEE, 1996.

[100] D. Zhou, R. Spee, G. Alexander, and A. Wallace, "A simplified method for dynamic control of brushless doubly-fed machines," in *Industrial Electronics, Control, and Instrumentation, 1996., Proceedings of the 1996 IEEE IECON 22nd International Conference on*, vol. 2, pp. 946–951, IEEE, 1996.

[101] W. R. Brassfield, R. Spee, and T. G. Habetler, "Direct torque control for brushless doubly-fed machines," *Industry Applications, IEEE Transactions on*, vol. 32, no. 5, pp. 1098–1104, 1996.

[102] D. Zhou, R. Spee, and G. C. Alexander, "Experimental evaluation of a rotor flux oriented control algorithm for brushless doubly fed machines," *Power Electronics, IEEE Transactions on*, vol. 12, no. 1, pp. 72–78, 1997.

[103] W. Brassfield, R. Spee, and T. Habetler, "Direct torque control for brushless doubly-fed machines," in *Industry Applications Society Annual Meeting, 1992., Conference Record of the 1992 IEEE*, vol. 1, pp. 615–622, IEEE, 1992.

[104] D. Zhou, R. Spee, and A. Wallace, "Model reference adaptive speed control for doubly-fed machines," in *Industrial Electronics, Control, and Instrumentation, 1993. Proceedings of the IECON'93., International Conference on*, pp. 1175–1180, IEEE, 1993.

[105] A. R. Muñoz and T. A. Lipo, "Dual stator winding induction machine drive," *Industry Applications, IEEE Transactions on*, vol. 36, no. 5, pp. 1369–1379, 2000.

[106] H. Shoudao, W. Yan, L. Youjie, and W. Yaonan, "Fuzzy-based power factor control for brushless doubly-fed machines," in *Intelligent Control and Automation, 2002. Proceedings of the 4th World Congress on*, vol. 1, pp. 587–591, IEEE, 2002.

[107] J. Poza, E. Oyarbide, and D. Roye, "New vector control algorithm for brushless doubly-fed machines," in *IECON 02 [Industrial Electronics Society, IEEE 2002 28th Annual Conference of the]*, vol. 2, pp. 1138–1143, IEEE, 2002.

[108] S. Shao, E. Abdi, and R. McMahon, "Vector control of the brushless doubly-fed machine for wind power generation," in *Sustainable Energy Technologies, 2008. ICSET 2008. IEEE International Conference on*, pp. 322–327, IEEE, 2008.

[109] J. Chen, W. Zhang, B. Chen, and Y. Ma, "Improved vector control of brushless doubly fed induction generator under unbalanced grid conditions for offshore wind power generation," *Energy Conversion, IEEE Transactions on*, vol. 31, no. 1, pp. 293–302, 2016.

[110] C. Ming, J. Yunlei, H. Peng, and W. Qingsong, "Unbalanced and low-order harmonic voltage mitigation of stand-alone dual-stator brushless doubly-fed induction wind generator," *Industrial Electronics, IEEE Transactions on*, 2017.

[111] P. Han, M. Cheng, and Z. Chen, "Dual-electrical-port control of cascaded doubly-fed induction machine for EV/HEV applications," *Industry Applications, IEEE Transactions on*, vol. 53, no. 2, pp. 1390–1398, 2017.

[112] M. Hutton and B. Friedland, "Routh approximations for reducing order of linear, time-invariant systems," *Automatic Control, IEEE Transactions on*, vol. 20, no. 3, pp. 329–337, 1975.

[113] A. N. Michel and R. K. Miller, *Qualitative analysis of large scale dynamical systems*. Elsevier, 1977.

[114] D. D. Šiljak, *Large-scale dynamic systems: stability and structure*, vol. 2. North Holland, 1978.

[115] L. Jocic, M. Ribbens-Pavella, and D. Siljak, "Multimachine power systems: Stability, decomposition, and aggregation," *Automatic Control, IEEE Transactions on*, vol. 23, no. 2, pp. 325–332, 1978.

[116] A. Titli and P. Bertrand, *Analyse et commande des systèmes complexes*. Cépaduès, 1979.

[117] M. Ribbens-Pavella and F. Evans, "Direct methods for studying dynamics of large-scale electric power systems—a survey," *Automatica*, vol. 21, no. 1, pp. 1–21, 1985.

[118] M. Kidouche, *Systèmes non linéaires de grande dimension*. University 20 August 1955 – Skikda, 2013. Postgraduate seminar.

[119] A. Dell'Aquila, M. Marinelli, V. G. Monopoli, and A. Lecci, "Optimized resonant control for shunt active power filters," in *Power Electronics and Motion Control Conference, 2006. EPE-PEMC 2006. 12th International*, pp. 877–882, IEEE, 2006.

[120] A. M. Dumitrescu, G. Griva, R. Bojoi, V. Bostan, and R. Magureanu, "Design of current controllers for active power filters using naslin polynomial technique," in *Power Electronics and Applications, 2007 European Conference on*, pp. 1–7, IEEE, 2007.

[121] J. M. Retif, *Automatique régulation.* National Institute of Applied Sciences of Lyon, 2008.

[122] R. Herzog, *Réglage robuste appliqué.* University 20 August 1955 – Skikda, 2014. Postgraduate seminar.

[123] G. Zames, "Feedback and optimal sensitivity: Model reference transformations, multiplicative seminorms, and approximate inverses," *Automatic Control, IEEE Transactions on*, vol. 26, no. 2, pp. 301–320, 1981.

[124] J. C. Doyle, K. Glover, P. P. Khargonekar, and B. A. Francis, "State-space solutions to standard H_2 and H_∞ control problems," *Automatic Control, IEEE Transactions on*, vol. 34, no. 8, pp. 831–847, 1989.

[125] J. C. Doyle, B. A. Francis, and A. R. Tannenbaum, *Feedback control theory.* Macmillan Publishing Company, 1990.

[126] B. M. Chen, *Robust and H_∞ Control.* Springer Science & Business Media, 2000.

[127] J. Ackermann, *Robust control: the parameter space approach.* Springer Science & Business Media, 2002.

[128] K. J. Åström, *Control System Design.* University of California, 2002.

[129] H. Serhoud and D. Benattous, "Simulation of grid connection and maximum power point tracking control of brushless doubly-fed generator in wind power system," *Frontiers in Energy*, vol. 7, no. 3, pp. 380–387, 2013.

[130] M. A. Mahboub, S. Drid, M. Sid, and R. Cheikh, "Robust direct power control based on the lyapunov theory of a grid-connected brushless doubly fed induction generator," *Frontiers in Energy*, vol. 10, no. 3, pp. 298–307, 2016.

[131] M. A. Mahboub, S. Drid, M. Sid, and R. Cheikh, "Sliding mode control of grid connected brushless doubly fed induction generator driven by wind turbine in variable speed," *International Journal of System Assurance Engineering and Management*, vol. 8, no. 2, pp. 788–798, 2016.

[132] A. Laouafi, M. Mordjaoui, A. Medoued, T. E. Boukelia, and A. **Ganouche**, "Wind power forecasting approach using neuro-fuzzy system combined with wavelet packet decomposition, data preprocessing, and forecast combination framework," *Wind Engineering*, vol. 41, no. 4, pp. 235–244, 2017.

[133] A. Laouafi, M. Mordjaoui, S. Haddad, T. E. Boukelia, and A. **Ganouche**, "Online electricity demand forecasting based on an effective forecast combination methodology," *Electric Power Systems Research*, vol. 148, pp. 35–47, 2017.

[134] K. Protsenko and D. Xu, "Modeling and control of brushless doubly-fed induction generators in wind energy applications," *Power Electronics, IEEE Transactions on*, vol. 23, no. 3, pp. 1191–1197, 2008.

[135] S. Shao, T. Long, E. Abdi, and R. A. McMahon, "Dynamic control of the brushless doubly fed induction generator under unbalanced operation," *Industrial Electronics, IEEE Transactions on*, vol. 60, no. 6, pp. 2465–2476, 2013.

[136] X. Wang, H. Lin, and Z. Wang, "Transient control of the reactive current for the line-side converter of the brushless doubly-fed induction generator in stand-alone operation," *Power Electronics, IEEE Transactions on*, vol. 32, no. 10, pp. 8193–8203, 2017.

[137] G. Zhang, J. Yang, Y. Sun, M. Su, W. Tang, Q. Zhu, and H. Wang, "A robust control scheme based on ISMC for the brushless doubly fed induction machine," *Power Electronics, IEEE Transactions on*, vol. 33, no. 4, pp. 3129–3140, 2018.